

THE 4D LIVING GENOME

by

Julianna Arlene Sherman Goelzer



A dissertation

submitted in partial fulfillment

of the requirements for the degree of

Doctor of Philosophy in Biomolecular Science

Boise State University

August 2021

© 2021

Julianna Arlene Sherman Goelzer

ALL RIGHTS RESERVED

BOISE STATE UNIVERSITY GRADUATE COLLEGE

DEFENSE COMMITTEE AND FINAL READING APPROVALS

of the dissertation submitted by

Julianna Arlene Sherman Goelzer

Dissertation Title: The 4D Living Genome

Date of Final Oral Examination: 16 June 2021

The following individuals read and discussed the dissertation submitted by student Julianna Arlene Sherman Goelzer, and they evaluated her presentation and response to questions during the final oral examination. They found that the student passed the final oral examination.

Matthew L Ferguson, Ph.D.	Chair, Supervisory Committee
Eric Hayden, Ph.D.	Member, Supervisory Committee
Brad Morrison, Ph.D.	Member, Supervisory Committee
Allan Albig, Ph.D.	Member, Supervisory Committee

The final reading approval of the dissertation was granted by Matthew L. Ferguson, Ph.D., Chair of the Supervisory Committee. The dissertation was approved by the Graduate College.

DEDICATION

This dissertation is dedicated to my grandmother, Esther Sherman. She was the ultimate educator who called greatness out of every child she ever taught. I was blessed to have her in my corner from day one.

ACKNOWLEDGMENTS

Throughout my graduate school journey, I have received a great deal of support. I would first like to thank my primary advisor, Dr. Matthew L. Ferguson, whose expertise was invaluable in training not only my technical skills, but my thinking and communicating skills as a scientist. I would like to thank my committee for their assistance. They have gone above and beyond to assist me in grant writing, experimental design, and career advice.

I would also like to thank my collaborators at NCI, specifically Dr. Daniel Larson and Dr. Diana Stavreva who contributed significantly to the glucocorticoid study. I would also like to thank Dr. Gunes Uzer, Matthew Goelzer, and Dr. Corey Neu for their collaborations on the Nuclear Mechanobiology review that is highlighted in Appendix II. Additionally, I would like to acknowledge the collaborations of Ulas C. Coskun, Alexander Vallmitjana, Anh Hyunh, Yuansheng Sun, Shih-chu “Jeff” Liao, Sunil Shah, Enrico Gratton, and Beniamino Barbieri who contributed to the orbital tracking work showcased in chapter 2. Finally, I would like to thank Dr. Mike Pool, Ethan Davis, Abigail Figueroa, Gretchen Kunz, and Iris Torres for their assistance and support.

I would like to thank Dr. John Korstad and Dr. William Ranahan II for their encouragement and support in setting me on this path of scientific discovery. In addition, my parents for their encouragement and support in my educational journey. Finally, I could not have completed this dissertation without the support of my husband Matthew

who not only encouraged and supported me, but also provided insightful discussions towards the completion of this project.

ABSTRACT

Over the last few decades great advances have been made in our understanding of gene expression and the human genome. In 2003 the human genome was sequenced for the first time, allowing us to discover its true importance in human health. While sequencing the human genome was a great advance, it ultimately created more questions than it answered. It is known that the genomic sequence is extremely important in genome regulation, however recent studies have shown that the 4D (spatiotemporal) organization and dynamics of the living genome plays an equally critical role in regulation of gene expression. A key factor in the spatiotemporal genome is the temporal and spatial coordination of transcription factors required for gene expression. We focus on addressing both the spatial and temporal aspects of the genome through a cutting-edge microscopy technique known as 3D Orbital Tracking Fluorescence Correlation Spectroscopy (3DOT-FCCS) in conjunction with Molecular Dynamics simulations. The synergistic use of these techniques will provide a clearer picture of the rules that govern the human genome.

TABLE OF CONTENTS

DEDICATION.....	iv
ACKNOWLEDGMENTS.....	v
ABSTRACT	vii
LIST OF TABLES	xii
LIST OF FIGURES	xiii
LIST OF ABBREVIATIONS.....	xvi
CHAPTER ONE: INTRODUCTION.....	1
Background.....	1
The Human Genome Project	1
Gene Expression & Central Dogma.....	1
DNA Elements.....	3
Epigenetics	4
Light Microscopy.....	5
Optical Challenges	8
Aims	9
Outline of Dissertation.....	9
CHAPTER 2: NANO-RESOLUTION IN VIVO 3D ORBITAL TRACKING SYSTEM TO STUDY CELLULAR DYNAMICS AND BIO-MOLECULAR PROCESSES.....	11
Abstract.....	11
Introduction.....	12

Materials and Methods.....	16
The System Schematic.....	16
Tracking Procedure	17
Results and Discussion.....	20
Gene Activation.....	20
Transport of Lysosomes	23
Conclusion.....	25
CHAPTER THREE: LIGAND DEPENDENCE OF REAL-TIME GENE ACTIVATION BY THE NUCLEAR RECEPTOR GLUCOCORTICOID BY SINGLE MOLECULE LIVE CELL 3D ORBITAL TRACKING FLUORESCENCE CROSS CORRELATION SPECTROSCOPY.....	27
Abstract	27
Introduction	28
3D Orbital Tracking	29
Fluorescence Correlation Spectroscopy	30
RNA Labeling.....	32
Glucocorticoid Receptor.....	34
Methods.....	34
Plasmids and Cell Lines.....	34
Microscope.....	35
Orbital Tracking	36
Software.....	37
Data Analysis	37
Results	39
Transcription Factor Dwell Times	40

RNA Dwell Times	44
Cross Correlation Binding Time.....	47
Binding Efficiency	50
Molecule Number	51
Data Validation.....	52
Future Directions.....	58
Splicing.....	58
DNA Labeling	58
RNA Mango	59
Conclusion	59
Supplemental.....	61
CHAPTER FOUR: PREDICTIVE MODELING OF THE LIVING GENOME.....	66
Abstract.....	66
Biomolecular Sequencing.....	66
Molecular Dynamics Simulations	68
Models and Methods	70
Single Molecule Tracking Data.....	75
Conclusions.....	83
Future Directions.....	84
CHAPTER FIVE: CONCLUSIONS AND FUTURE DIRECTIONS	87
Conclusions.....	87
3D Orbital Tracking in Organoid Models.....	87
Introduction	87

Matrigel Proposed Experiments	89
Significance.....	89
Conclusions	90
REFERENCES.....	91
APPENDIX I.....	133
APPENDIX II	149

LIST OF TABLES

Table 3.1	TF (Red) Autocorrelation Two-Component Fits.....	43
Table 3.2	TF (Red) Autocorrelation Three-Component Fits.....	44
Table 3.3	RNA (Green) Autocorrelation Fits	47
Table 3.4	TF-RNA Cross Correlation Fits.....	50
Table 4.1	Single Molecule Tracking Gene Set	77
Table 4.2	Proposed Simulations.....	82
Table AII.1	Common in vitro mechanical force stimulation methods and their major studied outcomes.....	169
Table AII.2	Fluorescence Labeling Technologies.....	179
Table AII.3	Fluorescence Imaging Techniques.....	184

LIST OF FIGURES

Figure 1.1	The Central Dogma	2
Figure 1.2	Particle Tracking	6
Figure 1.3	Optics Triangle	7
Figure 2.1	Schematic of Alba Confocal Microscope	17
Figure 2.2	Schematic of a particle tracking experiment	18
Figure 2.3	Imaging Screenshot	21
Figure 2.4	Example Fluorescent Trace and Correlation Function	23
Figure 2.5	Example Lysosome Data	24
Figure 2.6	Lysosome Diffusion	25
Figure 3.1	3D Orbital Tracking Fluorescence Cross Correlation Spectroscopy	32
Figure 3.2	Glucocorticoid Receptor (Transcription Factor) Dwell Times	41
Figure 3.3	Model comparison of Transcription Factor Autocorrelation using a Bayesian Information Criterion (BIC)	42
Figure 3.4	RNA Dwell Times	45
Figure 3.5	Model comparison of RNA autocorrelation using a Bayesian Information Criterion (BIC)	46
Figure 3.6	Cross Correlation Analysis of TF-RNA	49
Figure 3.7	Efficiency measured by FCCS (using $G_x(0)/G_g(0)$)	51
Figure 3.8	TF, RNA, and TF-RNA Number	52
Figure 3.9	3DOT-FCCS Negative Control	53

Figure 3.10	Consensus in live-cell binding measurements.....	54
Figure 3.11	Order-of-magnitude discrepancy between FRAP and 2P-FCS	56
Figure 3.12	Gillespie Simulation to Validate Microscopy Results	57
Figure 3.13	Supplemental Figure 1: Model comparison of Transcription Factor Autocorrelation using a Bayesian Information Criterion (BIC).....	61
Figure 3.14	Supplemental Figure 2: Model comparison of RNA Autocorrelation using a Bayesian Information Criterion (BIC).....	62
Figure 3.15	Supplemental Figure 3: Example fluorescence traces and carpet plots	63
Figure 3.16	Supplemental Figure 4: Example carpet plots, fluorescent traces, and resulting correlation functions	63
Figure 3.17	Supplemental Figure 5: Residual Graphs.....	64
Figure 3.18	Supplemental Figure 6: Example of cells post induction (Green Only) ...	64
Figure 3.19	Supplemental Figure 7: Example of induced cells	65
Figure 4.1	Core Genome Model Components.....	70
Figure 4.2	Modeling TAD length.....	72
Figure 4.3	Loop Size Simulation.....	73
Figure 4.4	The kinetic features of human transcription.....	75
Figure 4.5	Sequencing Features of Interest for MYH9	78
Figure 4.6	Sequencing Features of Interest for ERRFI1.....	79
Figure 4.7	Sequencing Features of Interest for RAB7A.....	79
Figure 4.8	Sequencing Features of Interest for RHOA	80
Figure 4.9	Sequencing Features of Interest for SLCA1.....	80
Figure 4.10	Sequencing Features of Interest for RPAP3.....	81
Figure 4.11	On Time Simulation.....	83
Figure 4.12	Example CTCF Traces Compared Across Cell Types.....	85

Figure 5.1	MCF10A Matrigel Time Course.....	88
Figure 5.2	Future Directions.....	90
Figure A.1	Methods of Fluorescently Labeling RNA.....	143
Figure A.2	CRISPR/Cas13 + RNA Mango Live-cell fluorescent RNA Labeling	147
Figure AII.1	Nuclear Structure.....	168

LIST OF ABBREVIATIONS

DNA	Deoxyribonucleic Acid
TSS	Transcription Start Site
TAD	Topologically-associated Domain
LAD	Lamin-associated Domain
3DOT	3D Orbital Tracking
FCCS	Fluorescence Cross Correlation Spectroscopy
3DOT-FCCS	3D Orbital Tracking Fluorescence Cross Correlation Spectroscopy
FRAP	Fluorescence Recovery After Photobleaching
MSD	Mean Squared Displacement
PALM	Photo-Activated Localization Microscopy
STORM	Stochastic Optical Reconstruction Microscopy
STED	Stimulated Emission Depletion Microscopy
NSOM	Near Field Scanning Optical Microscopy
FFT	Fast Fourier Transform
BIC	Bayesian Inference Criteria
GR	Glucocorticoid Receptor
MMTV	Mouse Mammary Tumor Virus Promoter
Cort	Corticosteroid
Dex	Dexamethasone

SARS	Severe Acute Respiratory Distress Syndrome
FCS	Fluorescence Correlation Spectroscopy
CSS	Charcoal-Stripped Serum
LFD	Laboratory for Fluorescence Dynamics
SPT	Single Particle Tracking
Chia-PET	Chromatin Interaction Analysis with Paired-End Tags
Chip-Seq	Chromatin Immunoprecipitation sequencing
Hi-C	High Resolution Chromatin Conformation Capture
LJ	Lennard-Jones
CV	Coefficient of Variation
FiSH	Fluorescence in-situ hybridization
GFP	Green fluorescent protein
lncRNA	long-noncoding RNA
SELEX	Systematic Evolution of Ligands by EXponential Enrichment
FRET	Förster Resonance Energy Transfer
IF	Immunofluorescence
JF	Janelia Fluor
Fabs	Fluorescent Antibody Fragments
LINC	Linker of Nucleoskeleton and Cytoskeleton
ONM	Outer Nuclear Membrane
PNS	Perinuclear Space
INM	Inner Nuclear Membrane

KASH	Klarsicht, ANC-1, and Syne Homology
MSC	Mesenchymal Stem Cell
ECM	Extracellular Matrix
BAF	barrier-to-autointegration factor
LIV	Low intensity vibration
Yap	Yes-associated-protein
AFM	Atomic Force Microscopy
LEM	LAP2 β , emerin, MAN1
NM-I	Nuclear Myosin-1
HRR	Homologous Recombination Repair
NHEJ	Nonhomologous end-Joining
NER	Nucleotide Excision Repair
LBR	Lamin Binding Receptor
FSS	Fluid Shear Stress
MEF	Mouse Embryonic Fibroblasts
CHO	Chinese Hamster Ovary
gRNA	Guide RNA
TIRF	Total Internal Reflection Fluorescence
HiLo	Highly Inclined and Laminated Optical Sheet

CHAPTER ONE: INTRODUCTION

Background

The Human Genome Project

By the middle of the 20th century great advancements had been made in science: atomic fission was harnessed for energy production; penicillin was discovered; and deoxyribonucleic acid (DNA) was identified as the “code of life”. With the identification of DNA as the biomolecule that stores the genomic information required for life, scientists sought out to decipher and sequence the human genome. The goal of this monstrous endeavor was twofold: record the entire nucleotide sequence; and construct a framework from the genetic code for the advancement of personalized medicine (Lander et al. 2001; Collins 1999; Collins, Morgan, and Patrinos 2003). By 2003 the human genome had been successfully sequenced and a framework for how the human genome functions was created. However, this achievement brought an explosion of data that indicated the inner workings of human genome and its expression were more complicated than previously thought.

Gene Expression & Central Dogma

Gene expression is largely governed by the central dogma of biology. The central dogma states that DNA is used to produce mRNA through a process known as transcription. This nascent RNA is then used as a template to produce protein through translation. While initially appearing to be a very straightforward process, there are many intricacies and biomolecules that play a critical role in these core biochemical processes

(Hager, McNally, and Misteli 2009). The general flow of information is known, as well as many of the players, but the dynamics of this intricate molecular dance are largely unknown within a living cell. Investigation into transcription of genes revealed that alternative splicing of transcribed genes mRNA and alternative transcription start sites (TSS) located inside genes bridges accounts for the large disparity of genes and proteins. While revealing the complicated nature of gene expression and building upon our understanding of the genome, alternative splicing and alternative TSS does not account for the regulation of the genome. DNA elements such as CTCF sites, Enhancers, Promoters, and Topologically Associated Domains (TADs) that were long thought to be of minimal importance have emerged as critical regulators of the kinetics of transcription.

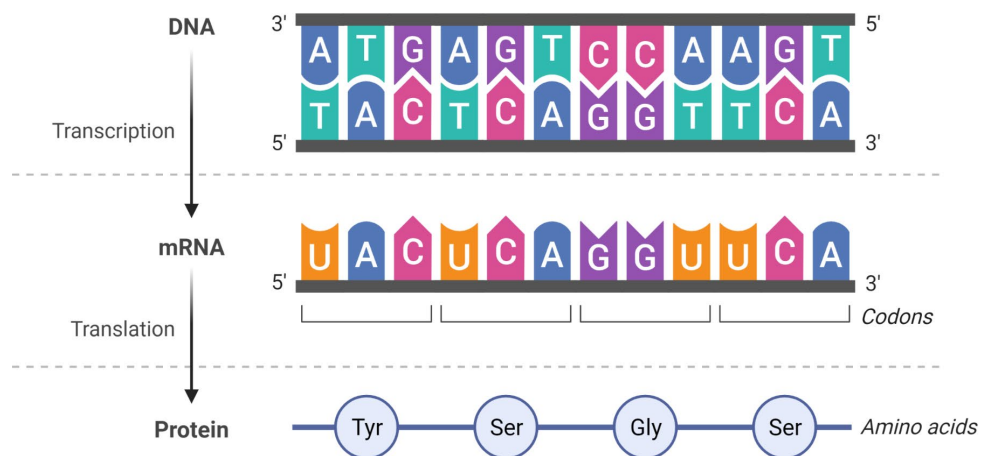


Figure 1.1 The Central Dogma

The core pillar of genetics is the central dogma which states that DNA is used as a template to produce RNA, which is used as a template to produce protein. The process of going from DNA to RNA is known as transcription. The process of going from RNA to protein is known as translation.

DNA Elements

CTCF binding sites are one of the regulators of genome structure and function. They are specific sequences within the genome where cohesin can bind and form a DNA loop (Rao et al. 2017; Sanborn et al. 2015; Rao et al. 2014) and often act as insulators for small discrete sections of the genome. They are largely conserved across cell types and organisms (Rao et al. 2014). In a 2017 paper by Rao et al., cohesin was degraded by auxin, leading to rapid large changes in contact maps, but “minimal” changes in genome wide gene expression (Rao et al. 2017).

Productive transcription also requires that the promoter for the gene of interest be accessible and within a nucleosome free region. Promoters are short nucleotide sequences located near the transcription start site. Eukaryotic promoters are usually around 100-1000 nt long and vary based on gene and the species of the organism. These promoter regions are where enhancers loop in and assist in forming the initiation complex (Robson, Ringel, and Mundlos 2019). Enhancers are also short DNA regions, ranging between 50–1500 bp. Protein activators (like p300) bind to enhancers to increase the chances that a particular gene will be transcribed (Pennacchio et al. 2013). Since enhancers are DNA elements that regulate other genes, they are known as cis-acting elements. Typically, they are located less than 1 Mbp on the same chromosome as the gene they are targeting (Maston, Evans, and Green 2006). They can be up or downstream of the target gene’s start site. Interestingly, recent evidence suggests that enhancers and promoters are one in the same. Enhancer or promoter sites have varying strengths, but they both promote transcription (Andersson and Sandelin 2020). Some are more targeted to be “super enhancers” or strong promoters, but many enhancers and promoters have the capacity to

act as both enhancers and promoters to some degree. The main difference is just whether they are acting on an adjacent gene or one more distantly located.

Epigenetics

Scientists and medical professionals observed instances where individuals inherited detrimental mutations but did not express the physiological trait of the mutation (Dupont, Armant, Brenner 2009). This observation led to the discovery of the field of epigenetics, the regulation of the genome through conformational changes of the genome's physical structure. DNA is tightly bound to histone proteins that create tightly packaged, organized histone-DNA structures (Klemm et al. 2019). Termed chromatin, this histone-DNA structure is the main building block of the highly packaged structure of chromosomes (Mondal et al. 2010). Research revealed that chromatin has two main conformations: heterochromatin and euchromatin. Heterochromatin is tightly packed, physically inhibiting gene transcription of enclosed genes by blocking binding of transcription complexes (Dame RT 2005). Contrastingly, euchromatin is marked by open conformations of DNA allowing for transcription complexes to bind to enclosed genes and proceed with gene expression (Dame RT 2005). Chromatin has specific histone modifications that correlate with heterochromatin and euchromatin, such as H3K27me3 indicating heterochromatin and H3K9ac for euchromatin (Jamieson et al. 2016). Discovery of heterochromatin and euchromatin expanded our understanding of the genome and built upon the framework of the genome, but unfortunately, these discoveries still did not fully explain the regulation of the genome. Recently, the 3D organization of the genome was discovered to also play a role in the epigenetic regulation of the genome. Studies utilizing chromosome interactions, such as Hi-C and 4C, revealed that

chromosomes interact with each other and with other nuclear structures. These nuclear interactions play a role in regulating gene expression (Lieberman-Aiden et al. 2009). Chromosome conformation studies discovered that chromosomes have interacting domains with other chromosomes called Topological-associated-domains (TADs) (Braccioli and de Wit 2019). Additionally, chromosome domains that associate with the nuclear envelope lamina proteins are termed (LADs) and are associated with increased heterochromatin, repressing gene expression (Guelen et al. 2008). While further revealing the intricacies of the genome and its regulation, these revelations into epigenetic regulation of the genome have failed to investigate one more important aspect of the genome: spatiotemporal regulation.

Light Microscopy

Light microscopy has emerged as an invaluable tool in the quest to unlock the inner workings of the genome. This mainstay technique offers both spatial and temporal resolution with relatively minimal perturbation to the sample as compared with many other biophysical techniques. Unlike biochemical techniques, which require the DNA or RNA to be extracted and purified, light microscopy, and often more specifically fluorescence microscopy, allows for the investigation of molecular interactions and biomolecular dynamics within a living cell. This in turn provides insights into their biological functions that were missing from the human genome project.

A further advance in the visualization of the genome through microscopy came in the form of single particle tracking which facilitated the shift from qualitative to quantitative measurements through imaging. Single particle tracking microscopy, a valuable tool in characterizing the genome, uses the same mathematical concepts that

early astronomers used to discover stars and planets in the night sky that were then translated into models of the universe (Figure 1.2). These studies provide information on the motion and behavior of single molecules like DNA, RNA, and protein.

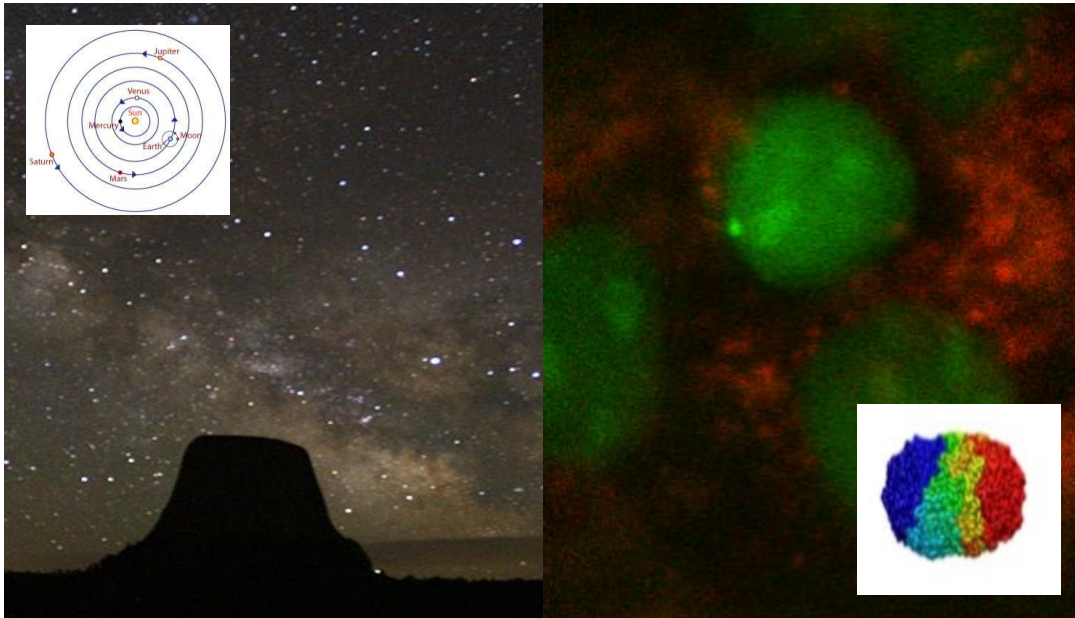


Figure 1.2 Particle Tracking

Early astronomers tracked bright points of light in the night sky and were able to create and perfect models of our solar system (left). Similarly, fluorescently labeled biomolecules can be tracked over time using live cell microscopy. This live cell tracking experiments can be used to begin building and perfecting models of the genome (right). Figure adapted from (“Night Sky Viewing” n.d.; Fankhauser n.d.; Sanborn et al. 2015)

Equation 1: $\Delta r = w / \sqrt{N}$

Equation 2: $N = \epsilon \Delta t$

There are two main functions important for single molecule imaging. Equation 1 shows that the spatial resolution (Δr) is determined by the point spread function width (w) divided by the square root of the number of photons collected (N). Equation 2 shows that the number of photons (N) is determined by molecular brightness (ϵ) with units of

Optical Challenges

The major challenge in studying the kinetics of the genome has been with optical technology. There are three main desirables with microscopy: speed, resolution, and signal-to-noise (Figure 1.3). Currently all three cannot be optimized in a single experiment, so microscopists are forced to choose based on the experiment. Resolution is necessary to differentiate between biomolecules located near each other, and as shown in the equations above is limited by the point spread function and number of photons collected per molecule. Speed is necessary to capture molecular dynamics on faster timescales. Signal-to-noise ratio needs to be high quality in order for the microscopist to be able to differentiate between background noise and a valuable signal.

3D orbital tracking seeks to build on the ideas of particle tracking while addressing the optical challenges at hand through the adjustment of the scanning pattern (Anzalone, Annibale, and Gratton 2014; Valeria Levi, Ruan, and Gratton 2005; V. Levi et al. 2005). 3D orbital tracking takes data at high speeds that have high spatial and temporal resolution as well as quality signal-to-noise ratio. Orbital tracking also provides faster sampling and longer measurements than traditional microscopy, while minimizing photobleaching. However, to achieve these attributes only a small volume can be scanned and measured. In essence by sacrificing the evaluation of the entire field of view for a smaller region of the image one can have all three of these optical desirables in real time, thus allowing for data collection in 3D + 1D. 3D orbital tracking (3DOT) can be enhanced through the synergistic application of fluorescent labeling with orbital tracking and fluorescence cross correlation spectroscopy (FCCS), providing the ability to study gene activation, splicing, and transcriptional bursting (Donovan et al. 2019; Stavreva et

al. 2019). Using these methods, we can begin to address the lingering questions of how the genome works and fundamentally what directs its behavior. The development of 3D orbital tracking fluorescence cross correlation spectroscopy will be discussed in depth in chapters 2 and 3.

Aims

The first aim of this dissertation is to develop a live cell, single molecule microscopy technique that can improve speed, resolution, and signal-to-noise ratio in such a way that transcription kinetics could be measured in a living cell. The live cell imaging will be followed up with in-silico validation. The goal of this work is to develop a suite of methods that would allow for the prediction of genome behavior and gene expression. Finally, future experiments will be proposed to further this method and move toward not only a live cell dynamics study, but an organ level biomolecular kinetics study. Additionally, further information on fluorescent labeling strategies for live cell single molecule imaging will be provided along with further applications of 3D orbital tracking.

Outline of Dissertation

Chapter 2 provides further information on the technique of 3D orbital tracking, highlighting its versatility in not only measuring transcription kinetics, but also the molecular dynamics of lysosomes.

Chapter 3 describes the development of 3D orbital tracking fluorescence cross correlation spectroscopy (3DOT-FCCS). It includes not only the methodology of this new technique, but also experiments performed with it that measure and characterize the differences between two glucocorticoid ligands, dexamethasone and corticosteroid. One

question asked was: Can the differences in dexamethasone and corticosteroid in transcriptional activation and RNA synthesis be measured within a living cell? The results of this study were then compared to previous Fluorescence Recovery After Photobleaching (FRAP) experiments and different in-silico models.

Chapter 4 highlights preliminary results from Molecular Dynamics simulations and bioinformatics

Chapter 5 proposes future 3DOT-FCCS live-cell experiments to study transcription dynamics in organoid models.

Appendix I includes further information on biomolecular labeling methods currently available for visualizing DNA, RNA, and protein for single-cell, live cell imaging.

Appendix II includes background information on biomolecules involved in nuclear structure and function. It then reviews how biomechanical processes affect the chromatin and nuclear structure. Finally, it explores state-of-the-art live-cell methods for measuring nuclear structure and mechanics with a particular emphasis on techniques that can be used to visualize DNA, RNA, and protein dynamics.

CHAPTER 2: NANO-RESOLUTION IN VIVO 3D ORBITAL TRACKING SYSTEM TO STUDY CELLULAR DYNAMICS AND BIO-MOLECULAR PROCESSES

Abstract

We present a microscopy technique, orbital particle tracking, in which the scanner scans orbits around species, unlike a raster imaging technique in which the scanner scans an area one line at a time. By analyzing the fluorescence emission intensity variation along an orbit, the location of a species in the orbit can be determined with precision of a tenth of a nanometer in a millisecond time scale, and the orbit can be moved to the new location of the species through a feedback loop if any movement is detected. This technique can be extended to two scanning orbits, one above and one below the sample plane to track the sample in 3D space. It can be used in vitro or in vivo to track a motion of a sample or to understand the dynamics of the sample. Additional detectors can help reveal the correlation between events with different emission spectrums. We have performed two different experiments with the system to show the capability of the technique. In the first example, we track a transcription site to understand the relationship between transcription factor - DNA binding and RNA transcription (Stavreva et al. 2019; Donovan et al. 2019). By labeling a transcription factor with Halo-JF646 and nascent RNA with PP7-GFP, we were able to cross correlate fluorescence intensity to discover temporal coordination between transcription factor DNA binding and resulting gene activation. In the second experiment, we tracked lysosomes in live cells to understand the nature of the transport whether it is an active

transport or a free diffusion (Valeria Levi and Gratton 2007). Trajectories of a total of 24 lysosomes are recorded during the experiment. The mean squared displacement (MSD) curves of the trajectories showed some clear differences between the behaviors of the lysosomes which were attributed to the active transport along microtubules as opposed to freely diffusing lysosomes.

Introduction

In the last two decades many novel super-resolution microscopy techniques have been developed to image cellular structures beyond the diffraction limit. Some examples of these techniques are photo-activated localization microscopy (PALM) (Betzig et al. 2006), stochastic optical reconstruction microscopy (STORM) (Rust, Bates, and Zhuang 2006; Zhuang 2009) [5-6], stimulated emission depletion (STED) (Hell and Wichmann 1994) microscopy, near field scanning optical microscopy (NSOM) (Synge 1932, 1928). The significance of these developments led to a Nobel Prize in 2014 where Betzig, Moerner, and Hell were awarded the Nobel Prize for their contribution to the development PALM of (Betzig and Moerner) and STED microscopy (Hell). Simultaneously, new techniques have been developed to study molecular dynamics of cellular structures (Moerner and Orrit 1999; Ha et al. 1996; Lu, Xun, and Xie 1998; Shashkova and Leake 2017). Although the molecular dynamics of individual structures were initially deduced from the studies based on bulk structures, recent technological improvements have provided new tools to understand the dynamics of an individual, single-molecule structure. Interests in biomolecular dynamics have been one of the major forces in developing super-resolution microscopy techniques, FLIM-FRET experiments, etc. Since structures drift or migrate over time, these techniques are time-

limited when studying structures while they travel through the observation volume, which in turn affects the precision of the study. Many solutions have been proposed to extend experiment/observation periods. Some examples are attaching the biological structures to the surface to avoid or minimize drift or trapping the molecules in a capsule (Kudalkar, Davis, and Asbury 2016; Leslie, Fields, and Cohen 2010; J.-Y. Kim, Kim, and Lee 2015; Cohen and Moerner 2008). These methods are very perturbative processes since the results of experiments might strongly depend on the environment.

Independently, many methods were developed to track structures. Most of them use cameras as a part of wide-field imaging systems to track molecules (Betzig et al. 2006; Rust, Bates, and Zhuang 2006; Zhuang 2009; Yildiz et al. 2003). Post-process computer algorithms analyze data to build the trajectories that the structure took. These methods provide limited information on 3D trajectories. The 3D information is based on images recorded by microscopes with a modified optical path. One way to modify the optical path is by using a cylindrical lens in the optical path (Kao and Verkman 1994). This results in astigmatism in the image which can be used to calculate the axial position of the structure. Another way is to obtain images from dual focal planes to determine the axial position of structures (Kao and Verkman 1994). In either case, the range in which the structure can be determined is limited to a couple of micrometers of the imaging plane.

Another group of methods uses a closed-loop feedback system to control the scanning system of a confocal microscope (Berg 1971; Lessard, Goodwin, and Werner 2007; Cang et al. 2006; Enderlein 2000; V. Levi et al. 2003; Kis-Petikova and Gratton 2004; Germann and Davis 2014; S. Hou, Lang, and Welsher 2017). These methods

position the confocal volume of the excitation beam on the molecule of interest and collect its emission signal. The feedback system calculates the molecule's position as it drifts and in the millisecond temporal range the confocal volume is repositioned back on the molecule's position by the feedback system. These techniques have a wider spatial range of observation field of view, i.e., they can track an object for tens of micrometers in all directions including axial direction.

Here we discuss one of the methods that uses a closed-loop feedback system. It is called 3D orbital tracking. It was first proposed by Enderlein in 2000 (Enderlein 2000) and was first implemented in 2003 by Gratton (Enderlein 2000; V. Levi et al. 2003). It is based on a laser scanning confocal microscope. The Galvo mirrors of the microscope are driven to move the excitation beam in a circular orbit around a structure of interest such that the radius of the orbit is comparable to the radius of the confocal volume. The intensity of the fluorescence emission along the orbit is analyzed with a Fast Fourier Transform (FFT) based algorithm. The modulation of the first harmonic helps the feedback system calculate the size of the drift and the phase of the first harmonic helps it calculate the direction of the drift. Based on the calculations, the position information is used to update the center of the new circular orbit in the XY plane. The frequency of the orbits is limited by the Galvo mirror response time and is on the order of 1kHz. Generally, multiple orbits are scanned before each feedback repositioning to reduce noise.

There are multiple ways to extend the technique to track particles in the axial direction (Berg 1971; Cang et al. 2006; Enderlein 2000; Annibale, Dvornikov, and Gratton 2015). Our technique is extended to 3D by scanning two sets of orbits, one set

of orbits scans above the structure and another one scans below the structure. A piezoelectric stage can be used to move the image plane relative to the sample to collect signals from two spatially separated orbits along the axial direction. The difference in the average intensity of the two orbits is used to localize the structure along the axial direction.

The response time of the piezoelectric stage is around 5ms and is the major limitation on this technique. Generally, the temporal resolution of this technique is around 32ms with a spatial resolution of 20nm in each direction. The structures with diffusivity up to 0.04 are successfully tracked with the 3D orbital tracking system.

This technique is very versatile as it can be implemented to various confocal microscopes even to a STED microscope (Lees and Gratton 2019). In addition, data can be collected with multiple channels to study many biomolecular dynamics independently along the orbit.

Here we present two different applications as a proof of concept (Stavreva et al. 2019; Donovan et al. 2019; Valeria Levi and Gratton 2007). In the first experiment, a locus site of a cell is tracked, and the characteristics of gene expression are studied over time in an Alba microscope. The main purpose of the experiment is to determine how the binding of a transcription factor correlates with transcription RNA at an active gene. In the second experiment, lysosomes in live cells are studied with an Alba STED microscope. The purpose of the experiment is to determine the type of transport whether it is an active transport or free diffusion of the lysosomes.

Materials and Methods

The System Schematic

Figure 2.1 shows the schematic of a generic ISS Alba confocal microscope (<http://www.iss.com/microscopy/instruments/albav5.html>). Generally, Alba can host GaAsP (H7422p, by Hamamatsu), hybrid PMTs (R10467, by Hamamatsu), or avalanche photodiodes (APDs by Excelitas). Each excitation and emission dichroic wheels (D1 and D2) can hold 5 dichroic. Similarly, each filter wheel (EMs) can hold 5 filters. In an Alba, the detection channels are supported by dedicated variable pinhole apertures. The excitation chamber hosts Galvo mirrors (Cambridge Technologies). They are used to scan a raster image or an orbit in the XY image plane. The image plane is shifted by a high-speed piezoelectric stage (Nano-F25HS by MadCity Labs, Madison, Wi) during experiments in the axial axis. A long working distance objective is needed to avoid any crash between the objective and stage. Both of the experiments are performed on a Nikon Ti-U inverted microscope with a CFI Plan Apochromat 60X 1.2 NA water immersion objective (Nikon Instruments Incorporated, Melville, NY). The Galvo mirrors and the piezo device are controlled by an IOtech 3000 Data Acquisition card (Measurement Computing Corporation, Norton, MA). The same card is used to collect signals from the detectors. Data acquisition is performed by the SimFCS software (Laboratory for Fluorescence Dynamics, University of California, Irvine). Based on the feedback from the SimFCS, the IOtech card repositions the stage and centers the Galvo mirrors to compensate for the movement of the sample. The ISS Alba can be coupled to commercial microscopes from Olympus, Nikon or Zeiss.

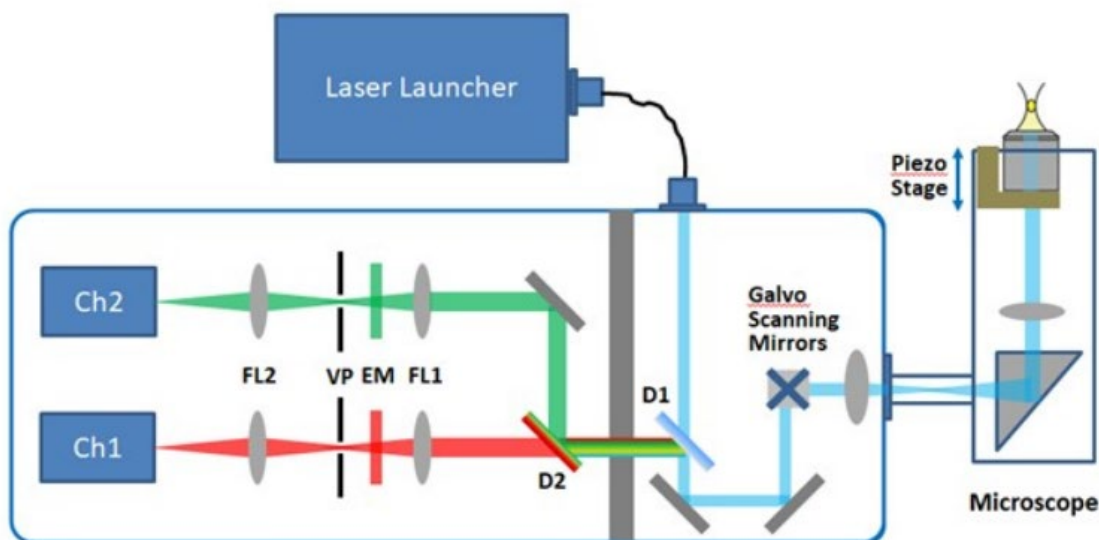


Figure 2.1 Schematic of Alba Confocal Microscope

For the gene expression experiments, the Alba confocal microscope was equipped with a 488nm laser and a 633nm laser. They were used in combination with a dual bandpass filter, zet488-640m (Chroma, Bellows Falls VT). The emission beam was split using a long-pass filter, et655lp (Chroma) and emission filters, ET700/75m (Chroma) and 525/50 (Semrock, Rochester NY). There were two SPCM-ARQH Avalanche Photodiode (Pacer, Palm Beach, FL) detectors with dark counts <100/s. Alba was coupled to a Nikon Ti-U inverted microscope with a CFI Plan Apochromat 60X 1.2 NA water immersion objective (Nikon Instruments Incorporated, Melville, NY).

Tracking Procedure

An experiment starts by locating a particle of interest in a raster image in the XY plane. After setting up the tracking parameters like orbit radius, pixel-time, pixel numbers along an orbit, number of orbits, and the axial distance between two imaging planes, the center of the initial orbit is defined by clicking on the particle in the image. Once the tracking procedure starts, the excitation beam is driven on a circular orbit around the particle. In a typical experiment, 4 or 8 orbital periods are used for each feedback calculation. The half set of orbits is traced in the upper image plane and the other half is traced in the lower image plane. Figure 2.2A illustrates the upper and lower

image plane orbits as well as a particle (black dot) and the point spread function of the excitation beam (blue oval volume). Figure 2.2B shows intensity profiles along the orbits. The blue curve shows the intensity profile during a feedback period from a simulation. In this example 4 orbits are scanned, two of them are in the first image plane and the other two are in the second image plane. As it is visible, the first two cycles have a higher intensity than the last two cycles have. This information is used to locate the axial position of the particle. The pink curve is the cumulative intensity profile for all the orbits. The shape of this profile is studied to extract location information of the particle on the XY image plane. The feedback algorithm analyzes the data on-fly to determine the coordinates of the particle and updates the scanner system to compensate for any particle movement.

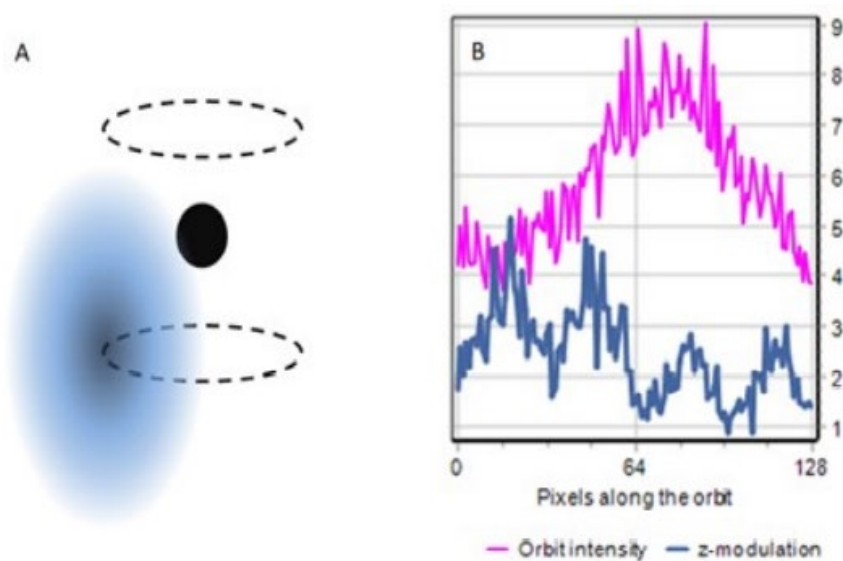


Figure 2.2 Schematic of a particle tracking experiment

A. The panel shows the position of the point spread function of a laser beam relative to a particle. The upper and lower orbits are represented with dashed lines. B. Intensity profiles along the orbit are shown here. The pink data is the cumulative intensity profile for all the orbits, and blue data shows the intensity profile for a feedback cycle. The system has scanned 4 orbits (2 up, 2 down orbits) for each feedback cycle in this example.

For the gene expression experiments, cells were labeled for 20 minutes with JF646 dye and grown or placed in 35mm dishes with #1.5 coverslips (Cellvis, Mountain View, CA). Cells were grown overnight in media and transcription was induced 10-20 minutes before imaging. Then they were placed inside a pre-warmed Okolab stage incubator maintained at a temperature of 37C, 5% CO₂ (mammalian cells) and 100% humidity or 30C and 100% humidity (*S. cerevisiae*). The cells were kept in the incubator until transcription sites appeared. Transcription sites usually appeared as diffraction-limited spots inside the nucleus of a cell within 4 hours after induction. When an active transcription site was identified the laser power was lowered to reduce photobleaching and orbital tracking was initiated.

Tracking of transcription sites was tracked with four orbits with a ~87nm radius. The first two orbits were scanned 145nm above the transcription site followed by another two orbits 145nm below it. Each orbit consisted of 64 points with a pixel dwell time of 1024 μ s per pixel. Each orbit lasts 65.5ms with a total sampling time of 262 ms or a 3.8 Hz sampling rate for each feedback loop. The orbital tracking system tracked the fluorescently labeled transcription factor molecules in the red channel and saved the signal from RNA in the green channel simultaneously.

In the second experiment, lysosomes in live HeLa cells are tracked. The cells are incubated with LysoTracker Deep Red (ThermoFisher) at 75nM for two hours and then washed. An Alba-STED microscope is used to track the lysosomes. In this case, for the 3D, the microscope objective is mounted on a tunable lens (Optotune) instead of the piezo-electric stage. This allows much faster movement in the Z-direction since there is no actual motion of the objective, simply its focal length is electrically modified, at the

cost of adding optics to the system and hence reducing the number of photons collected.

Lysosomes sites were tracked in multiple cells. Experiments lasted generally between 10 and 50 seconds. Orbital tracking feedback algorithm parameters were chosen for best performance considering the relative brightness of the images and the observed speed of the lysosomes. Tracking was updated every four orbits for best signal to noise ratio. We used 64 points per orbit and a dwell time of 64 μ s per point, yielding an orbit time just over 4ms and of radius 70 μ m. An image was taken before and after each tracking experiment to check for instances of tracking jumping between lysosomes in cases of high density in the field of view.

Results and Discussion

Gene Activation

When a sample is ready, it is imaged by repeated raster scans until the transcript site becomes active. Figure 2.3A and B shows two sample images where the transcript sites appeared as green dots in the RNA signal channel. Figure 2.3C shows an intensity profile along the orbit, the z and the intensity modulation. Figure 2.3D shows 3D-trajectory recorded during the experiment. Intensity profiles along the orbit can be studied in "carpet plot" during post data analysis. Figures 2.3E and 2.3F show examples of carpet plots. Carpet plots show fluorescence intensity along the orbit vs. time. The pattern that is shown in the RNA channel (Figure 2.3E) confirms that the system tracked the particle without any suspicious activity, like losing the site or jumping to another site. Simultaneously, the red channel records intensity signals from GR molecules. The carpet map of the red channel (Figure 2.3F) shows an intermittent signal in the red channel assumed to be binding of fluorescently labeled GR molecules.

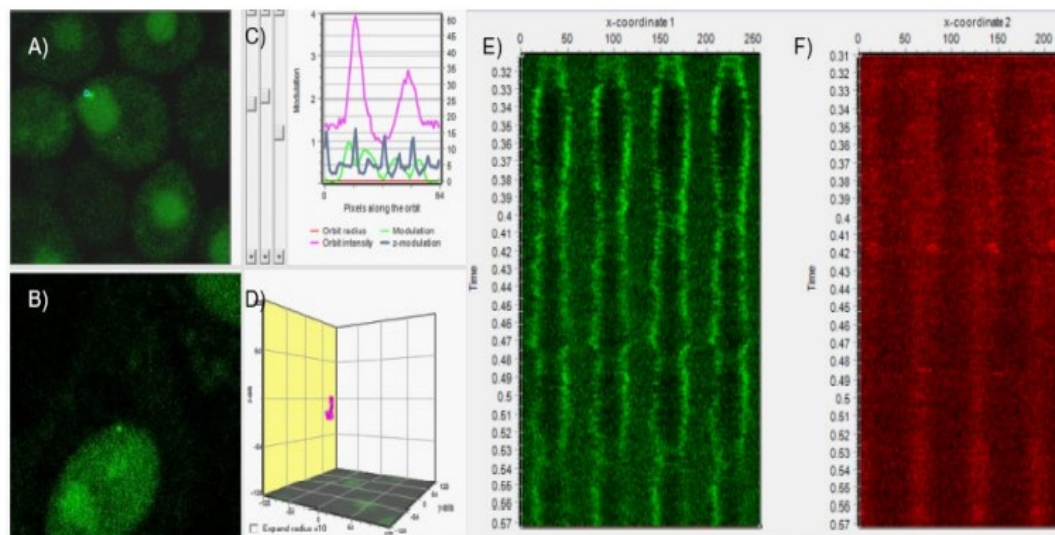


Figure 2.3 Imaging Screenshot

PP7 labeled transcription site screenshots in A. *S. cerevisiae* and B. Murine mammary epithelial cells. The nucleus of the cell is filled with GFP labeled PP7 coat protein. An active gene shows up as a diffraction-limited spot. C. Orbit intensity, modulation and z-modulation of orbital tracking. D. 3D trajectory of the transcription site during orbital tracking. E, F. Carpet plot of Green and Red signal during an orbital tracking experiment.

To test the correlation between the two channels, average intensity values along the orbit are calculated for both channels. Figure 2.4 shows such intensity profiles over time for Gal10 RNA and Gal4 fluorescence emission. The initial rise in the intensity profile is usually due to lock-in on the transcription site. Sections of the fluorescence intensity traces which appear to be higher than the background level in the carpet plots were selected for active transcriptions. Auto and cross correlation functions of the fluorescent signal were calculated in the standard way from the average fluorescence intensity traces. Early and late parts of the trace which included locking of the active feedback loop (~50 cycles) and initial strong photo-bleaching (~100 cycles) were excluded from analysis as were late parts of the traces of indefinite duration where the gene was no longer active (loss of green signal). Correlation functions were averaged

over 10-20 measurements. In order to estimate the average number of molecules at the transcription site, the background fluorescence level was needed and was assumed to be equal to the minimum of fluorescence intensity traces over an entire measurement as described in (Schwille et al. 1999). This resulted in very robust and reproducible correlation functions from which the dwell time of transcription factor molecules, RNA and temporal relationships could be estimated as described above. Figure 2.4 insert shows an example of the correlation function which is obtained from the intensity profile data.

Correlation functions were fit to models using the LMFIT package (Newville et al. 2016) in Python 2.7. For autocorrelation functions, a single component exponential or sinc function were used and for cross correlation functions, a shifted Gaussian was used. Model fits were evaluated using Bayesian Inference Criteria (BIC). The RNA autocorrelation was the best fit with a sinc function; transcription factor autocorrelation function was the best fit using a single exponential fit. The cross correlation of the two channels reveals the relationship between the activity on a Gal10 transcription site and the Gal4 binding process at the site. The intensity signals reveal that two events are correlated and the activity in the Gal4 channel lags the activity in the RNA Gal10 channel by 80 seconds.

Data analysis was performed using custom software written in IDL (Harris Geospatial Solutions, Broomfield CO) and Python 2.7 (Continuum Analytics, Austin, TX).

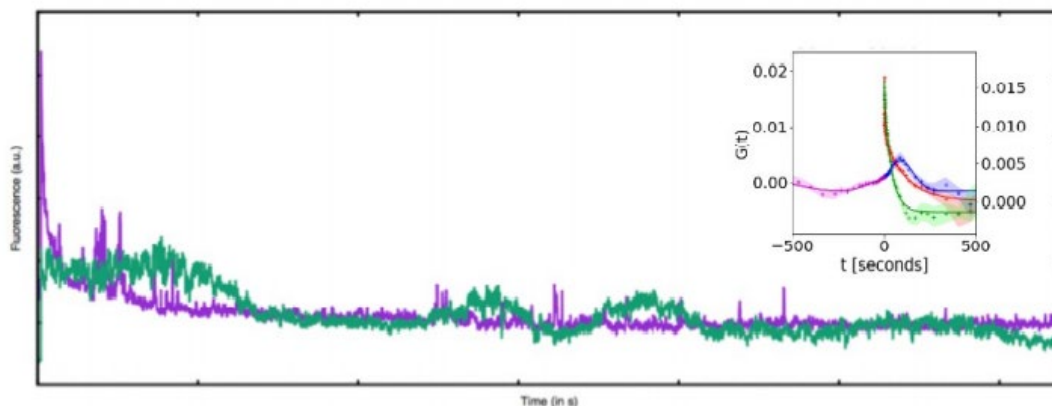


Figure 2.4 Example Fluorescent Trace and Correlation Function

Above is a characteristic trace of Gal4 and Gal10 RNA fluorescence intensity. (inset) Cumulative autocorrelation functions of Gal4 (red) and Gal10 RNA (green) as well as cross correlation showing 60s delay between Gal4 binding and transcription of Gal10 RNA.

Transport of Lysosomes

A total of 24 lysosomes were tracked in different cells. Each experiment lasted between 10s and 50s. Experimental parameters were adjusted for the best performance considering the brightness and the speed of the particle, and the noise in the signal.

Images of samples are recorded before and after the experiment to confirm the experimental success. Figure 2.5B shows a typical intensity vs. feedback cycle graph. At the beginning of each experiment, there is usually a mismatch between the center of the first few cycles and the particle, which manifests as a lower intensity value while the system locks on the particle, after which the intensity value rises once it is centered. As the experiment continues, the photo-bleaching results in decreasing intensity values.

Figure 2.5A shows a trajectory of a lysosome in 3D. Based on trajectories, mean squared displacement (MSD) curves are calculated excluding the initial milliseconds where the intensity is still rising since it corresponds to the locking-on. Figure 2.5C and 2.5D show two distinct cases of MSD curves. In each curve, the brown area represents the variance

of the MSD. The first part of the curves -initial 0.3s- is used to fit a straight line from which the 3D free diffusion MSD values are obtained (also called micro-diffusion). The cases in which the MSD curve tends to horizontal asymptote is attributed to confinements that limit the range a lysosome can travel in a free diffusion event; the cases in which the MSD curve increases with a trend above linearity is interpreted as case where the lysosome is attached to some molecular mechanism that is driving motion in a particular direction (Valeria Levi and Gratton 2007).

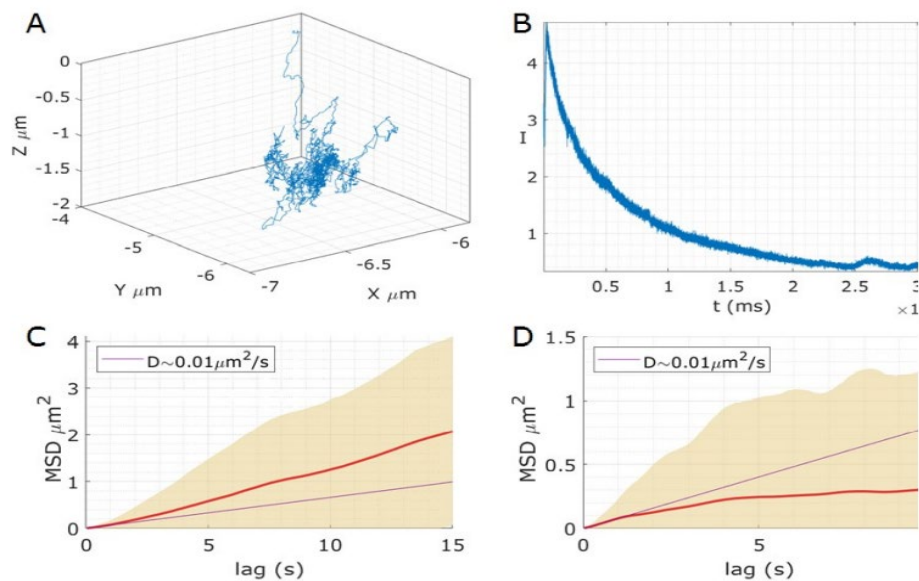


Figure 2.5 Example Lysosome Data

A. Example 3D trajectory of a lysosome. Initial drop in Z corresponds to the lock-in phase. B. Intensity profile during the tracking experiment. The decay in intensity is due to the photobleaching. C. MSD curve for a candidate of active transport. D. MSD curve for an example showing confinement.

Figure 2.6A shows all the MSD curves for all the 24 experiments together.

Figure 2.6B summarizes all MSD values altogether in a single graph and Figure 2.6C presents the same data in a histogram. The average value for the MSD is calculated as $0.096 \pm 0.004 \mu\text{m}^2/\text{s}$ for 20 experiments after excluding 4 outlier values. This result is

slightly above the reported value in the literature of $0.071\mu\text{m}^2/\text{s}$ (Bandyopadhyay et al. 2014). We consider the higher value as being due to the fact that the method we used to separate the outliers is somewhat arbitrary and/or an active transport process dominates the diffusion process.

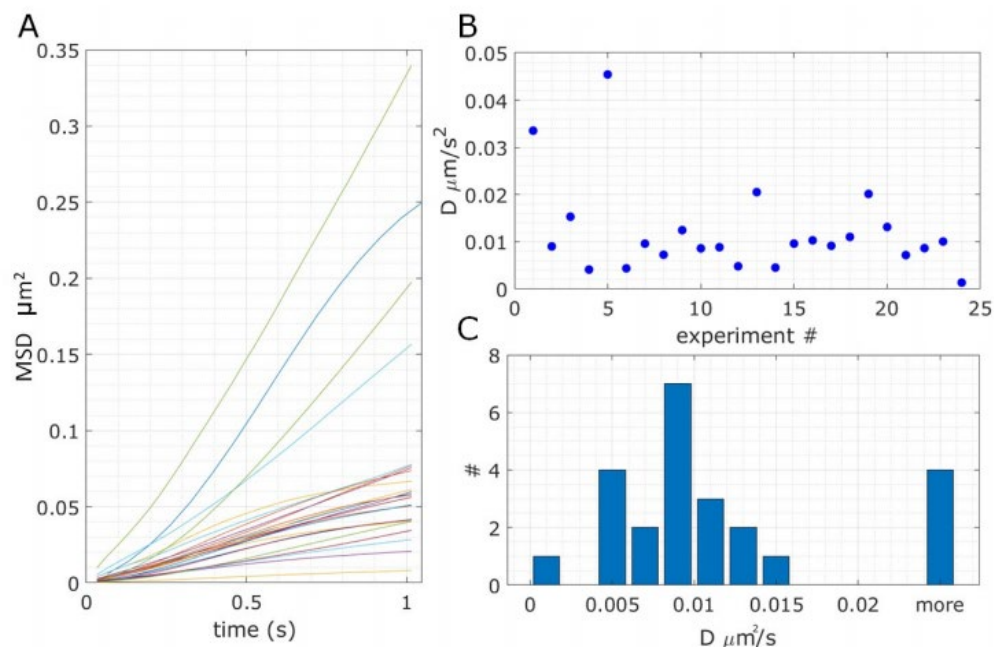


Figure 2.6 Lysosome Diffusion

A. MSD curves for the 24 experiments. B. Micro-diffusion values obtained for each of them shown as a series. C. Histogram of the series with a binning of 0.002.

Conclusion

In conclusion, we integrated the 3D orbital tracking to an ISS Alba system. We have tested the system with two applications. In the first experiment, we track lysosomes with diffusion of $0.1\mu\text{m}^2/\text{s}$ which would be very useful to study the motion of lysosomes and many other structures. In the second application, we have tracked an active transcription site. As we track the site, we have studied the activity of transcription in vivo which reveals a relationship, correlation, and timing between transcription factor

bindings and transcription at the site. Briefly, the 3D particle tracking system provides a unique tool to track a site or molecule and study molecular dynamics in vivo as a function of the location.

CHAPTER THREE: LIGAND DEPENDENCE OF REAL-TIME GENE ACTIVATION
BY THE NUCLEAR RECEPTOR GLUCOCORTICOID BY SINGLE MOLECULE
LIVE CELL 3D ORBITAL TRACKING FLUORESCENCE CROSS CORRELATION
SPECTROSCOPY

Abstract

In-vitro kinetic studies conducted on isolated components have provided valuable information on the timing and assembly of large molecular complexes, but they can be misleading or incomplete in the context of a living cell. Thus far this has been the best method of studying transcriptional kinetics due to a severe lack of reproducible in vitro experiments that could also be visualized in vivo. Therefore, we have developed 3D orbital tracking fluorescence cross correlation (3DOT-FCCS), a novel method, to visualize in real-time an active site of transcription in a living cell by fluorescently labeling within a mammalian cell and sampling at a high rate. This method allows for observation of single molecules and the determination of the temporal correlation between transcription factors and pre-mRNA.

In this article, we describe our novel methodology along with its advantages and disadvantages in detail and discuss applications and future directions of this approach. We believe that this methodology has a bright future to shed light on the molecular mechanisms involved in regulation of the genome as well as other areas of molecular and cellular biology such as translation, receptor mediated endocytosis, viral ingress and egress, and possibly neurological function. In order to illustrate the method and further

explore gene activation, we report results of experiments observing live cell glucocorticoid receptor (GR) activation of a Mouse Mammary Tumor Virus Promoter (MMTV) reporter gene by two ligands, the native ligand corticosteroid (Cort) and a synthetic one dexamethasone (Dex). Both of these have been used widely to treat inflammation (Barnes 2006) and more recently Severe Acute Respiratory Distress Syndrome (SARS) caused by the novel coronavirus SARS-nCov-2 (J.-W. Yang et al. 2020). Our results show that GR activated by Dex binds longer than Cort to our reporter gene but that it produces slower initiation rate and longer termination times of nascent mRNA and therefore less mRNA per cell perhaps resulting in weaker hormone response and poor clinical outcomes observed (Zoorob and Cender 1998).

Introduction

Gaining a deeper understanding of the genome and the interactions taking place on a molecular level in living cells is particularly difficult. But attaining a better knowledge of the temporal dynamics of stochastic biomolecular processes and interactions is critical for understanding gene regulation and the process of transcription that in turn controls cellular metabolism. Through 3D orbital tracking (3DOT), in combination with fluorescence cross correlation spectroscopy (FCCS), we can visualize the transcription process. This is done by observing the temporal relationships between pre-mRNA transcription at a MMTV promoter and the protein-DNA binding of the transcription factor glucocorticoid receptor (GR). This study establishes that we can effectively track these molecules of interest, fluorescently labeled pre-mRNA (labeled by PP7-GFP) and the transcription factor, GR (labelled by Halo-JF646) during the process of transcriptional activation (under induction by corticosteroid and dexamethasone). This

method allows for observation of a single molecule and the determination of the temporal correlation between GR binding to the DNA and the activation of mRNA synthesis. The data collected improves our knowledge of how eukaryotic organisms regulate transcription and sheds light on previously unknown details about transcriptional activation and temporal coordination. 3DOT-FCCS has the capacity to be expanded to the transcriptional processes of other genes, many of which could have weighty implications for our understanding of genome biology and human health and disease.

3D Orbital Tracking

3D orbital tracking was first described in a series of papers by Levi et al. (V. Levi et al. 2003; Valeria Levi, Ruan, and Gratton 2005; V. Levi et al. 2005; Anzalone, Annibale, and Gratton 2014). It modifies the traditional raster laser pattern that scans the sample line by line to a laser scanning pattern that is a series of circular orbits (Figure 3.1A). With this adapted scanning pattern, the fluorescent molecule of interest is excited indirectly when the laser passes around it. This results in a longer imaging window (V. Levi et al. 2003; Valeria Levi, Ruan, and Gratton 2005). Through the analysis of the fluorescence emission intensity fluctuations along an orbit, the precise location of a molecule of interest can be determined within 20 nm in the millisecond time scale (Valeria Levi, Ruan, and Gratton 2005) (Figure 3.1B). If any movement is detected, the orbit can be adjusted to the updated location of the molecule being tracked through a feedback loop. Two scanning orbits, one above and one below the sample plane, can be performed to expand the tracking into 3D space. It was first applied to transcription using a 200x array (Annibale and Gratton 2015), and more recently to acquire quantitative, single-cell, live data on transcription factor binding and elongation (Donovan et al. 2019;

Stavreva et al. 2019), as well as study lysosome active transport and free diffusion (Valeria Levi, Ruan, and Gratton 2005; Coskun et al. 2020).

Fluorescence Correlation Spectroscopy

Fluorescence Correlation Spectroscopy (FCS) analyzes the fluctuations in fluorescence intensity in a small observation volume to analyze molecular diffusion processes and binding or synthesis kinetics (Magde, Elson, and Webb, 1974).

Fluctuations in intensity can be indicative of multiple important processes, some of which include conformational changes, protein folding, rotational motion, changes in the number of molecules present, and diffusion. When fluctuations in intensity are due to changes in the number of molecules within the observation volume, the rate of motion, concentration of particles, and changes in a particle's inherent fluorescence can be determined (Figure 3.1C). Correlation functions are often used to extract information from the fluorescence signal. Correlation function analysis is conducted by separating the intensity time trace into a stationary average and a rapidly fluctuating term $F(t) = \langle F \rangle + \delta F(t)$. Autocorrelations are calculated using $G(\tau) = \langle \delta F(t) \cdot \delta F(t + \tau) \rangle / \langle F \rangle^2$ (Krieger et al. 2015) where $\langle \cdot \rangle$ denotes $\lim_{T \rightarrow \infty} 1/T \int_0^T dt$. Following the central limit theorem, the amplitude of the resulting autocorrelation curve is inversely proportional to the number of molecules present. The decay time of the autocorrelation curve is indicative of the typical dwell time of each molecule within the laser. The longer the curve the slower they are moving.

An extension of FCS is fluorescence cross correlation spectroscopy (FCCS) which allows for two color, two molecule analysis. Fluorescent signals from two different fluorophores are recorded simultaneously. In addition to being able to calculate the

autocorrelations of the two molecules, a cross correlation can be calculated as well. The cross correlation can be used to determine association between the two molecular species using $G_{rg}(\tau) = \frac{\langle \delta F_r(t) \times \delta F_g(t+\tau) \rangle}{\langle F_r(t) \rangle \langle F_g(t) \rangle}$. Much like the autocorrelation, the cross correlation reveals the number of molecular complexes and the rate at which they are moving. This can be valuable for determining not only molecular motion, but also associative binding.

Our method combines the well-established techniques of Two-Color Fluorescence Correlation Spectroscopy (FCCS) and 3D orbital tracking (3DOT) to track the kinetics of multiple biomolecules within a living cell in real-time. The 3DOT scanning pattern is employed to collect fluorescence fluctuations over time (Figure 3.1D). The collected fluorescence fluctuations are then analyzed using the FCS analysis techniques described above.

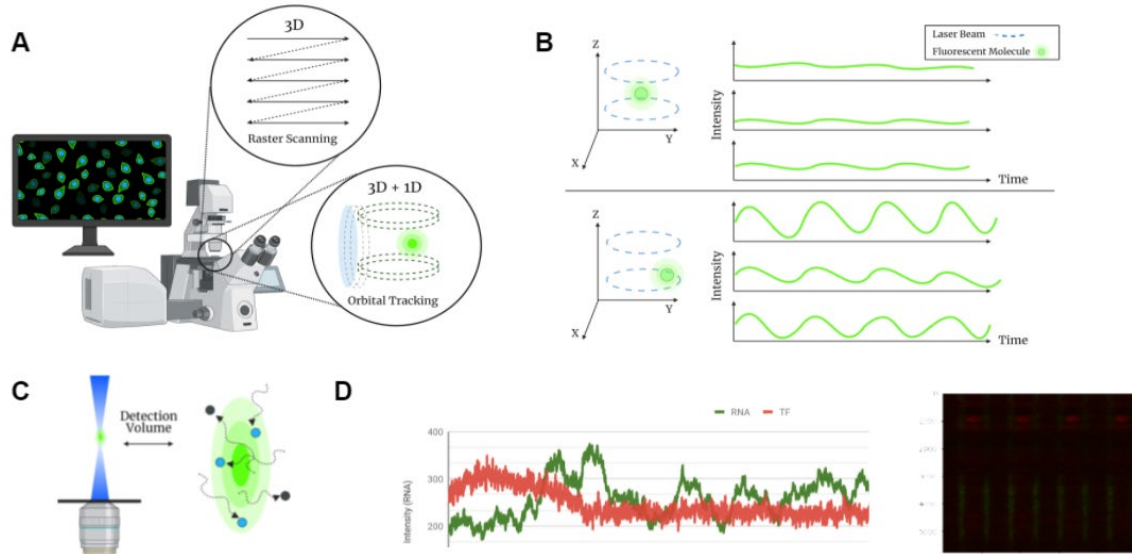


Figure 3.1 3D Orbital Tracking Fluorescence Cross Correlation Spectroscopy

A. Orbital tracking uses a laser scanning or confocal microscope with a modified scanning pattern. Instead of raster or line scanning, orbital tracking changes the laser pattern to a series of orbits above and below the point of interest. B. 3DOT-FCCS collects data as fluctuations in fluorescence over time. Based on how close the molecule of interest is to the orbit, how bright it is, and how fast it is moving determines the fluctuations in fluorescence over time. C. Live cell fluorescence cross correlation spectroscopy (FCCS) determines the kinetics of a fluorescent molecule based on how fast it is moving, brightness, and how long it is in the detection volume. D. During a 3DOT-FCCS experiment, measured fluorescence fluctuations over time are shown as a carpet plot, with each row being a series of orbits. These carpet plots can then be used to generate a fluorescence trace. The red fluorescent traces are the data on the TF and the green fluorescent traces are the data on the RNA. The red peaks first indicate that TF binding occurs prior to RNA transcription.

RNA Labeling

The MS2 RNA labeling strategy was first reported by Bertrand et al. (1998). By integrating a 24x repeat of a 20-mer sequence from the RNA genome of the MS2 bacteriophage into the *ASH1* gene of *Saccharomyces cerevisiae* and labeling the MS2-capsid protein with GFP, active transcription was visualized under a digital microscope for the first time. Later in 2008, a second bacteriophage, PP7 (Chao et al. 2008) was utilized with a tighter binding to visualize the *MDM1* gene (Larson et al. 2011) and

introns of the HBB gene (Martin et al. 2013). Finally, MS2 and PP7 were combined with two color imaging to visualize both coding and non-coding regions of the human HBB reporter gene and endogenous Gal locus (Coulon et al. 2014; Lenstra et al. 2015). While MS2 and PP7 allow fluorescent labelling of nascent transcripts in living cells, novel labelling methodologies such as dCas13 (L.-Z. Yang et al. 2019) and RNA Mango (Dolgosheina et al. 2014; Panchapakesan et al. 2017) are promising future directions for the labeling of endogenous transcripts and reducing the fluorescent background caused by nuclear localization of fluorescent capsid proteins.

While up to 98 hairpins and as low as 12 have been used, 24 repeats of the hairpin seem to provide the maximum brightness and photostability with the minimum negative effects. Care must be made to modify the sequence of each hairpin and linker to limit difficulty in cloning and silencing of the final construct. Early versions of the MS2 hairpin cassette contained a pseudo stop codon and could not be used in intergenic regions. PP7 capsid protein binds with a higher affinity than MS2, thus requiring a lower capsid protein expression level and allowing for a higher signal to background ratio for RNA and transcription sites. High levels of capsid protein aggregate in the nucleoli. This can make fluctuation analysis difficult near those locations in the nucleus. Therefore, the promoter for the capsid protein must be chosen carefully. The nuclear concentration must not be so high that it overwhelms fluorescence signals from the RNA and transcription site but not so low that the RNA hairpins cannot bind fluorescent labels (Ferguson and Larson 2013; Wu et al. 2014).

Glucocorticoid Receptor

Glucocorticoids, steroid hormones required for development and homeostasis, play a critical role in metabolism and disease. Glucocorticoid hormones act as an activation ligand to the glucocorticoid receptor (GR). GR is a ligand-regulated transcription factor. Glucocorticoid binding occurs cytosolically, inducing a conformational change in GR which activates a nuclear localization sequence, allowing for translocation to the nucleus (Taves et al. 2019). Nuclear GR is known to form homodimers and homotetramers which together bind specific DNA sequences to and act as specific transcription factors (Presman et al. 2017). It holds significant value to the pharmaceutical industry, as it is one of the mostly highly targeted proteins due to its potent anti-inflammatory functions. It is expressed in almost all tissues. There are two main glucocorticoid receptor ligands, Dex and Cort. Cort is the naturally occurring ligand and Dex is the synthetic derivative. Both ligands have been used to treat inflammation (Barnes 2006), and more recently have been explored as treatments for Severe Acute Respiratory Distress Syndrome (SARS) caused by the novel coronavirus SARS-nCov-2 (J.-W. Yang et al. 2020).

Methods

Plasmids and Cell Lines

The mouse mammary adenocarcinoma cells were routinely cultured in Dulbecco's modified Eagle's medium containing 4.5 g/L glucose, L-glutamine, and sodium pyruvate (Corning 10-013-CM; Corning, NY), 10% fetal bovine serum, and 1% penicillin-streptomycin, at 37°C in a humidified atmosphere of 5% CO₂. Cells were

cultured in the presence of 5 µg/mL tetracycline (Sigma–Aldrich) to prevent expression of a stably integrated GFP-GR.

The *MMTV*-PP7 reporter was generated using the PonA-CFP-SKL-24xPP7 construct which was previously described by Palangat and Larson (Palangat and Larson 2016). Since the D4B2D10 parental cell line (Walker, Htun, and Hager 1999) expresses GFP-GR and endogenous GR, both were disrupted using tetracycline and CRISPR-Cas9 technology respectively (Sander and Joung 2014). Additionally, these D4B2D10 cells were infected with a fluorescent coat protein lentiviral expression vector for the PP7 viral coat protein that binds the PP7 RNA hairpins (Palangat and Larson 2016). Puromycin selection and single cell subcloning was used to obtain a cell line with low expression of PCP-FGP, as well as 4 integrations of the *MMTV*-PP7.

GR-HALO was introduced into the genome of the D4B2D10 cells as described in (Stavreva et al. 2019). All cells were maintained in growth media supplemented with 10µg/ml tetracycline to prevent GFP-GR expression. Induction of HALO-GR was accomplished by changing the media to DMEM + Dextran charcoal-stripped serum (CSS) in the absence of tetracycline. This was done 24 hours prior to induction with Dex or Cort.

Microscope

Orbital tracking was performed on an ISS Alba FCS microscopy (Champaign, IL). Two excitation channels, 488 nm and 633 nm were used in combination with a dual band pass filter (Chroma, Bellows Falls VT). A long pass filter was used to split the emitted light. Photon counting was conducted with two SPCM-ARQH Avalanche

Photodiodes (Pacer, Palm Beach, FL). Dark counts were maintained $<300/s$. Data collection was conducted using SimFCS 3.0 software (Laboratory for Fluorescence Dynamics, University of California, Irvine). A 1MHz IOtech 3000 Data Acquisition card (Measurement Computing Corporation, Norton, MA) was used in conjunction with a Nano-F25HS high speed z piezo (Mad City Labs Incorporated, Madison, WI) and Nikon Ti-U inverted microscope with a CFI Plan Apochromat 60X 1.2 NA objective (Nikon Instruments Incorporated, Melville, NY). Proper microscope alignment was validated in xyz using 3D imaging of fluorescent beads. The estimated point spread function alignment of both channels is 60 nm. A 0.5-2x variable beam expander was placed in front of the 488nm laser to improve alignment in the z direction. When conducting FCCS using one photon excitation, proper alignment of both lasers is critical to obtaining accurate results (Schwille et al. 1999).

Orbital Tracking

Prior to live cell imaging, cells were transferred into 35mm dishes with #1.5 coverslips (Cellvis, Mountain View, CA) and allowed to grow in DMEM with 10% Charcoal Stripped FBS overnight. They were labeled for 20 minutes with JF646 dye (0.5 μ M) (Grimm et al. 2016) and induced with Dex or Cort (100nM) 10–20 minutes before imaging (Figure 3.18). Tetracycline was present in the media of the cells to suppress the expression of GFP-GR. Samples were placed inside a prewarmed Okolab stage incubator maintained at a temperature of 37°C, 5% CO₂ and 100% humidity. Samples were imaged on the microscope for 20min to 4h after induction. When a diffraction limited active transcription site was identified, the laser power was lowered and orbital tracking was initiated according to the available literature (Kis-Petikova and Gratton 2004; Annibale

and Gratton 2015; V. Levi et al. 2005; Valeria Levi, Ruan, and Gratton 2005; V. Levi et al. 2003). The excitation power of the lasers was reduced to a point where less than 25% of initial signal would be lost to photobleaching. Measurements generally lasted around 20 minutes per transcription site. Active transcription sites (Figure 3.19) were tracked using two laser orbits of radius $\sim 87\text{nm}$. One orbit was performed 145nm above the active transcription site and one was performed 145nm below the transcription site. Each orbit consists of 64 points with a pixel dwell time of $1024\mu\text{s}$ per pixel.

Software

3D orbital tracking was performed using Globals for Images: SimFCS v3 developed by Enrico Gratton of the Laboratory for Fluorescence Dynamics (LFD), University of California Irvine. Data analysis was performed using custom written software in IDL v5 and Python v2.7. Models were fit to data using LMFIT.

Data Analysis

Fluorescence intensity data collected appears in carpet plots of angle vs. time (Figure 3.1D). Sections of these fluorescence intensity traces were selected as active transcription events based on the appearance of a strong signal above the background. The standard method of calculating temporal correlation function from the fluorescent DC signal was performed by taking half the average photon intensity over the 4-orbital period (Kis-Petikova and Gratton 2004).

Data analysis was conducted using custom software written in Python. Temporal correlation analysis of the fluorescent signal was calculated from the DC component (Kis-Petikova and Gratton 2004). 10-20 measurements of correlation functions generated

from individual transcription sites were averaged to generate the average dwell times and number of molecules. Correlation functions were fit to six different models using the LMFIT package (Newville et al. 2016).

Multiple models were tested for each of the autocorrelations. These include single exponential, double exponential, triple exponential, and power law distribution for the TF red autocorrelation. Single exponential, double exponential, triple exponential, and sinc were evaluated for the RNA green autocorrelation. The five models tested were chosen based on models previously described for FCS data (Bacia and Schwille 2003; Höfling and Franosch 2013; Bacia, Kim, and Schwille 2006; Coskun et al. 2020). The single component exponential model is typically used to fit data in which the diffusion of the molecule of interest is faster than the integrations time (~ 1 ms) and the binding obeys a single off rate chemical kinetic equation (Michaleman Ribiero et al. 2009). The double and triple exponential models are often used to fit data in which the autocorrelation function has multiple characteristic decays. This is often indicative of multiple behaviors of the biomolecule of interest, such as specific and non-specific binding of a transcription factor (Michaleman-Ribiero et al. 2009). A power law model, or fractional Brownian motion model was also tested. In this model increments of Brownian motion are no longer independent. This model is often used to fit data in which the biomolecules are constrained within a particular region (Höfling and Franosch 2013; Garcia et al. 2021). This makes it an ideal model for transcription factor data. Sinc, similar the single exponential, is a model that fits to primarily one state, but unlike the single exponential, sinc is oscillatory (Coskun et al. 2020). This makes it a good model for transcriptional bursting in which multiple distinct bursts of RNA synthesis are observed. Each of these

models was tested on five separate transcription activation data sets (two experimental data sets were induced with corticosteroid and three were induced with dexamethasone).

The goodness of fit to the models was evaluated using Bayesian Inference Criteria (BIC) and Reduced chi-squared statistic. Both statistical tests consider the observed experimental variance and the expected, or theoretical variance. Reduced chi-squared analysis is the ratio of the experimental variance to the theoretical variance. The closer this value is to one, the more acceptable the variance. This model assumes that there are enough data points and that the proper number of parameters is being used (Taylor 1997). BIC calculates how well the data supports the hypothesis, or the proposed model. It is calculated using not only how well the data fits the proposed model, as in the case of Reduced chi-squared, but it also accounts correctly for how many parameters are being used to fit the data. In essence, any data set could in theory score perfectly against itself, therefore the more parameters used to fit the data, the higher the penalty. The more negative the BIC value is, the better the model fit. Therefore, BIC preferentially chooses the best fit with the simplest model (Gelman et al. 2013).

Results

Simultaneous measurement of the intensity of the HALO-tagged GR molecules and the GFP-tagged RNA at an individual TS were measured using 3DOT-FCCS for both Dex and Cort induced transcription (Figure 3.2A and Figure 3.4A). Representative traces of the experiments are shown in Figure 3.1D and Figure 3.12. The intensity profiles of the RNA (green) and GR (red) over time revealed red peaks representing binding of GR

molecules, followed by increased green signal, which corresponds to RNA transcription (Figure 3.1D).

Transcription Factor Dwell Times

GR molecules tagged with HALO and JF646 dye (Figure 3.2A; Table 3.1; Table 3.2) were imaged using 3DOT-FCCS. The measured fluctuations in fluorescence over time were used to perform autocorrelation analysis. This analysis yielded the number of molecules present and their binding rates based on the height and length of the curve respectively (Figure 3.2D). Autocorrelation analysis of the GR (red) data was conducted for two Cort data sets and three Dex data sets (Figure 3.2C). The dwell times of the transcription factor (TF) were shorter overall for Cort than for Dex (Figure 3.2B). Multiple models were tested on the TF autocorrelation data including single exponential, double exponential, triple exponential, and power law distribution. Bayesian Inference Criterion (BIC) analysis revealed that the best fit of the data is a two-component exponential fit (Figure 3.3 and Figure 3.13). This fit signifies a ~0.5 second nonspecific binding of the transcription factor to the DNA followed by a second longer specific binding to a Glucocorticoid Response Element in the promoter region of the reporter (Figure 3.3). Samples that show significant photobleaching often fit best to a three-component exponential model because they have a third photobleaching term that can often overwhelm meaningful data.

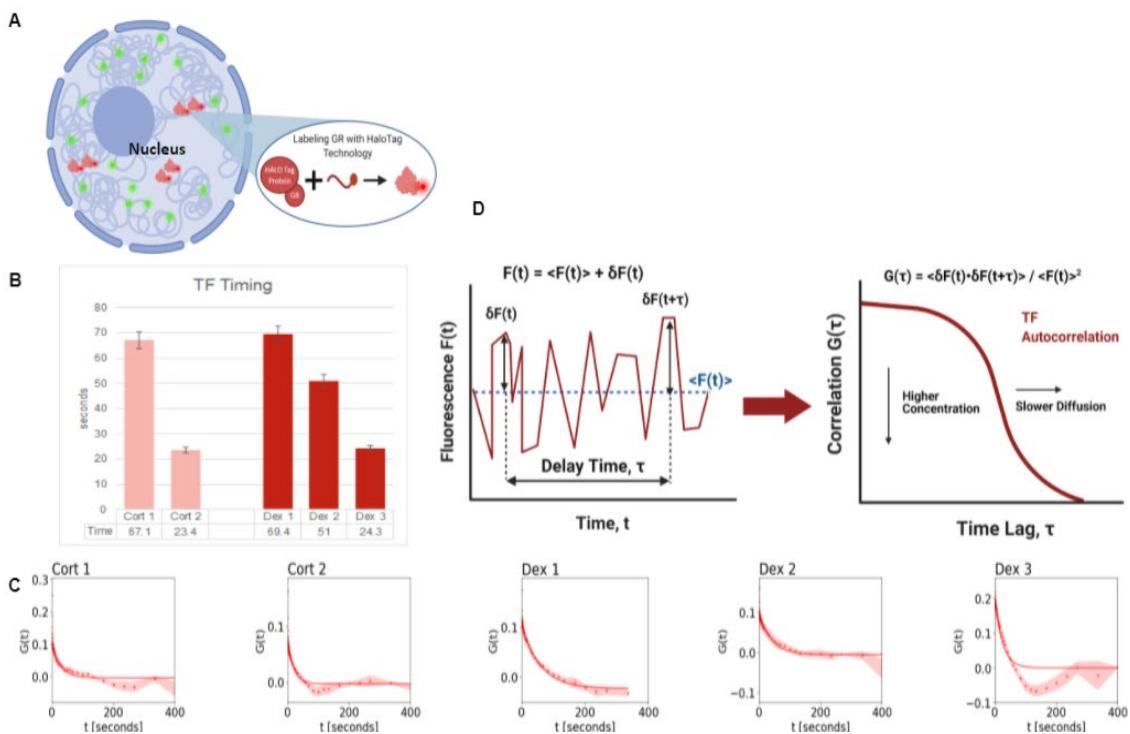


Figure 3.2 Glucocorticoid Receptor (Transcription Factor) Dwell Times

A. HaloTag Technology was used to label Glucocorticoid (GR). JF646 dye was added prior to imaging. B. GR dwell times were calculated using the autocorrelation function. Binding times were as follows: Cort 1 = 67.1 +/- 10.3s, Cort 2 = 23.3 +/- 1.69s, Dex 1 = 69.4 +/- 3.42s, Dex 2 = 50.9 +/- 4.40s, Dex 3 = 24.3s. C. The autocorrelation functions of GR binding compared across all five data sets. The double exponential analysis curves are shown here. Figure 3.13 shows the autocorrelation curves for all models tested. D. Autocorrelation functions can be used to calculate the number of molecules bound. This is found through the amplitude of the curve which is equal to 1/N. The rate at which the molecules are moving can be found through the length of the curve. The slower the molecules are diffusing, the longer the curve will be.

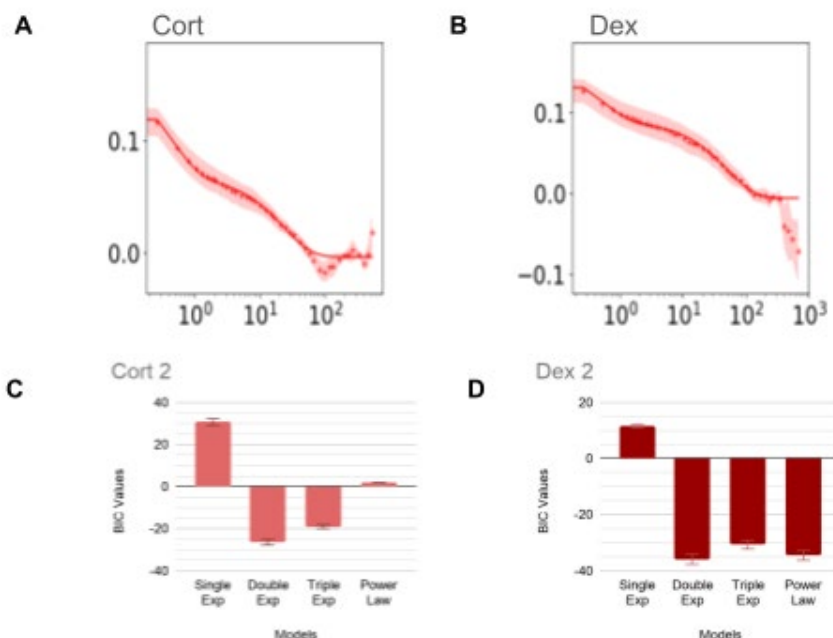


Figure 3.3 Model comparison of Transcription Factor Autocorrelation using a Bayesian Information Criterion (BIC)

A. Example corticosteroid autocorrelation data set analyzed with double exponential fit with an exponential time scale. B. Example dexamethasone autocorrelation trace analyzed with double exponential fit with an exponential time scale C. Reported BIC Values for example corticosteroid data set for models tested. The double exponential is most negative, and therefore the best model for this data. D. Reported BIC Values for example dexamethasone data set for models tested. The double exponential is most negative, and therefore the best model for this data.

The Tau, or time component for each dataset was calculated using the autocorrelation. This was performed for both the TF and the RNA autocorrelations (Table 3.1, 3.2, 3.3). Tau and Tau2, both time components for the double exponential model are reported in the below table. Additionally, A1 was calculate. $A1 = 1/N$, and therefore it can be used to determine the number of molecules present. Error was calculated for Tau, Tau2, and A1 and is also reported along with the Reduced chi-squared and BIC values. The error, Reduced chi-squared, and BIC are indicative of data quality and goodness of fit for the model.

Table 3.1 TF (Red) Autocorrelation Two-Component Fits

The below table compares the reported tau and A1 for the TF red autocorrelation. Tau and Tau2 are the two-timing components in the double exponential model. The first component is consistently around 0.5 seconds. This is thought to be indicative of TF non-specific binding. Tau2 varies more significantly but is typically between 20-70 seconds. This second component is longer and more variable because it corresponds to transcription. A1 is equal to $1/N$, with N being the number of molecules present. The Reduced chi-squared and BIC values are used to determine the goodness of fit for each data set.

Data Set	Tau (τ)	Tau2 (τ)	A1 ($1/N$)	Reduced chi-squared	BIC
Cort 1	1.1 +/- 0.21	67.1 +/- 10.3	0.149 +/- 0.0180	4.70e-01	-16.4
Cort 2	0.43 +/- 0.07	23.3 +/- 1.69	0.093 +/- 0.0083	3.79e-01	-26.4
Dex 1	0.67 +/- 0.12	69.4 +/- 3.42	0.068 +/- 0.0056	1.96e-01	-48.9
Dex 2	0.53 +/- 0.12	50.9 +/- 4.40	0.069 +/- 0.0069	3.09e-01	-35.8

Table 3.2 TF (Red) Autocorrelation Three-Component Fits

The below table compares the reported tau and A1 for the TF red autocorrelation. Tau, Tau2, and Tau3 are the timing components in the triple exponential model. The first component is consistently around 0.5 seconds. This is thought to be indicative of TF non-specific binding. Tau2 and Tau3 are longer and more variable because they correspond to transcription. A1 is equal to $1/N$, with N being the number of molecules present. The Reduced chi-squared and BIC values are used to determine the goodness of fit for each data set.

Data Set	Tau (τ)	Tau2 (τ)	Tau3 (τ)	A1 (1/N)	Reduced chi-squared	BIC
Cort 1	0.46 +/- 0.12	8.62 +/- 3.08	112.5 +/- 28.7	0.138 +/- 0.018	2.68e-01	-33.3
Cort 2	0.43 +/- 0.08	23.4 +/- 6014	23.3 +/- 1426	0.093 +/- 0.0091	4.02e-01	-19.1
Dex 1	0.061 +/- 0.0025	0.28 +/- 0.032	15.8 +/- 2.18	107.7 +/- 7.93	2.93e-02	-116.2
Dex 2	0.32 +/- 0.19	2.67 +/- 3.79	54.9 +/- 6.56	0.055 +/- 0.021	3.10e-01	-30.6

RNA Dwell Times

RNA molecules tagged with PP7 loops and GFP (Figure 3.4A; Table 3.3) were imaged using 3DOT-FCCS. The measured fluctuations in fluorescence over time were used to perform autocorrelation analysis. This analysis yields the number of molecules present and their diffusion rates based on the height and length of the curve respectively (Figure 3.4C). Autocorrelation analysis of the RNA (green) data was conducted for two

Cort data sets and three Dex data sets (Figure 3.4B, D). Multiple models including single exponential, double exponential, triple exponential, and sinc were evaluated for the RNA green autocorrelation. BIC analysis revealed that the best fit of the data is a two-component exponential fit. This fit signifies a 0.5 second nonspecific binding of GFP-CP to the PP7 loops followed by a second longer term that signifies RNA dwell time (Figure 3.5).

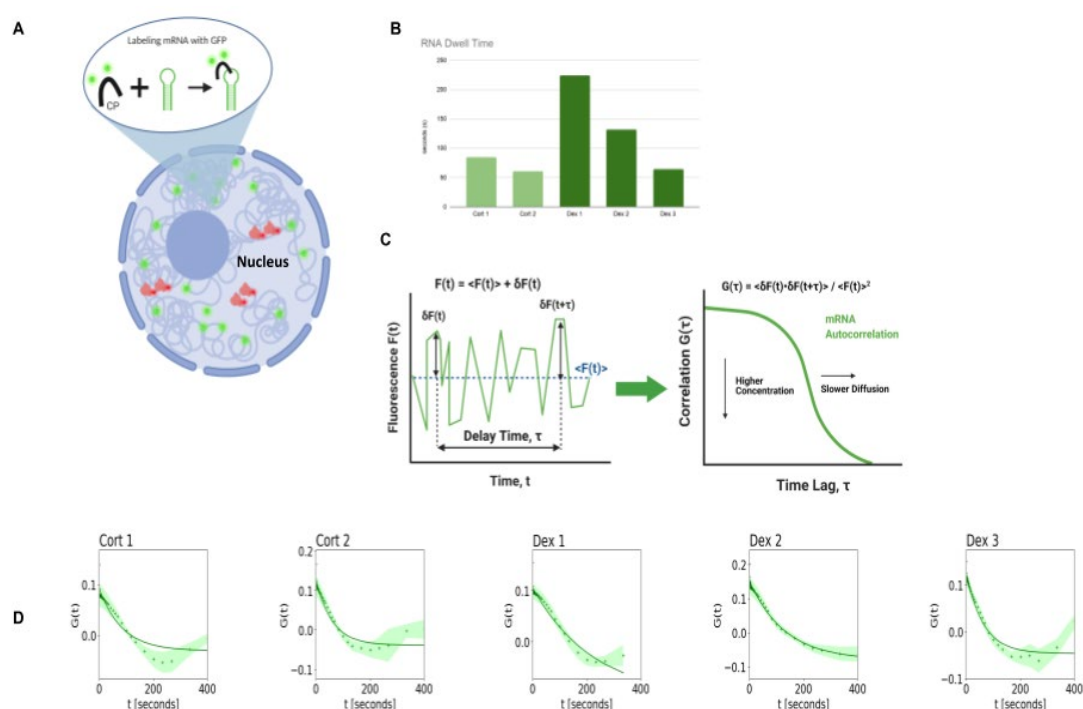


Figure 3.4 RNA Dwell Times

A. 24 PP7 stem loops tagged with GFP were used to label mRNA. B. RNA dwell times were calculated using the autocorrelation function. RNA dwell times are as follows: Cort 1 = 88.4 +/- 12.1s, Cort 2 = 62.6 +/- 7.9s, Dex 1 = 250.6 +/- 50.6s, Dex 2 = 137.1 +/- 5.4s, Dex 3 = 64.3s. C. The autocorrelation functions of RNA dwell time were compared across all five data sets. The double exponential analysis curves are shown here. Figure 3.14 shows the autocorrelation curves for all models tested. D. Autocorrelation functions can be used to calculate the number of molecules bound. This is found through the amplitude of the curve which is equal to $1/N$. The rate at which the molecules are moving can be found through the length of the curve. The slower the molecules are diffusing, the longer the curve will be.

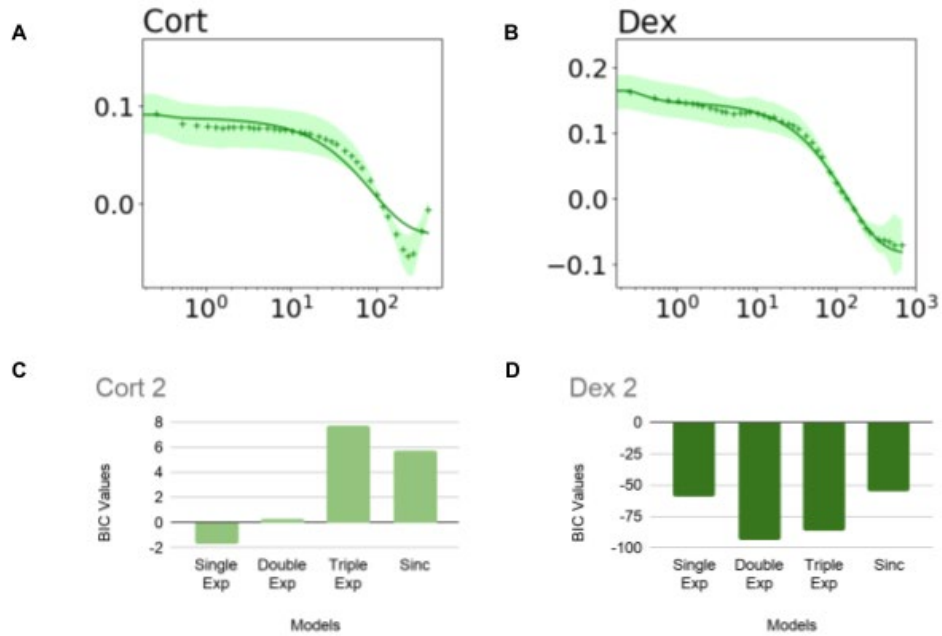


Figure 3.5 Model comparison of RNA autocorrelation using a Bayesian Information Criterion (BIC)

A. Example Corticosteroid autocorrelation data set analyzed with double exponential fit with an exponential time scale. B. Example dexamethasone autocorrelation trace analyzed with double exponential fit with an exponential time scale C. Reported BIC Values for example corticosteroid data set for models tested. The single exponential is most negative, and therefore the best model for this data. D. Reported BIC Values for example dexamethasone data set for models tested. The double exponential is most negative, and therefore the best model for this data.

Table 3.3 RNA (Green) Autocorrelation Fits

The below table compares the reported Tau and A1 for the RNA green autocorrelation. Tau and Tau2 are the two-timing components in the double exponential model. The first component is consistently less than 0.5 seconds. This is thought to be indicative of GFP-coat protein binding. Tau2 varies more significantly but is typically between 60 and 300 seconds. This second component is longer and more variable because it corresponds to transcription. A1 is equal to $1/N$, with N being the number of molecules present. The Reduced chi-squared and BIC values are used to determine the goodness of fit for each data set.

Data Set	Tau (τ)	Tau2 (τ)	A1 (1/N)	Reduced chi-squared	BIC
Cort 1	0.0948 +/- 0.192	88.4 +/- 12.1	0.0509 +/- 0.0160	7.27e-01	0.565
Cort 2	0.0971 +/- 0.258	62.6 +/- 7.9	0.0436 +/- 0.0193	7.29e-01	0.291
Dex 1	0.1186 +/- 0.079	250.6 +/- 50.6	0.0513 +/- 0.0087	3.63e-01	-25.6
Dex 2	0.2276 +/- 0.074	137.1 +/- 5.4	0.0544 +/- 0.0069	7.74e-02	-94.1

Cross Correlation Binding Time

The cross correlation, which considers proximity, or interactions between TF and RNA, was evaluated for both Dex and Cort data sets (Figure 3.6D). Figure 3.6A shows an example Dex and Cort correlation curve. Red is the autocorrelation of TF binding. Green is RNA autocorrelation of RNA dwell time. Blue is the positive correlation indicating TF binding followed by RNA synthesis. Pink is the negative correlation indicating RNA synthesis prior to TF binding. Figure 3.6B shows the comparison in

representative Cort and Dex correlation curves. The Dex curve has a significantly higher amplitude than the Cort curve indicating that there are less TF-RNA molecules present. The height of the cross correlation is inversely proportional for the number of molecules ($(\# \text{ of TF-RNA}) / (\# \text{ of Red Molecules} * \# \text{ of Green Molecules})$). Additionally, the Dex curve is also longer than the Cort curve, which is indicative of a slower diffusion. Cort was consistently nearly twice as fast as Dex. This is also further shown in Figure 3.6C which shows the cross correlation on a log scale. These curves can be used to find the timing of the TF-RNA interactions. Aside from the Dex3 dataset which suffers from photobleaching, the Cort sets are overall significantly faster than the Dex datasets (Table 3.4).

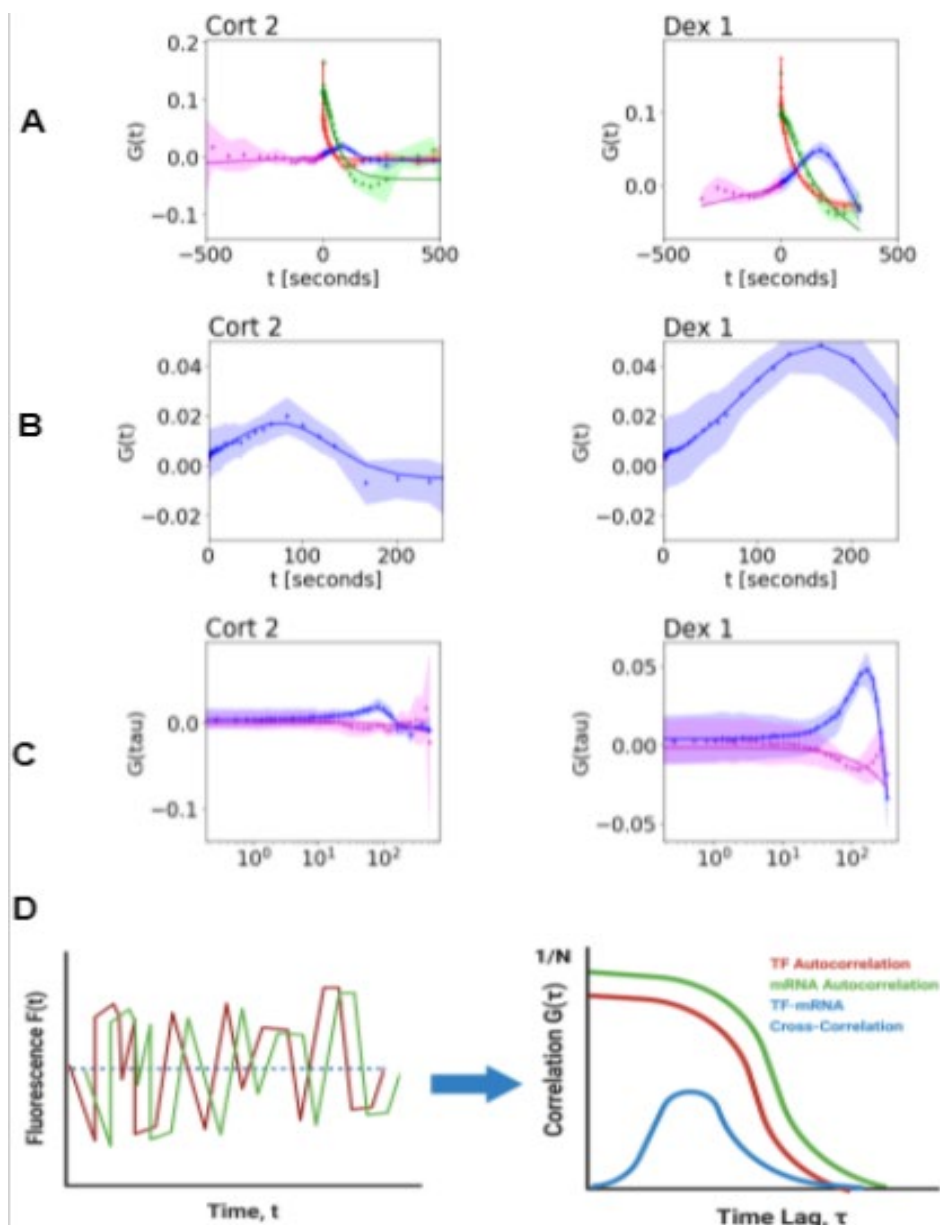


Figure 3.6 Cross Correlation Analysis of TF-RNA

A. Correlation Analysis (Red = TF autocorrelation, Green = RNA autocorrelation, Blue = RG cross correlation, Pink = GR cross correlation) B. The cross correlation functions of representative Dex and Cort datasets were compared. The Dex curve is visibly taller, which is indicative of less molecules (N). The length of the curve for Dex is also longer, which is indicative of a longer, slower timescale. This was shown with a linear timescale. C. The cross correlation functions of representative Dex and Cort datasets were compared on a logarithmic timescale D. Schematic of how fluorescent traces collected through orbital tracking can be used to calculate the cross correlation function. Fluorescent fluctuations over time are used to calculate the cross correlation with the following equation $G_{rg}(\tau) = \frac{\langle \delta F_r(t) \times \delta F_g(t+\tau) \rangle}{\langle F_r(t) \rangle \langle F_g(t) \rangle}$.

Table 3.4 TF-RNA Cross Correlation Fits

The below table compares the reported tau for the TF-RNA cross correlation. Tau is the timing of the TF binding and RNA synthesis. A1 is equal to $1/N$, with N being the number of TF-RNA or red-green molecules present. The Reduced chi-squared and BIC values are used to determine the goodness of fit for each data set.

Data Set	Tau (τ)	A1 ($1/N$)	Reduced chi-squared	BIC
Cort 1	67.2 +/- 3.24	0.0424 +/- 0.0011	1.87e-02	-142.1
Cort 2	52.2 +/- 5.27	0.0208 +/- 0.0018	6.12e-02	-101.2
Dex 1	99.5 +/- 2.10	0.0847 +/- 0.0022	2.99e-03	-207.9
Dex 2	64.4 +/- 8.16	0.0372 +/- 0.0035	2.15e-01	-51.1
Dex 3	189.3 +/- 73.84	0.3442 +/- 0.3436	1.52e-01	-60.4

Binding Efficiency

Not only can the number of TF, RNA, and TF-RNA molecules be measured from these experiments, but from these measurements the efficiency of TF binding can be determined. This is done by calculating the ratio of the cross correlation to autocorrelation amplitudes. This calculated value includes not only the efficiency of TF binding, but also the labeling efficiency of the HaloTag, which produces some errors in the estimates. Figure 3.7A-C shows the simulated and expected number of RNA and TF-RNA for varying levels of TF efficiency. Figure 3.7A shows a TF with a 15% efficiency, Figure 3.7B shows a TF with a 50% efficiency, and Figure 3.7C shows a TF with a 100% efficiency. The resulting number of TF-RNA for each simulation is shown in Figure 3.7D. These simulations collectively show that some nonproductive binding of TF is to be expected.

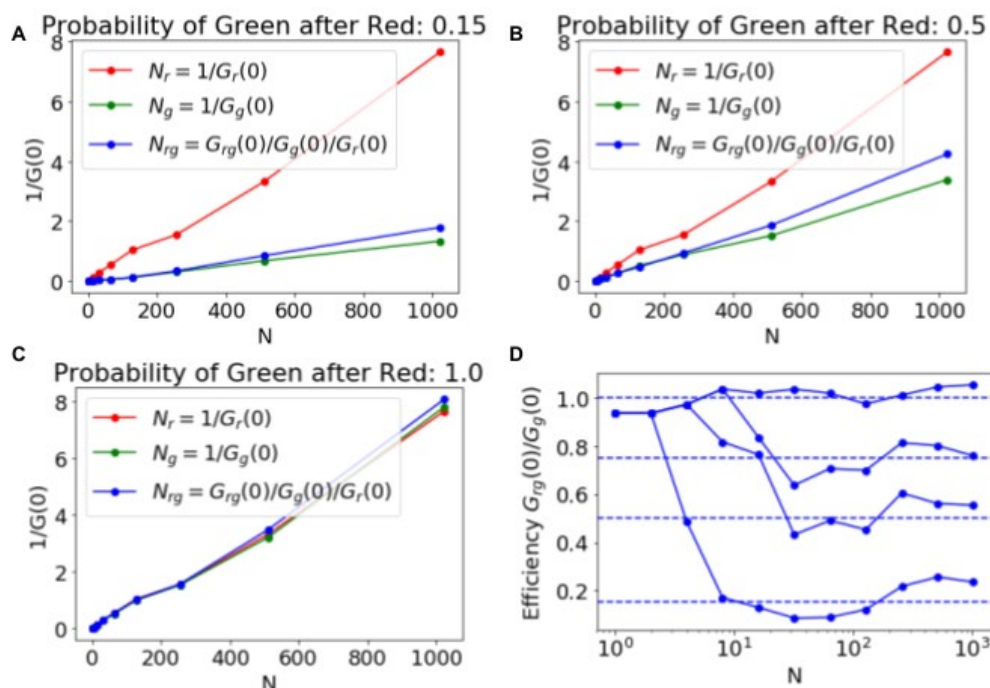


Figure 3.7 Efficiency measured by FCCS (using $G_x(0)/G_g(0)$)

A. Probability of Green after Red: 0.15 efficiency B. Probability of Green after Red: 0.5 efficiency C. Probability of Green after Red: 1.0 efficiency D. Efficiency $G_{rg}(0)/G_g(0)$

Molecule Number

The number of TF, RNA, and TF-RNA were calculated using the amplitudes of the auto and cross correlations. The number of TFs binding for Dex and Cort were all very similar. Cort datasets were calculated to be 3.6 and 6.1 TF binding. Dex datasets were calculated to be 4.7, 6.1, and 4.5 (Figure 3.8A). The number of TF binding is still suspect as HALO tagging can sometimes result in “dark” or unlabeled molecules. Figure 3.8B showed that there were consistently more RNA molecules being produced with the Cort ligand than with Dex. Excluding Dex 3, the number of TF-RNA were very similar between Cort and Dex (Figure 3.8C). It is likely that Dex 3 varies so drastically from the other samples because of significant photobleaching (Figure 3.13).

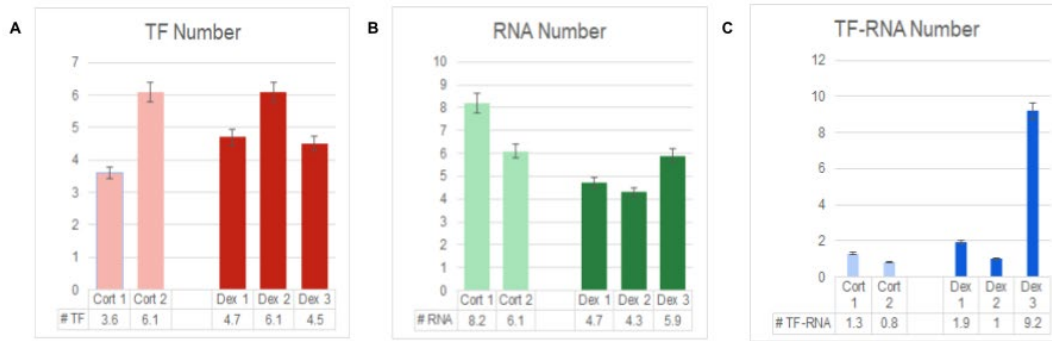


Figure 3.8 TF, RNA, and TF-RNA Number

The number of TF, RNA, and TF-RNA, for each of the five datasets, calculated using the auto and cross correlation amplitudes. The number of TF for each dataset were as follows: Cort 1 = 3.6, Cort 2 = 6.1, Dex 1 = 4.7, Dex 2 = 6.1, Dex 3 = 4.5. The number of RNA produced are as follows: Cort 1 = 8.2, Cort 2 = 6.1, Dex 1 = 4.7, Dex 2 = 4.3, Dex 3 = 5.9. The number of TF-RNA molecules are as follows: Cort 1 = 1.3, Cort 2 = 0.8, Dex 1 = 1.9, Dex 2 = 1.0, Dex 3 = 9.2.

Data Validation

Correlation and cross correlation analysis were validated using unlabeled GR samples as a negative control. Random spots in the nucleus were treated as transcription sites and tracked to validate the method. This data set was then analyzed and compared to the Dex and Cort data (Fig 3.9). This negative control showed that there was no cross-correlation when there is no active transcription site. Additionally, as a positive control cal bodies were tracked to show the validity of the method.

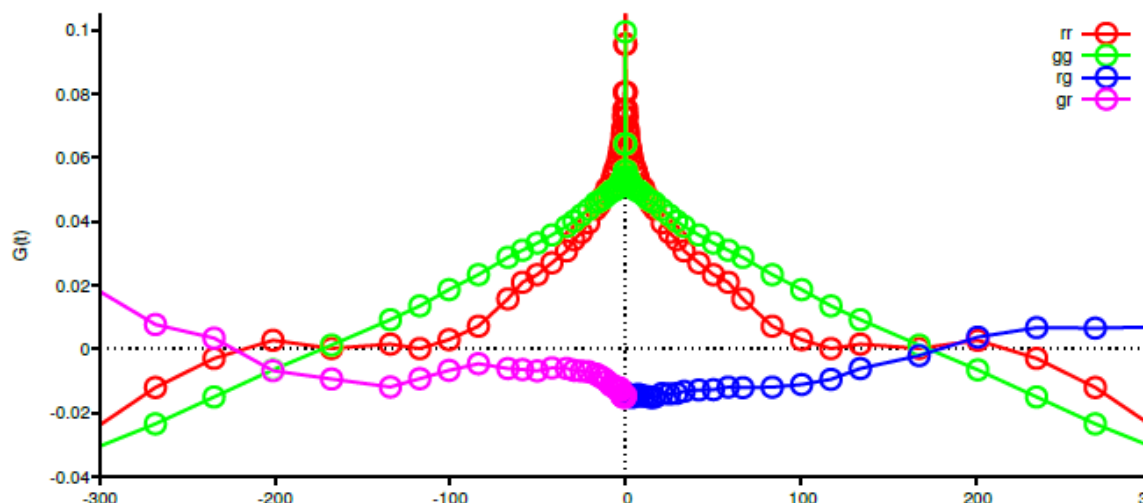


Figure 3.9 3DOT-FCCS Negative Control

Twelve separate sites in uninduced cells were tracked. This data was then used to calculate the auto and cross correlations. The data indicates that there is very little correlation in sites that are not actively transcribing. The red autocorrelation had a Reduced chi squared of 1.92 and a BIC of 34.9. The green autocorrelation had a Reduced chi squared of $8.65e-01$ and a BIC of 2.11. The cross correlation had a Reduced chi squared of $5.17e-02$ and a BIC of -108.2.

Over the last decade, since the advent of fluorescence techniques such as Fluorescence Recovery After Photobleaching (FRAP) (Sprague et al. 2004; Stavreva et al. 2004), Fluorescence Correlation Spectroscopy (FCS) (Michelman-Ribeiro et al. 2009; Stasevich et al. 2010) and Single Molecule Tracking (SMT) (Davide Mazza et al. 2012; Morisaki et al. 2014), measurements have been made to determine GR binding to a 200x array of Glucocorticoid Response Elements (GREs). These measurements have shown agreement with a residence time under Dexamethasone induction of 1-3 seconds (D. Mazza et al. 2013) (Figure 3.10). This disagrees quantitatively with the orbital tracking measurements reported here which show a residence time of 50-70 binding time. This begs the question: why the disagreement?

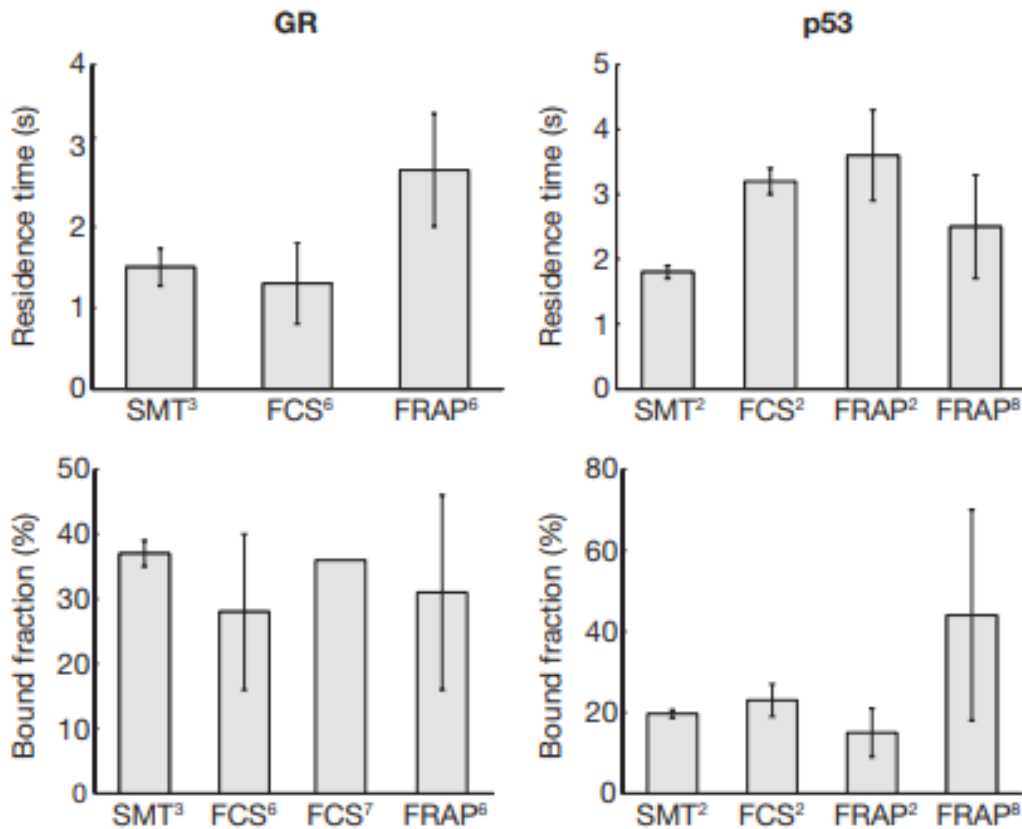


Figure 3.10 Consensus in live-cell binding measurements

Consistent estimates for transcription factor residence times and bound fractions on chromatin have now been obtained using three different techniques (SMT, FCS, and FRAP) in five different studies applied to two different transcription factors (GR and p53). Bars show published mean values with errors when available (GR, s.d. for FRAP, FCS, and SMT; p53, s.e.m. for FRAP and FCS and 95% confidence interval for SMT). (Figure adapted from Mazza et al. 2013).

There are several possible explanations for the differences in this measurement.

One major difference between the measurements described here and previous measurements is that most previous measurements were made on a 200x array of GRE's whereas the measurements reported here were taken on a single MMTV promoter. A second important difference between the 3DOT-FCCS measurement and SMT and FCS measurements is that previous measurements of this type were dominated by

photobleaching significantly more than the 3DOT-FCCS measurements. This is probably not the case with FRAP measurements (Figure 3.11). The data here shows similar trends to the measurements made with fluorescence recovery after photobleaching (FRAP) and reported in 2004 (Stavreva et al. 2004). In this paper they reported that transcription induced with corticosteroid was faster than transcription that was induced with dexamethasone. Additionally, their results indicated that Cort did not bind as tightly as Dex. While no exact numbers reported, they did show the same trend.

Why would a measurement on a 200x array of GREs give a shorter residence time than a single integrated promoter? Early work on GREs showed that a bound GR molecule must react with a specific GRE binding site to produce a bound GR molecule (Stavreva et al. 2004). It could be that the mobility of a bound GR molecule is higher in the presence of 200 GRE's than just one. In the future, computer simulations may be able to resolve this discrepancy. Currently only 3DOT-FCCS can measure GR-GRE binding at a single site.

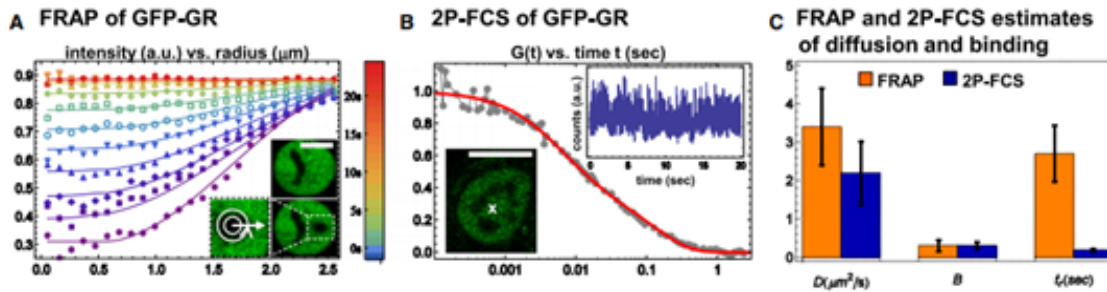


Figure 3.11 Order-of-magnitude discrepancy between FRAP and 2P-FCS

A. FRAP was performed in cells stably expressing GFP-GR. The bleach spot profile in postbleach frames was determined by radial averaging in concentric rings centered on the bleach spot (insert, white bar = 10 μm). Spatial profiles at select times are shown (color-coded according to the legend) along with a fit (solid lines) to a reaction-diffusion model that yielded a diffusion coefficient $D = 3.26 \mu\text{m}^2/\text{s}$, bound fraction $B = 0.39$, and binding residence time $t = 2.6\text{s}$. B. 2P-FCS was performed in the same cells as FRAP (lower insert, white bar 10 μm). Compared with FRAP, the expression of GFP-GR was reduced to enhance the relative size of fluctuations. Photon counts in the 2P excitation volume (white x) fluctuate about a constant mean throughout the measurement (upper insert, rebinned for illustration purposes), indicating no apparent photobleaching. The temporal autocorrelation $G(t)$ of these data (joined gray points) was averaged with that of analogous data to produce the displayed curve. A fit (solid red line) to the same reaction-diffusion model used for FRAP yielded $D = 2.46 \mu\text{m}^2/\text{s}$, $B = 0.30$, and $t = 0.16\text{s}$. C. A comparison between the FRAP and 2P-FCS estimate. Although estimates of B and t agree, estimates of t differ by $\sim 15\times$. (Figure adapted from Stasevich et al. 2010)

In addition to validating the findings with published literature, additional Gillespie simulations were performed to validate the live cell data (Figure 3.2-3.6). Gillespie simulations model stochastic processes. For this simulation we modeled Dex and Cort induced transcription using the binding times, dwell times, and molecule numbers that were measured using 3DOT-FCCS (Figure 3.12). Figure 3.12A-B shows the distribution of RNA expected for Dex and Cort respectively. Figure 3.12C-D shows the TF binding in pink and the resulting mRNA in green. These graphs appear very similar to the fluorescence fluctuation charts produced from the live cell data. The output of the simulation indicated that Cort and Dex would have similar numbers of TFs binding, but Cort would produce more RNA than Dex (Figure 3.12E-F). This was

consistent with the results of the live cell measurements. This in-silico work further underscores the validity of the measurements made by 3DOT-FCCS.

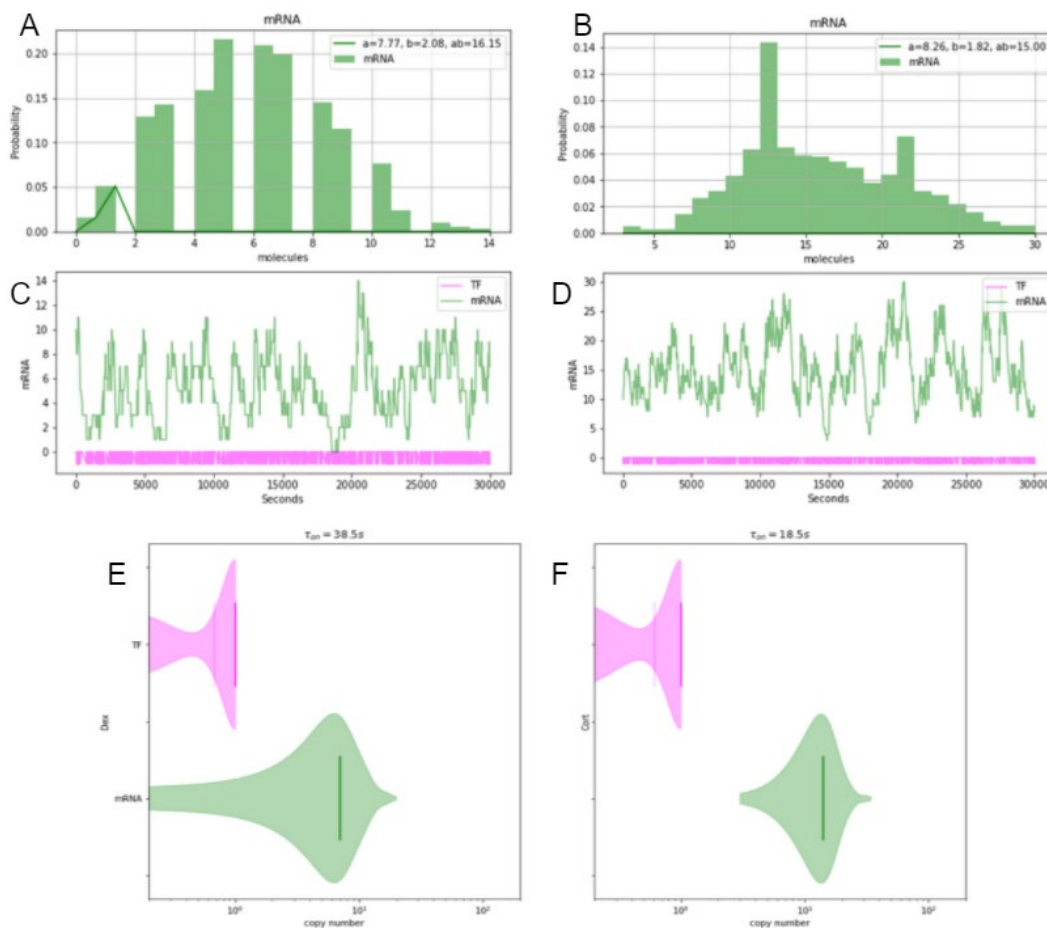


Figure 3.12 Gillespie Simulation to Validate Microscopy Results

The above panel shows the results of a Gillespie biochemical rate simulation. The number of transcription factor binding events, along with the binding times for dexamethasone and corticosteroid were used to determine the expected RNA copy number and RNA dwell time. A. RNA production distribution for dexamethasone. B. RNA production distribution for corticosteroid. C. mRNA production over time induced by dexamethasone. D. mRNA production over time induced by corticosteroid. E. Violin plots of expected transcription factor number and corresponding RNA copy number when induced with dexamethasone. F. Violin plots of expected transcription factor number and corresponding RNA copy number when induced with corticosteroid.

Future Directions

Here we have described the employment of 3DOT-FCCS for the study of transcriptional kinetics. Further work needs to be conducted to validate the accuracy of these kinetics measurements. While 3DOT-FCCS is consistent in the trends that it reveals, there is still a great deal of variation between identical samples. This method has a bright future if it continues to be optimized. Presumably, it could be employed for the study of other cellular processes such as splicing, chromatin reorganization, and RNA regulation.

Splicing

Splicing is the process of cutting out noncoding regions of RNA (introns) and joining together the coding regions (exons). Much like transcription, the kinetics of splicing are largely unknown. Moreover, most genome-wide measurements lack the time-resolution which would provide clues about the underlying biochemical mechanism. Measurements have been made with time lapse microscopy (Coulon et al. 2014), but 3DOT-FCCS measurements would provide more accurate results. Therefore, further exploration of the spliceosome and alternative splicing are necessary for our understanding of how the genome functions and how genes are regulated.

DNA Labeling

The data which was described here was taken using a two-color imaging scheme. While this clearly does work, it was not without challenges. DNA labeling would significantly improve the ability to track genes in the off state instead of just finding them when they are actively transcribing. This would improve the ease of data collection, as well as improve overall data quality. DNA labeling could likely be accomplished with

CRISPR/dCas9 labeling. Cas9 uses the CRISPR gene editing system for DNA labeling with a fluorescently labeled, nuclease dead Cas9 in combination with specifically engineered guide RNAs that bind to sets of fluorescent proteins (Ma et al. 2016). DNA labeling not only has the capacity to improve transcription kinetics data, but also open new possibilities for the study of chromatin dynamics and genome organization.

RNA Mango

RNA is the linchpin of the central dogma, and therefore the visualization of it is critical to understanding the inner workings of the genome. It has a wide range of functions including acting as the messenger of genetic information, silencing DNA, regulating RNA processing, and catalyzing translation. RNA Mango, and other RNA aptamers like it have recently been developed and promise to provide a virtually background-free method of live-cell RNA imaging made possible primarily through their fluorogenic properties upon ligand binding (Cawte, Unrau, and Rueda 2020). The use of RNA Mango in place of the MS2/PP7 system would improve signal-to-noise ratio, as well as open doors to the study of not only mRNA synthesis but also the study of many other regulatory RNAs.

Conclusion

Our analysis of Dex and Cort induced GR binding further highlights the differences between these two ligands. We find that dexamethasone typically induces transcription quicker than corticosteroids. However, corticosteroid produces more RNA. The novel technique of 3DOT-FCCS is applicable to a variety of biological questions, including the molecular dynamics of gene regulation. It allows for a fast-sampling rate without sacrificing signal-to-noise ratio or resolution.

Our results indicate that GR kinetics are ligand dependent. If, as our data suggest, corticosteroid has higher turnover and looser binding than dexamethasone, then it is likely that this could directly impact the clinical efficacy of glucocorticoid based treatments. Our data underscore the validity of 3DOT-FCCS and the importance of live-cell imaging for a characterization of transcriptional kinetics. While there is still work to be done in optimizing this technique, it is still a significant advance in measuring biochemical processes within a living cell.

Supplemental

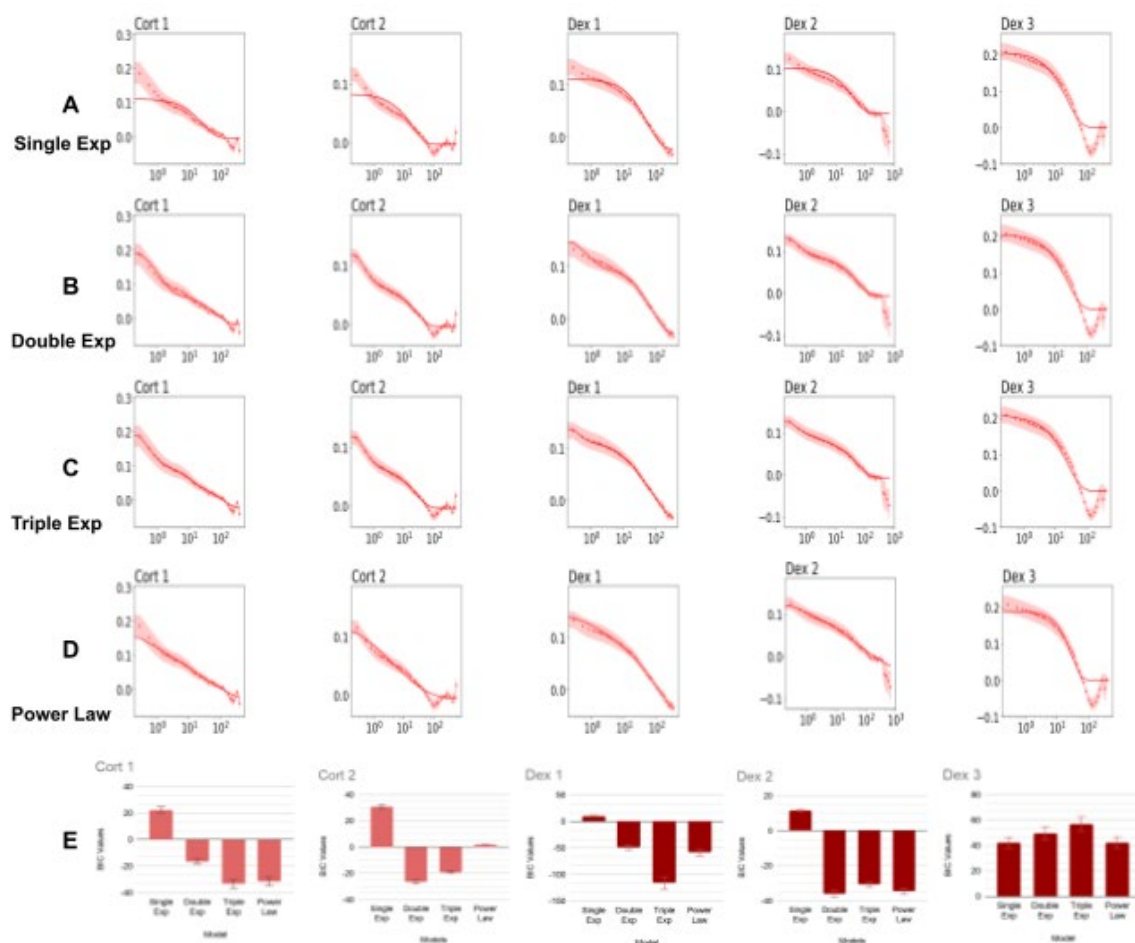


Figure 3.13 Supplemental Figure 1: Model comparison of Transcription Factor Autocorrelation using a Bayesian Information Criterion (BIC)

A. TF autocorrelation calculated with a single exponential fit and plotted on a logarithmic time scale. B. TF autocorrelation calculated with a double exponential fit and plotted on a logarithmic time scale. C. TF autocorrelation calculated with a triple exponential fit and plotted on a logarithmic time scale. D. TF autocorrelation calculated with a power law fit and plotted on a logarithmic time scale. E. BIC values calculated for each model and each data set. While some datasets might prefer different models, the double exponential performs well across all data sets.

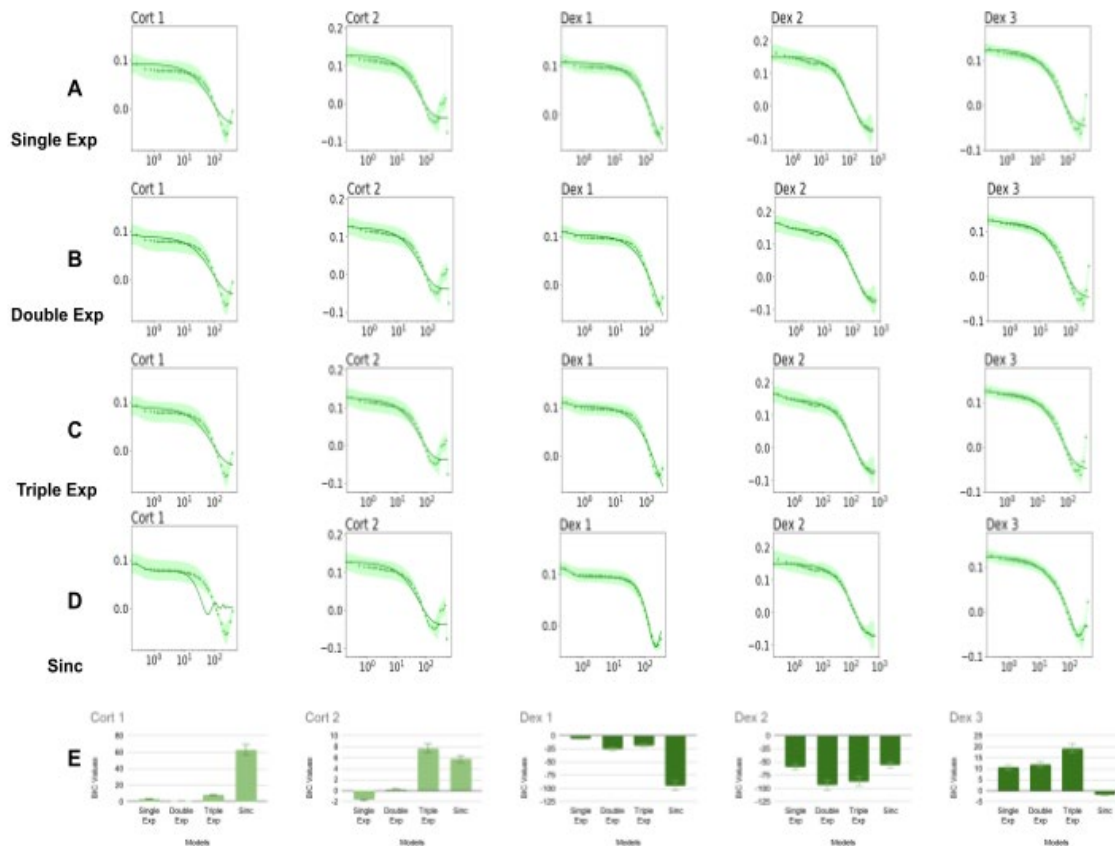


Figure 3.14 Supplemental Figure 2: Model comparison of RNA Autocorrelation using a Bayesian Information Criterion (BIC)

A. RNA autocorrelation calculated with a single exponential fit and plotted on a logarithmic time scale. B. RNA autocorrelation calculated with a double exponential fit and plotted on a logarithmic time scale. C. RNA autocorrelation calculated with a triple exponential fit and plotted on a logarithmic time scale. D. RNA autocorrelation calculated with a power law fit and plotted on a logarithmic time scale. E. BIC values calculated for each model and each data set. While some datasets might prefer different models, the double exponential performs well across all data sets.

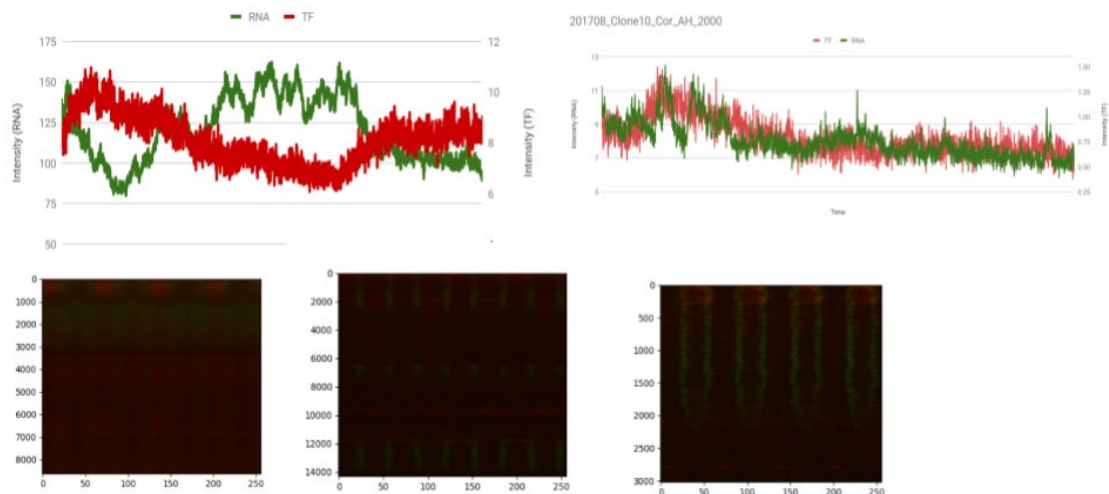


Figure 3.15 Supplemental Figure 3: Example fluorescence traces and carpet plots

Two example fluorescence traces and three carpet plots are shown. Both the traces and the carpet plots show that an increase in red fluorescence precedes an increase in green fluorescence. While this is expected, it does show that TF binding occurs prior to RNA synthesis.

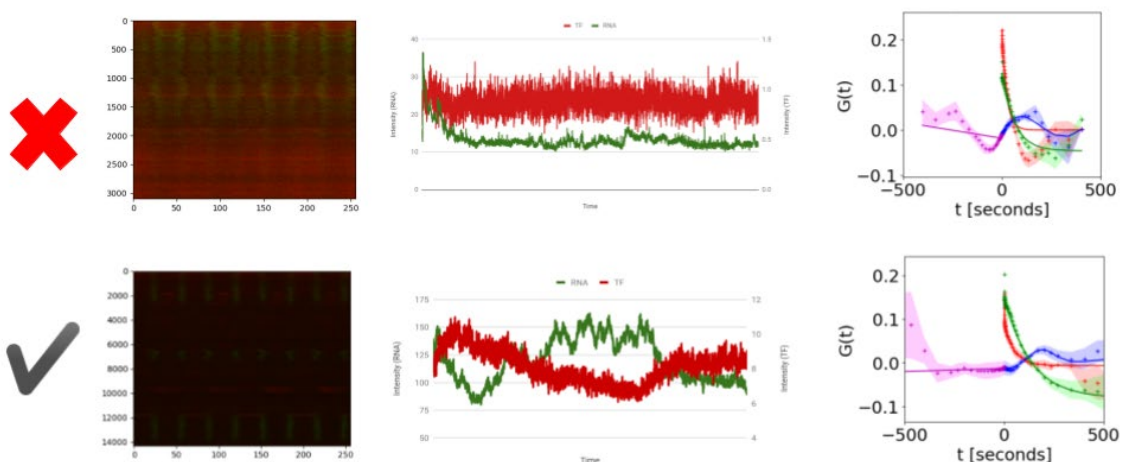


Figure 3.16 Supplemental Figure 4: Example carpet plots, fluorescent traces, and resulting correlation functions

Above are shown good and bad examples of 3D orbital tracking data. There is a delicate balance between having high enough laser power to provide ample signal and having too much, resulting in photobleaching and unusable data. The above carpet plot, trace and correlation function show what sort of data results when tracking is conducted with too high of laser power. The below example shows what a proper experimental carpet plot, trace, and correlation function should look like.

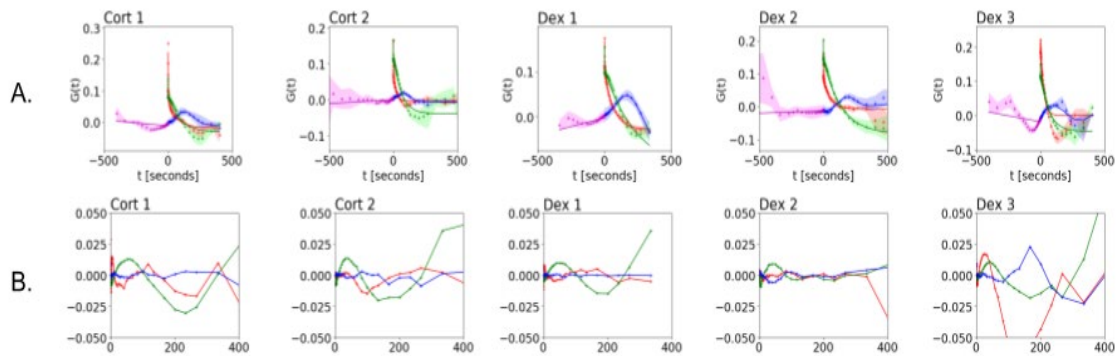


Figure 3.17 Supplemental Figure 5: Residual Graphs

A. Correlation functions for all five data sets. B. Residual graphs are shown for all five data sets. The closer the residual line curve is to zero the better the fit. This indicates that the double exponential fit for the red transcription factor autocorrelation is a valid one.

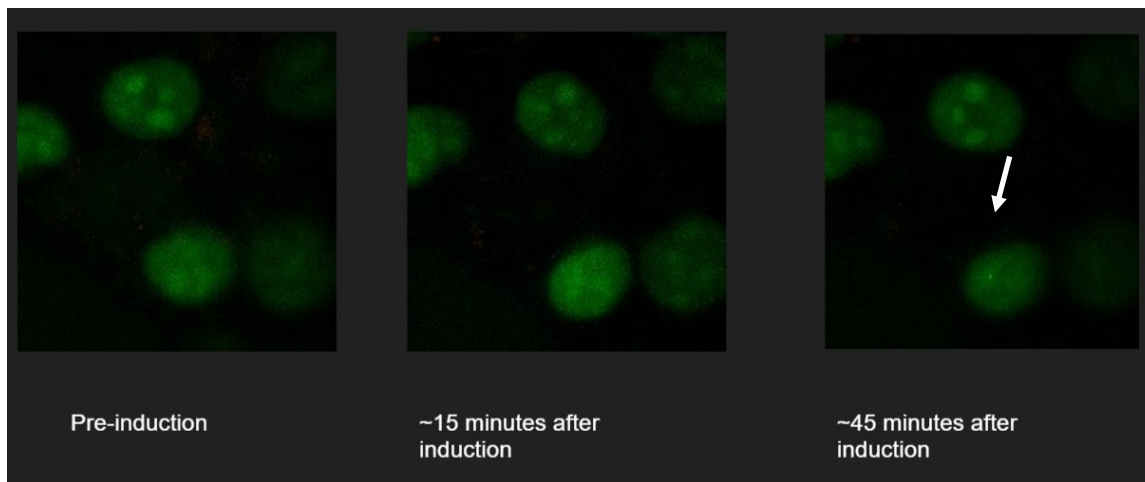


Figure 3.18 Supplemental Figure 6: Example of cells post induction (Green Only)

The above figure shows cells prior to induction, 15 minutes post-induction, and 45 minutes post-induction. The snapshot taken at 45 minutes post-induction shows an active transcription like that which would be tracked and quantified using 3DOT-FCCS. Cells were induced with Dex.

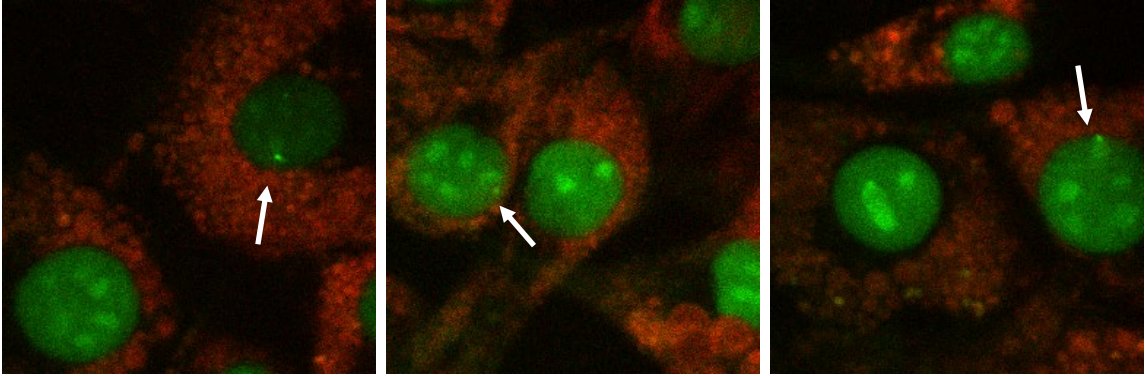


Figure 3.19 Supplemental Figure 7: Example of induced cells

Above is shown three representative images of active transcription sites. Cells were induced using Dex.

CHAPTER FOUR: PREDICTIVE MODELING OF THE LIVING GENOME

Abstract

Recent high-resolution contact mapping has made it possible to see the 3D organization of the nucleus on an unprecedented length scale (at 1kb resolution) (Rao et al. 2014; Sanborn et al. 2015; Rao et al. 2017). Since the average human gene is 12kb, this information is finally below a critical limit, and we are now able to understand the principles underlying epigenetic programming. One of the challenges of understanding the regulation of gene expression is developing tools and protocols that capture the complex spatiotemporal dynamics of these functions without compromising sampling rates, timescales, visibility of the sample, and all within a single living cell. The goal of our project is to develop a protocol for using 3D orbital tracking microscopy and in vivo RNA labeling to provide measurements of the cooperative binding of transcription factors and reprogramming of the human genome at a single active transcription site within a living cell. Using coarse grained modeling, GPU acceleration and Hi-C data, we intend to develop a dynamic model of the human genome to test an enhancer promoter looping model for transcriptional bursting and epigenetic regulation.

Biomolecular Sequencing

3D orbital tracking has significantly improved the quality of the live cell transcription kinetics data. This was the first step. Additional complementary biomolecular sequencing and computational techniques are needed to truly understand how the genome is behaving. Here several sequencing methods are highlighted including

chromatin interaction analysis with paired-end tags (Chia-PET), Chromatin Immunoprecipitation sequencing (ChIP-seq), and Chromosome Conformation Capture.

ChIA-PET, or chromatin interaction analysis with paired-end tags, is a technique that provides genome-wide sequencing information on chromatin-protein interactions. This high-resolution methodology gives base pair resolution (Lee et al. 2020). This method has been used independently to rediscover and validate known chromatin looping trends and CTCF sites (Phanstiel et al. 2015). Recently as a part of the ongoing Encyclopedia of DNA Elements (ENCODE) project, the cohesin-mediated chromatin loops and gene expression were analyzed for 24 human cell types. Housekeeping genes were found to have fewer contacts than dosage-sensitive genes which were more influenced by enhancer elements. Additionally, twenty eight percent of chromatin loops showed variation across cell types, though most variations were minimal (Grubert et al. 2020).

Chromatin Immunoprecipitation sequencing (ChIP-seq) has shed light on protein-chromatin interactions through the sequencing of DNA segments bound to proteins. To conduct ChIP-seq, chromatin within the nucleus is first isolated and fragmented, then antibodies against chromatin-associated proteins of interest are used to pull down these proteins and the DNA they are associated with. The DNA that these proteins were bound to is then sequenced, providing a clear picture of which genetic sequences are interacting with proteins. This technique has highlighted interactions between the nuclear lamina and chromatin termed Lamina-associated-domains (LAD) (Guelen et al. 2008), as well as unique epigenetic modification patterns (Wu et al. 2017; M. B. Meyer et al. 2016).

While ChIP-seq has been instrumental in determining protein-chromatin interactions, Chromosome Conformation Capture techniques, such as High-Resolution Chromatin Conformation Capture (Hi-C) and its predecessors (Dostie et al. 2006), have been invaluable in discovering patterns in chromatin-chromatin interactions. Hi-C has made it possible to see the 3D organization of the nucleus on an unprecedented length scale (at 1kb resolution) (Rao et al. 2014; Sanborn et al. 2015; Rao et al. 2017). Since the average human gene is 12kb, this information is finally below a critical limit, and we are now in a position to understand the principles underlying epigenetic programming. In Hi-C, DNA-DNA proximity ligations are performed, resulting in neighboring DNA being linearly ligated together for sequencing (Rao et al. 2017; Sanborn et al. 2015). From the resulting sequencing, contact matrices between chromosomes can be generated, providing information on chromatin interactions and 3D organization within the nucleus. This technique has recently shown that around 55 - 75% of loops mapped through Hi-C are conserved across cell type (Rao et al. 2014). One follow-up study in 2017 showed that while there is a distinct organization to the genome, TADs were largely conserved independent of CTCF binding. Additionally, this study also showed that overall gene expression in the short term was affected by genome structure, but not as significantly as previously proposed (Rao et al. 2017).

Molecular Dynamics Simulations

Computing technology is now at the point that molecular dynamics simulations can be used to understand the interplay between structure-to-function between macromolecules. Simulation times have been drastically reduced and are now approaching biologically relevant ones (Hospital et al. 2015). Coarse grained molecular

models have been used to study viral genome behavior (Indelicato, Cermelli, and Twarock 2019), viral capsid assembly (Fejer 2020), and chromatin folding (R. Zhou and Gao 2020). Much of the theoretical and mathematical groundwork has been laid through the study of the kinetics of polymer looping (Toan et al. 2008; Pastor, Zwanzig, and Szabo 1996), and now the task at hand is to apply them to the study of the human genome.

Using coarse grained modeling, GPU acceleration, and bioinformatics data, we intend to develop a dynamic model of the human genome to test an enhancer promoter looping model for transcriptional bursting and epigenetic regulation. There are three major components necessary for the development of a functional, predictive model of the genome: phase separation, chromatin looping, and transcription factor binding (Figure 4.1). The preliminary work described here will focus on chromatin looping through the determination of CTCF sites, enhancers, promoters, and gene characterization. This information will then be used to begin forming the framework for the eventual model. Single molecule tracking data on unique genes of interest will be used to inform and train the model.

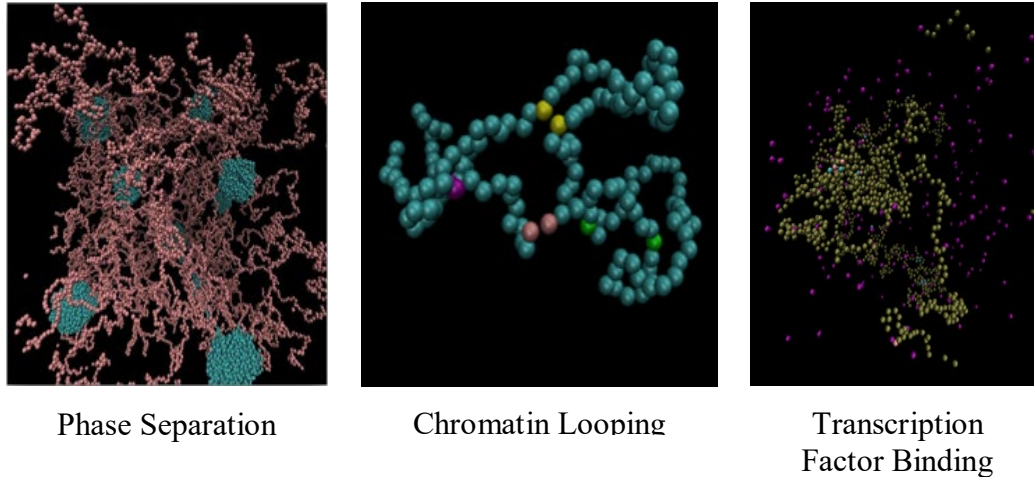


Figure 4.1 Core Genome Model Components

The left image shows a preliminary molecular dynamics simulation in HoomD of phase separation that would be akin to heterochromatin (blue) and euchromatin (pink). The middle image models the chromatin interactions of enhancers and promoters or CTCF forward and reverse sites. The blue beads are uncharged and therefore not attracted to any particular bead, while the yellow, pink, green and purple beads are all attracted to their like color match. The right image shows a preliminary molecular dynamics model of the transcription factor search process. Yellow beads signify the genome while purple beads signify individual transcription factors searching for the proper gene.

Models and Methods

Spherical simulation elements (“beads”) are used to represent 1kB of DNA. Bead interactions are modeled with the Lennard-Jones (LJ) potential $V_{LJ}(r) = 4\epsilon[(\sigma/r)^{12} - (\sigma/r)^6]$ where the parameters σ represent the size of simulation elements and ϵ represents the “stickiness”, or magnitude of the potential energy minimum between two beads. Here we test the length of the polymer (number of beads in the string) and the “stickiness” (ϵ) of particular beads. Additionally, we tested the freedom of the polymer, or the size of the simulation space relative to the size of the polymer. The HoomD Blue software package was used to run these dynamic high resolution polymer simulations (Ramasubramani et al. 2020).

The first step to this project was to begin modeling and testing different bead stickiness (ϵ) and different lengths of polymers. The stickiness of beads will be indicative of how attracted different genetic features, such as CTCF sites or enhancers and promoters, are to each other. The length of the polymer will model the length of a topologically associated domain (TAD). We found that length of the end-to-end distance is proportional to the square of the time it takes to turn on. The longer the string length, the longer it will take for the end beads to find each other, thus simulating that the larger the distance between CTCF sites, the slower they will be to find each other and turn the gene on. Additionally, the stickiness of the beads is critical because if they are not sticky enough, they will never interact with each other, but if they are too sticky, they will never come apart. This shows the importance of the proper level of molecular attractiveness between CTCF sites. If they are not attracted enough the gene will never turn on, but if they are too attracted it will never turn off.

Modeling TADs

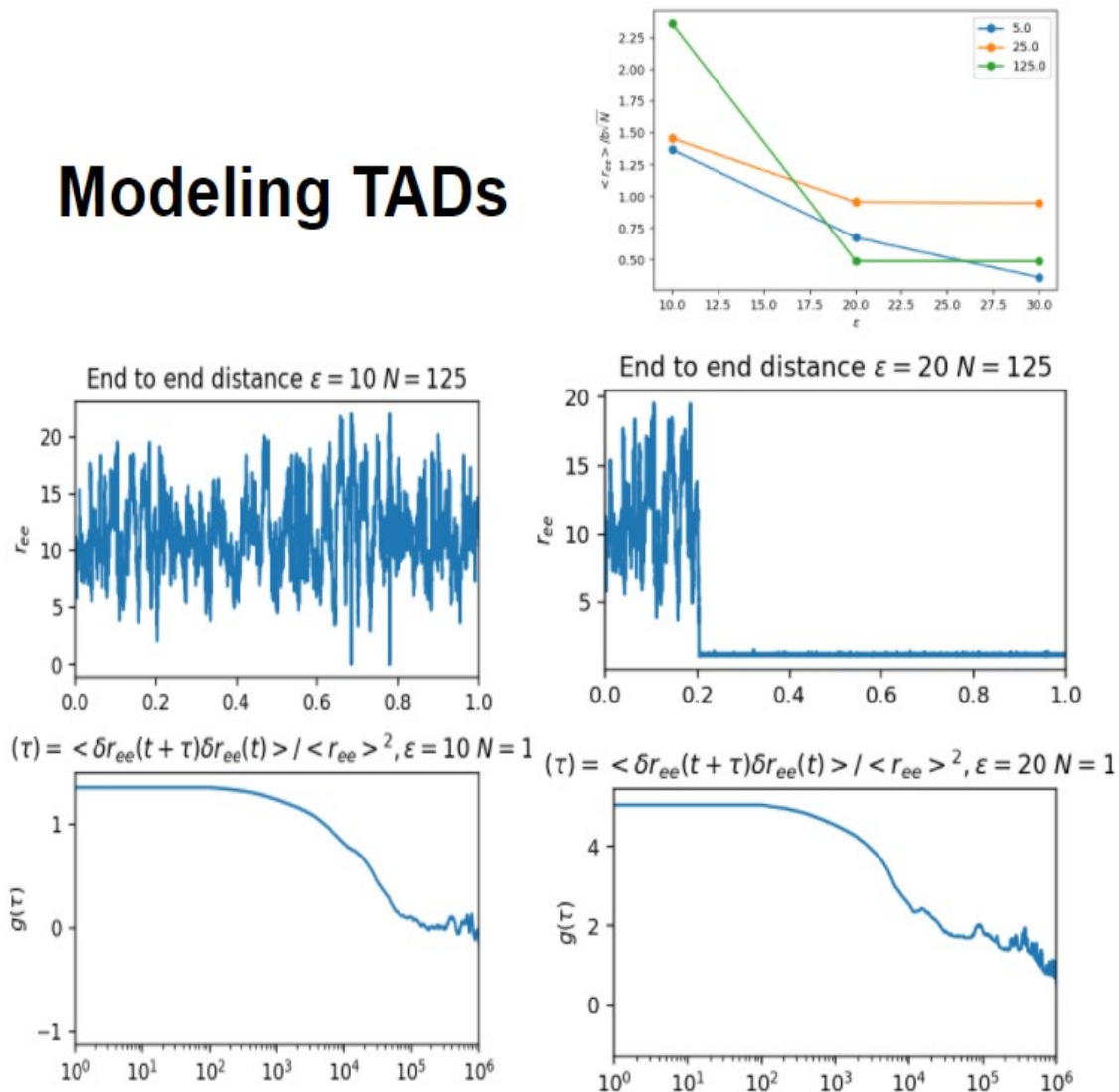


Figure 4.2 Modeling TAD length

The top graph shows the stickiness of the beads relative to how long the polymer is. The second row of graphs compare the two polymer chains that are 125 beads long. The left simulation has an epsilon of 10 and the right has an epsilon of 20. The right graph closes the loop much faster than the left one. The third row of graphs shows the autocorrelation of the above simulations.

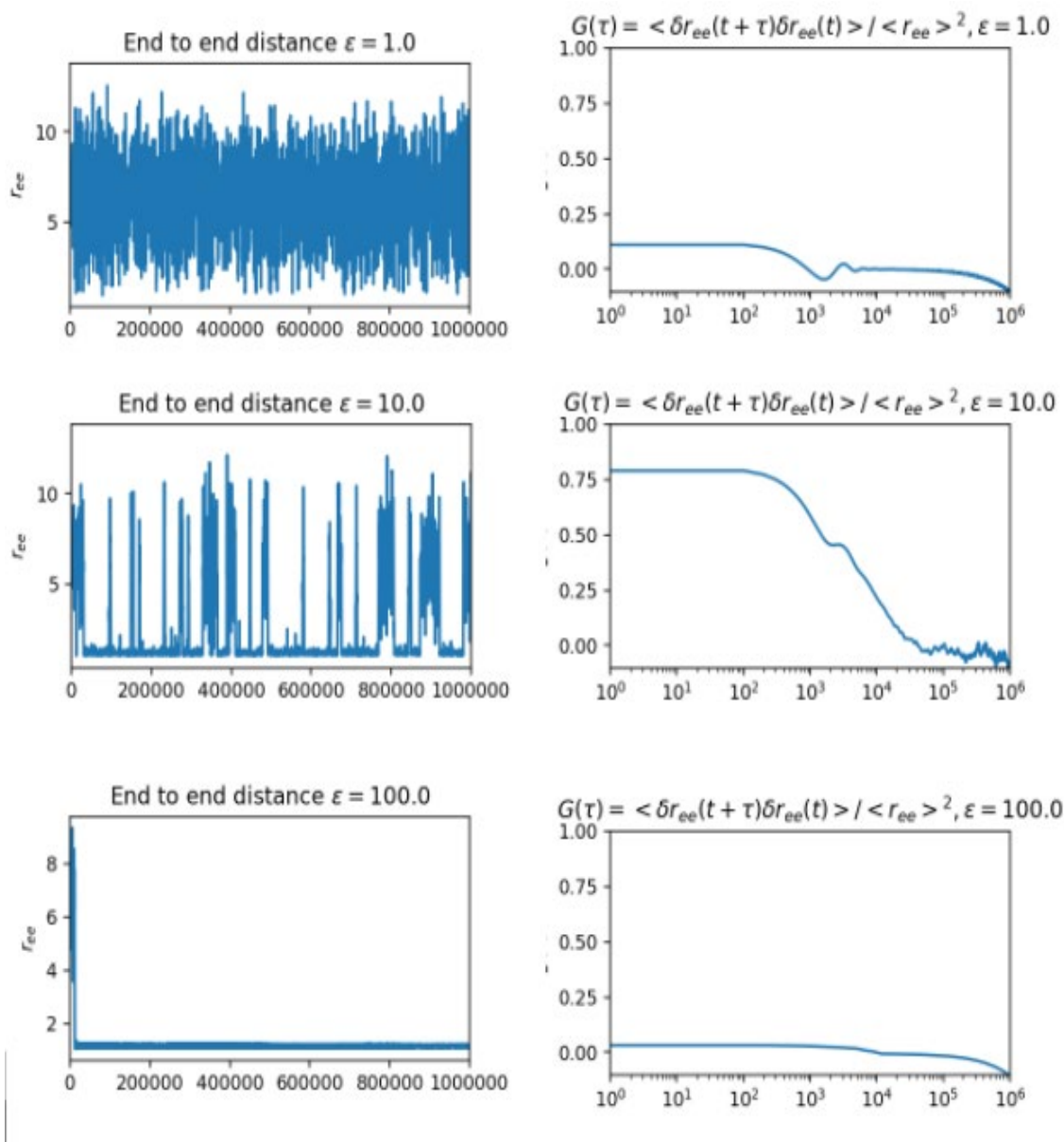


Figure 4.3 Loop Size Simulation

Epsilon was varied (1, 10, 100). The higher epsilon was the faster the loop closed and stayed closed. The left row shows end to end distance over time. The right row shows the corresponding autocorrelation curves for each epsilon tested. $G(\tau) = \langle \delta F(t) \cdot \delta F(t + \tau) \rangle / \langle F \rangle^2$ was used to calculate the autocorrelations.

Through the preliminary modeling and testing of the loop size and bead stickiness we were able to determine that the longer the polymer is, the less likely it is to form a loop (or form a bond between the sticky beads). Similarly, the stickier the bead the more

likely it is to form a bond and the less likely it is to fall off. This indicates that a higher epsilon is not always better. In the context of gene on and off rates it would be important for a gene to be able to turn both on and off, not simply on indefinitely. An epsilon of 10 (Figure 4.2) appears to be like the fluorescence fluctuation (raw data) and autocorrelation function data that is collected through 3D orbital tracking, therefore indicating that this would be an ideal starting point for modeling on and off times of gene expression.

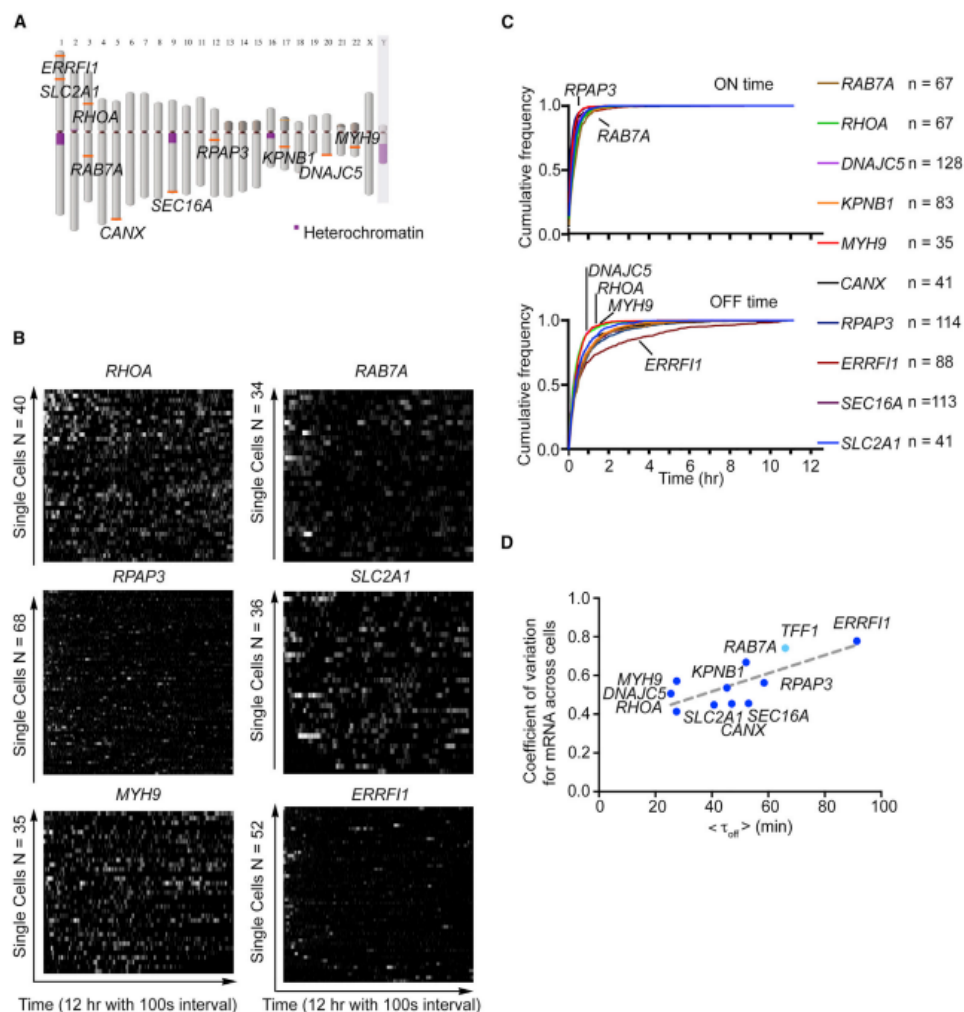


Figure 4.4 The kinetic features of human transcription

A. Ideogram of genes selected for clonal analysis. B. Heatmap of intensity traces from six genes. Each row represents a single cell recorded for 12h with 100-s intervals. Traces are sorted according to the duration of the first OFF period. C. Cumulative frequency of ON time and OFF time distribution for genes in panel A. D. The heterogeneity of mRNA in single cells correlates with transcription OFF time. Correlation between OFF time (T_{off}) and the coefficient of variation (CV) in single-cell mRNA distribution $R^2 = 0.54$. mRNA distribution for TFF1 is from our previous work (Rodriguez et al., 2019). (Figure adapted from (Wan et al. 2021)).

Single Molecule Tracking Data

The goal of these simulations is to be able to model and predict the behavior that is seen in single molecule tracking data. We have single molecule tracking data that

indicates a marked difference between 6 genes of interest that are all implicated in various ways in cancer. The six genes of interest are: ERRFI1, RPAP3, RAB7A, MYH9, RHOA, SLC2A1. The two especially unique ones are ERRFI1 and RPAP3. ERRFI1 has a much longer off time (Figure 4.4). RPAP3 has a much shorter on time. It is unclear from the live cell data why these gene activation times vary so wildly from each other. Below is preliminary characterization data on each of these genes that was procured using the NCBI and WashU databases.

Table 4.1 Single Molecule Tracking Gene Set

The below chart shows the six genes of interest, a brief description, gene length, exon number, the length of the TAD in which they typically reside, and their chromosomal location.

Gene	Description	Gene Length	# Exons	TAD Length	Chromosome Location
ERRFI1	Associated with cell growth. It is induced during cell stress and mediates cell. signaling.	14.6 kb	4	200 kb	1p36.23
RPAP3	RNA polymerase II-associated protein.	44.1 kb	17	**not in one TAD	12q13.11
RAB7A	RAS-related GTP-binding proteins that are important regulators of vesicular transport.	88.7 kb	6	420.5 kb	3q21.3
MYH9	Encodes a conventional non-muscle myosin.	106.7 kb	41	**not in one TAD	22q12.3
RHOA	Regulates cell shape, attachment, and motility. Overexpression is associated with proliferation and metastasis.	52.9 kb	5	109.6 kb	3p21.31
SLC2A1	Encodes a major glucose transporter in the mammalian blood-brain barrier.	24.3 kb	10	296.4 kb	1p34.2

The differences in gene features, while interesting, did not immediately reveal the unique on and off times observed in the single molecule tracking (SMT) data. This led to

a new hypothesis that the differences in CTCF sites and TAD length directly impacted how often a gene was turning on or off. Therefore, I used the WashU database and the Encode database to search for each of the 6 genes and the TADs that they were located within. CTCF sites were identified using Chip-seq tracks (GSE170996, GSE30263, GSE29611). They were then validated with Chia-PET tracks (GSE39495, GSE72816). All of this was conducted in the A562 cell line (it was also validated in HELA cells and MCF7 cells). Additionally, Chip-Seq tracks for p300 (a protein that binds to enhancer regions) were also analyzed using GEO data set GSM935401. This analysis yielded TAD length, the positioning of the gene of interest, promoter and enhancer location, and gene length. This will provide the basis for modeling these genes of interest. The bioinformatics analysis allowed for us to determine how many beads were required for each gene's simulation, the location of features of interest such as promoters and enhancers, and corresponding CTCF sites. Each bead within the simulation corresponds to 1 kb.

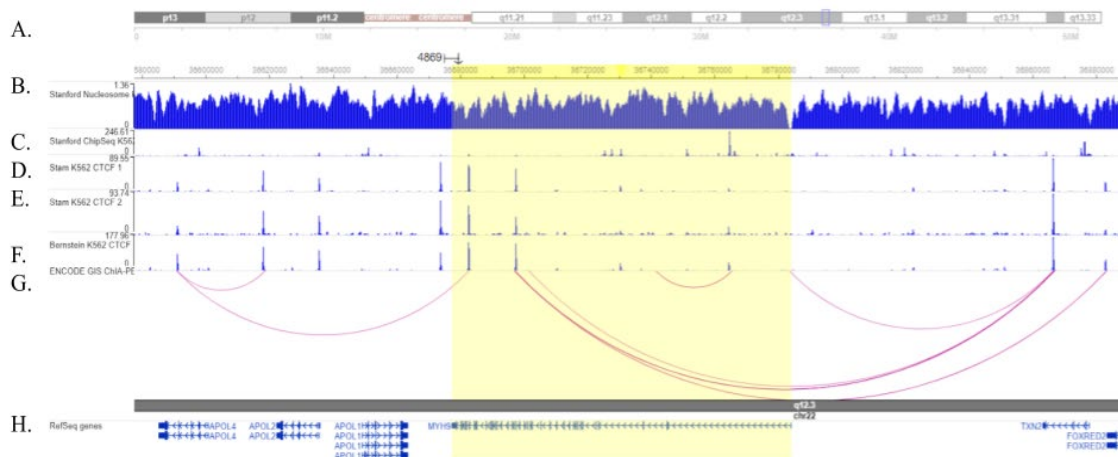


Figure 4.5 Sequencing Features of Interest for MYH9

A. Chromosome Location. B. Nucleosome positioning. C. Stanford p300 ChipSeq in K562 cells. D. Stam K562 CTCF Sample 1. E. Stam K562 CTCF Sample 2. F. Bernstein K562 CTCF. G. ENCODE GIS CHIA-PET. H. RefSeq Gene Location.

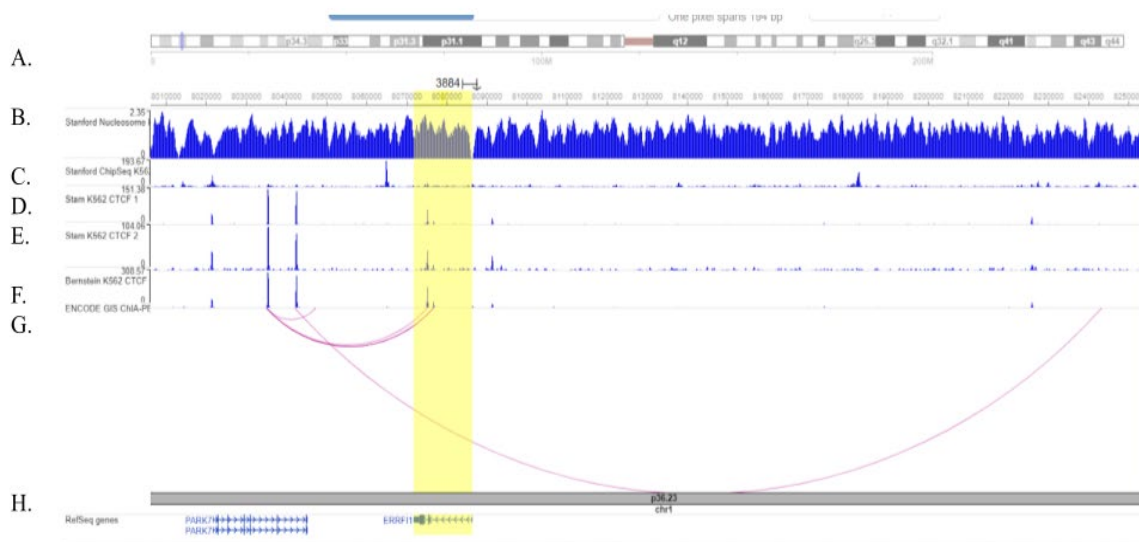


Figure 4.6 Sequencing Features of Interest for ERRFI1

A. Chromosome Location. B. Nucleosome positioning. C. Stanford p300 ChipSeq in K562 cells. D. Stam K562 CTCF Sample 1. E. Stam K562 CTCF Sample 2. F. Bernstein K562 CTCF. G. ENCODE GIS CHIA-PET. H. RefSeq Gene Location.

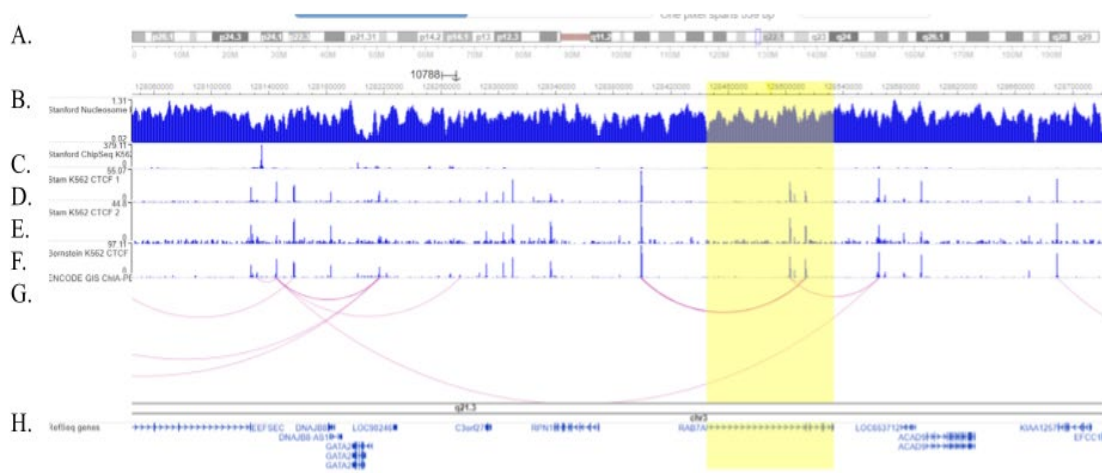


Figure 4.7 Sequencing Features of Interest for RAB7A

A. Chromosome Location. B. Nucleosome positioning. C. Stanford p300 ChipSeq in K562 cells. D. Stam K562 CTCF Sample 1. E. Stam K562 CTCF Sample 2. F. Bernstein K562 CTCF. G. ENCODE GIS CHIA-PET. H. RefSeq Gene Location.

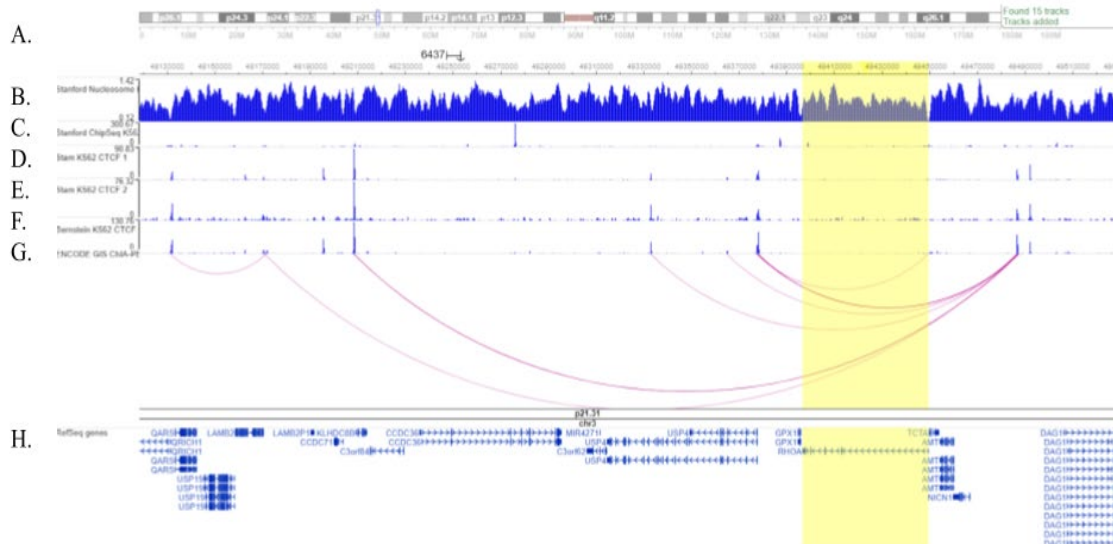


Figure 4.8 Sequencing Features of Interest for RHOA

A. Chromosome Location. B. Nucleosome positioning. C. Stanford p300 ChIPSeq in K562 cells. D. Stam K562 CTCF Sample 1. E. Stam K562 CTCF Sample 2. F. Bernstein K562 CTCF. G. ENCODE GIS CHIA-PET. H. RefSeq Gene Location.

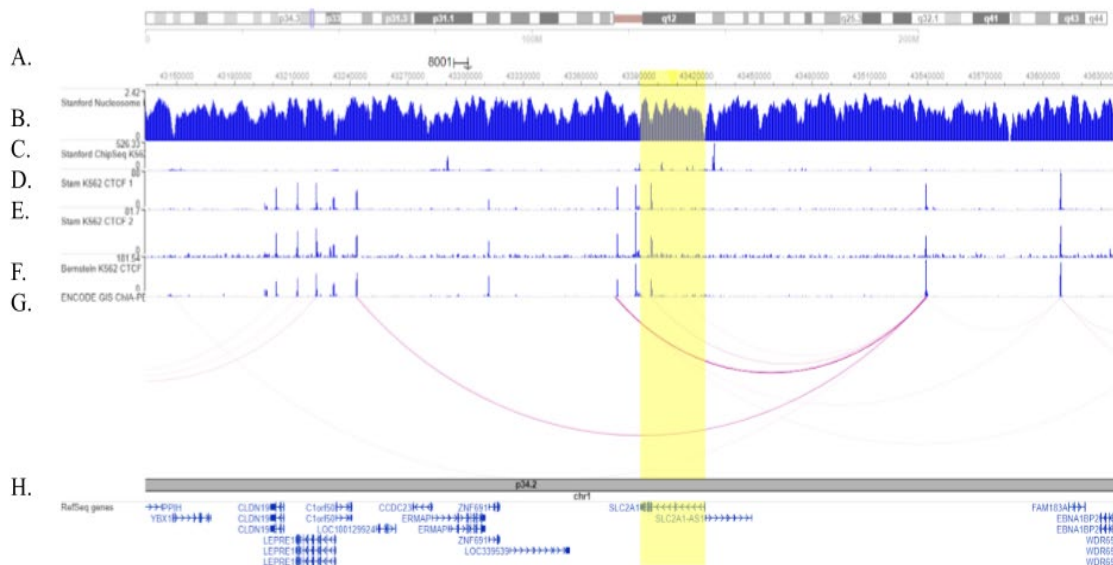


Figure 4.9 Sequencing Features of Interest for SLCA1

A. Chromosome Location. B. Nucleosome positioning. C. Stanford p300 ChIPSeq in K562 cells. D. Stam K562 CTCF Sample 1. E. Stam K562 CTCF Sample 2. F. Bernstein K562 CTCF. G. ENCODE GIS CHIA-PET. H. RefSeq Gene Location.

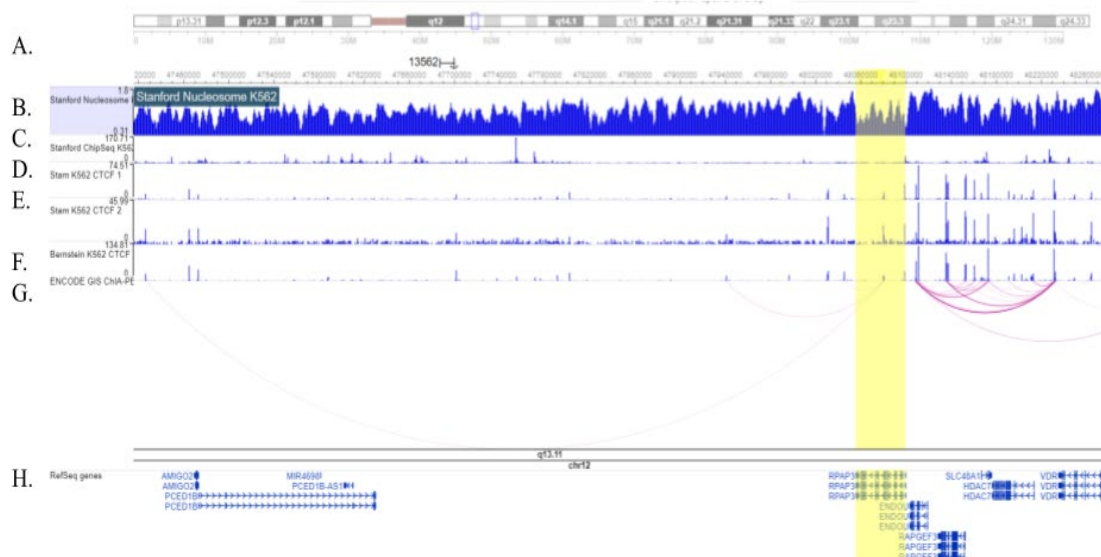


Figure 4.10 Sequencing Features of Interest for RPAP3

A. Chromosome Location. B. Nucleosome positioning. C. Stanford p300 ChIPSeq in K562 cells. D. Stam K562 CTCF Sample 1. E. Stam K562 CTCF Sample 2. F. Bernstein K562 CTCF. G. ENCODE GIS CHIA-PET. H. RefSeq Gene Location.

This bioinformatics search revealed that not every gene resided in a single TAD. Additionally, there are often multiple TADs that are possible within a single cell type, which adds a layer of complexity to the model. Below is the proposed specification for the initial modeling of the most straight-forward genes. The total number of beads in the simulation was determined using the TAD with the most read depth.

Table 4.2 Proposed Simulations

Each bead in the simulation represents 1kb of the genome. The total number of beads in the simulation is determined by the size of the TAD, or distance between CTCF sites, in which the gene typically resides. Beads are numbered in a linear fashion (ie. the first bead is #1).

Gene	Total Beads in Simulation	Beads in Gene (bead #)	Enhancer Location (bead #)	Promoter Location (bead #)
ERRFI1	200	31-44	23	45
RAB7A	421	301-390	58	300
RHOA	110	19-70	9	71
SLC2A1	296	149-177	48	178

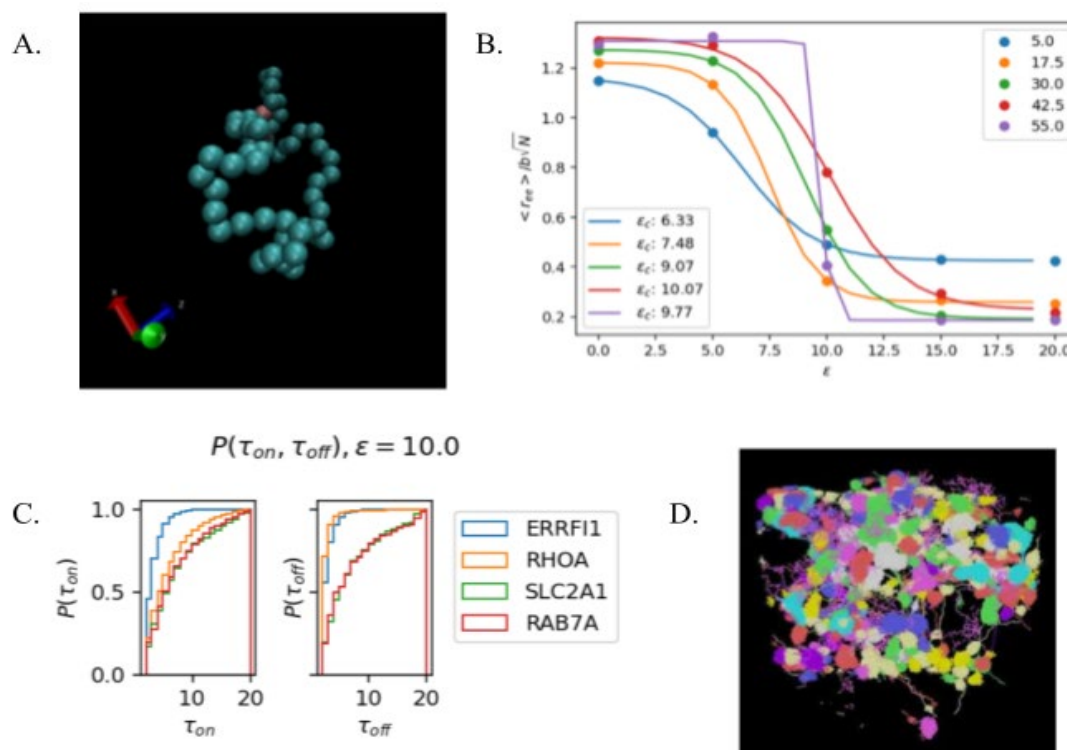


Figure 4.11 On Time Simulation

A. Molecular Dynamics Simulation of a single test gene that is 125 kb or 125 beads long. B. Test of ideal epsilon for loops varying sizes. 10.0 appears to be the ideal epsilon for polymers that are capable of opening and closing with ease. C. Simulated on/off times of ERRF11, RHOA, SLC2A1, and RAB7A. The length of the gene and length of the TAD described in Table 4.2 were used to perform a coarse grain models simulation. While not identical to the SMT data, these preliminary results show that ERRF11 is predicted to be ON more than the other genes in this set. D. Whole genome test simulation of 24 distinct polymers simulating 24 chromosomes in the human genome.

Conclusions

This preliminary study shows the validity of using available bioinformatics data as a basis for molecular dynamics simulation of the genome. Bioinformatics is a great starting point for developing a biologically relevant model, but it will eventually need to be supplemented with live cell single molecule tracking data. The main takeaway from this work to date is that CTCF sites and gene length are likely involved in the kinetics of gene expression, but they are not the only contributors to gene on/off rates. It is probable

that the determining factor of gene on/off rates is more complex than previously supposed. Further work needs to be done to the model to make it more physiologically relevant.

Future Directions

One of the lingering challenges with properly modeling this gene set is that while informative, the bioinformatics data is not clear cut. One such example is that not all the genes fall into one discreet TAD, which makes modeling individual genes a challenge. Another issue is that often multiple potential TAD boundaries show up in the bioinformatics data, and while there is usually one that clearly occurs most often, the current model does not account for the possibility of multiple TADs within the same region. There is the additional challenge of determining the proper cell type to evaluate these features within. Six different cell types were explored using the WashU database. While there are subtle differences, there were no significant differences between CTCF sites and TAD boundaries across cell types and most of the minor differences could be attributed to read depth. It is currently unclear whether these subtle nuances are significant enough to impact the validity of the coarse-grained model.

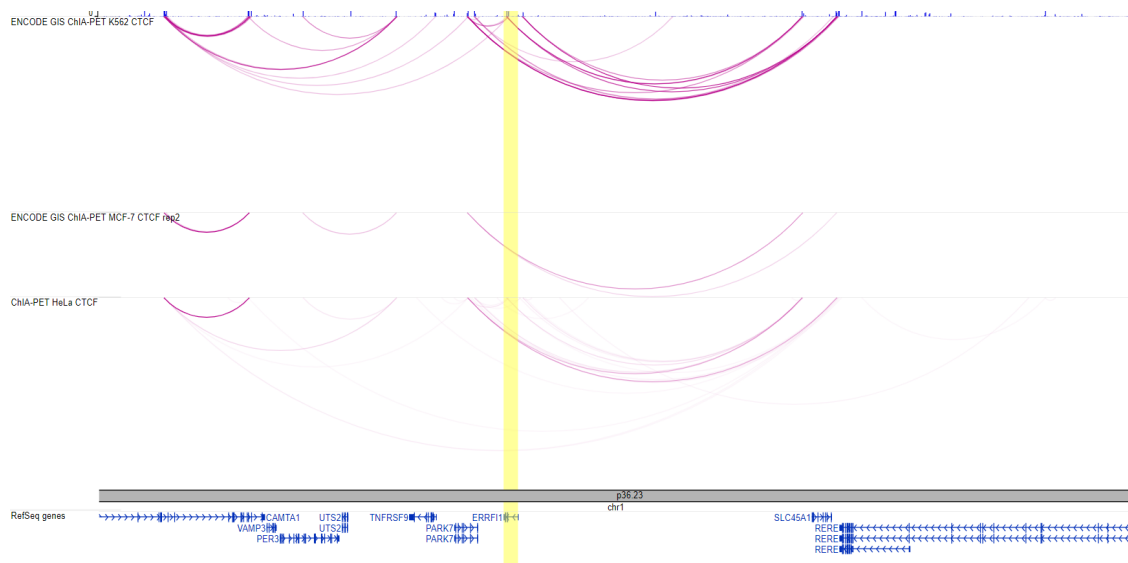


Figure 4.12 Example CTCF Traces Compared Across Cell Types

These example traces show the similarities of CTCF site interactions across cell types (HeLa, MCF-7, K562). Traces shown were collected using CHIA-PET.

Upon completion of the initial modeling of this gene set, the next major step in developing a predictive model for the molecular dynamics of the genome is to scale this up beyond the single gene level. Our preliminary work indicates that the genetic features in proximity to the gene of interest are involved in its activation and expression. Therefore, the next step would be to include the genes on either side of the gene of interest, and eventually the whole chromosome. It would also be critical to include not only TADs, but also LADs, but unfortunately this information is not readily available on the whole genome level. Further work also needs to be conducted on the various TADs that are possible. The Chip-seq and CHIA-PET data consistently shows multiple alternative pairs for CTCF sites. This high variability of TADs needs to be addressed in the simulation as it is scaled up. This could likely be done by making beads of various attractiveness, i.e., the most prominent CTCF sites would be most strongly attracted to

each other, but the other less prominent ones would still have some low level of attractiveness, therefore providing the variability that we see in the Chip-seq and Chia-PET data.

As previously stated, there are three major components to this model of the genome: phase separation, chromatin looping, and transcription factor binding. We are well on our way to having the chromatin looping component completed, but the inclusion of phase separation and transcription factor binding are still necessary.

CHAPTER FIVE: CONCLUSIONS AND FUTURE DIRECTIONS

Conclusions

The previous chapters demonstrated the need for a live cell imaging technique that can collect real-time data of active genes on the hour time scale, as well as a need to not only characterize the genome, but predict dynamic behavior. The work described in chapters 2 and 3 report the validity of a proof-of-concept imaging modality, 3D orbital tracking that can overcome optical limitations that have limited the applications of fluorescence microscopy to making dynamical measurements of gene behavior in real-time. 3D orbital tracking provides the temporal and spatial resolution necessary to begin evaluating the dynamical behavior of the genome. Through the utilization of this new microscopy scanning method, in conjunction with fluorescence cross correlation spectroscopy we were able to measure the dynamics of transcriptional activation and RNA synthesis within a living cell. Chapter 4 further reported that the measurements taken through single molecule tracking experiments in tandem with whole genome sequencing data could be used to begin developing a predictive molecular dynamics simulation for gene dynamics and expression.

3D Orbital Tracking in Organoid Models

Introduction

Molecular dynamics modeling and bioinformatics have further revealed the critical role that 3D organization plays in genome behavior. Therefore, the next step in improving the biological relevance of 3D orbital tracking data is to move into an

organoid model which better preserves genome organization and recapitulates an in-vivo environment than traditional 2D cell culture does. Just as benchtop experiments are not completely translatable to live cell experiments, 2D immortalized cell culture does not perfectly represent how a cell behaves in-vivo. Cells have been shown to behave differently based on the environment that they are in (Rønnov-Jessen and Bissell 2009; Mishra et al. 2014). While yet there is no good option for imaging a whole living human in single cell detail, 3D organoid imaging could provide a much more physiologically relevant method of characterizing genome behavior and transcription (Duval et al. 2017). An improved, physiologically relevant tissue culture model would result in a more complete characterization of the molecular mechanism of transcription that is relevant to human health.

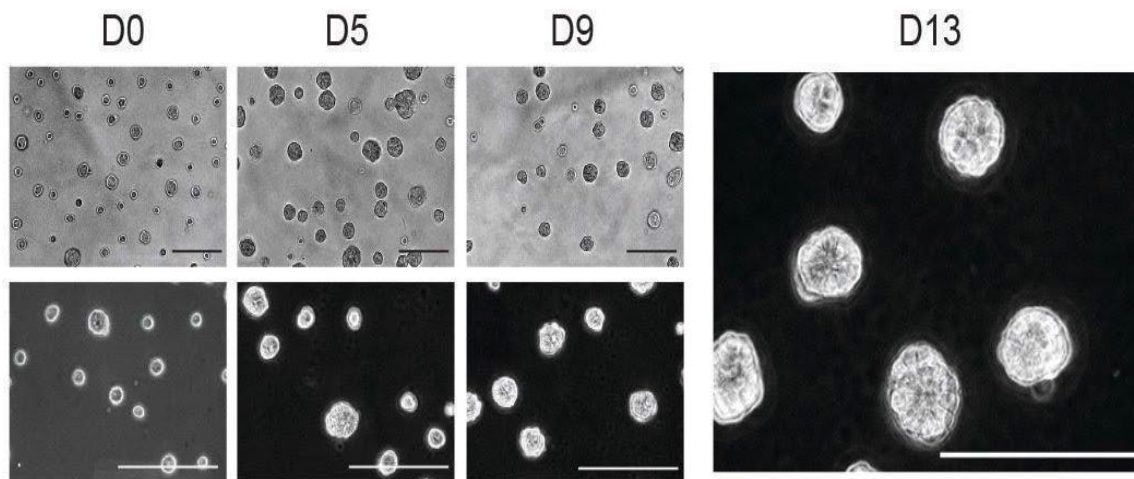


Figure 5.1 MCF10A Matrigel Time Course

Example time course of organoid formation in MCF10A cells. Cells form functional, symmetrical ductal structures like those seen in-vivo. Cells were seeded into the Matrigel matrix on Day 0 and imaged on Day 5, Day 9, and Day 13.

Matrigel Proposed Experiments

To further explore the role that cellular organization plays in genome behavior and transcription, modified mouse mammary cells that are labeled for 3D orbital tracking (as per the methods described in chapter 3) will be grown in Matrigel matrix according to established protocols (“Protocols” n.d.). Transcription of GR responsive genes will be induced using dexamethasone and corticosteroid (as per the methods described in chapter 3). Samples will then be imaged using 3D orbital tracking confocal microscope using TS-FCCS. Transcription sites will be tracked, and fluorescence traces analyzed (as per the data analysis described in chapter 3). Data generated will be used to determine how many RNAs are being produced and how long it takes to produce the GR-RNA, as well as differences in gene expression between cells cultured in 3D vs. 2D.

Significance

The data collected with 3DOT-FCCS is opening new doors for further exploration into fundamental biochemical processes through a dynamic view of single fluorescent molecules within living systems at high speeds. This data will improve our knowledge of how eukaryotic organisms regulate transcription and shed light on previously unknown details about transcriptional activation and temporal coordination. Conducting these experiments in a 3D environment would provide a more realistic environment to that which would be found in-vivo. This technique has the capacity to be expanded to the transcriptional processes of other genes, many of which could have weighty implications for our understanding of genome biology and human health and disease.

Conclusions

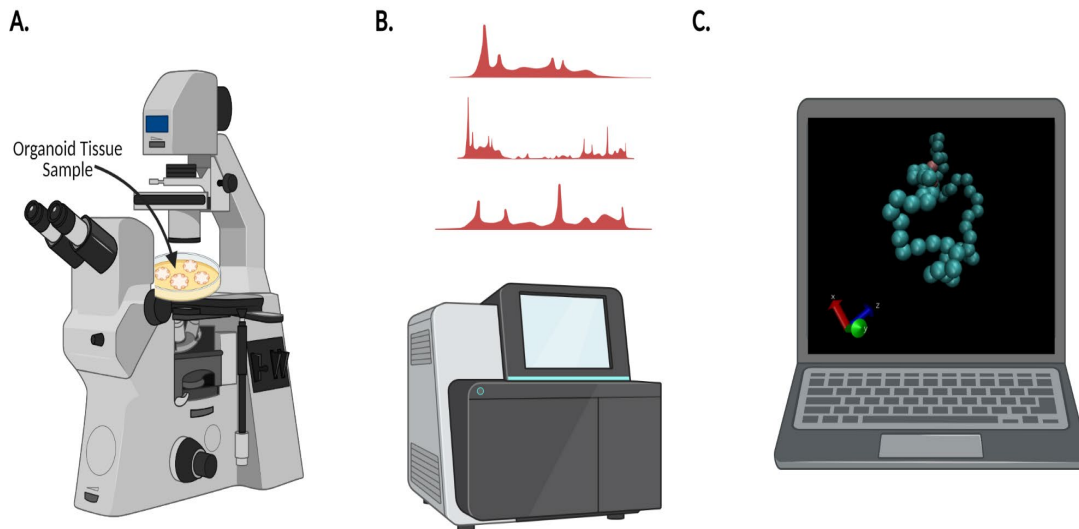


Figure 5.2 Future Directions

The quest to unlock the inner workings of the genome will be furthered through the synergistic use of cutting-edge imaging methods, novel sequencing methods, and in-silico modeling. A. Orbital Tracking Fluorescence Cross Correlation Spectroscopy in an organoid model B. Bioinformatics sequencing data C. Molecular Dynamics Simulations

The real challenge ahead is not developing a new imaging technique or analyzing bioinformatics data but synthesizing these complementary techniques together into a cohesive model of the human genome and how it behaves in real-time. This will be completed using cutting-edge microscopy techniques such as 3DOT-FCCS in conjunction with bioinformatics sequencing data like Hi-C, Chia-PET, and ChipSeq. These two arms of science, while powerful alone will synergistically provide invaluable insights when combined using molecular dynamics simulations. Together these methodologies will begin to move from describing and characterizing the genome to predicting the dynamics and organization of the 4D living genome.

REFERENCES

- Abusara, Z., R. Seerattan, A. Leumann, R. Thompson, and W. Herzog. 2011. "A Novel Method for Determining Articular Cartilage Chondrocyte Mechanics in Vivo." *Journal of Biomechanics* 44 (5): 930–34.
- Andersson, Robin, and Albin Sandelin. 2020. "Determinants of Enhancer and Promoter Activities of Regulatory Elements." *Nature Reviews. Genetics* 21 (2): 71–87.
- Annibale, Paolo, Alexander Dvornikov, and Enrico Gratton. 2015. "Electrically Tunable Lens Speeds up 3D Orbital Tracking." *Biomedical Optics Express* 6 (6): 2181–90.
- Annibale, Paolo, and Enrico Gratton. 2015. "Single Cell Visualization of Transcription Kinetics Variance of Highly Mobile Identical Genes Using 3D Nanoimaging." *Scientific Reports* 5 (March): 9258.
- Antoku, Susumu, Wei Wu, Leroy C. Joseph, John P. Morrow, Howard J. Worman, and Gregg G. Gundersen. 2019. "ERK1/2 Phosphorylation of FHOD Connects Signaling and Nuclear Positioning Alternations in Cardiac Laminopathy." *Developmental Cell* 51 (5): 602–16.e12.
- Anton, Tobias, Heinrich Leonhardt, and Yolanda Markaki. 2016. "Visualization of Genomic Loci in Living Cells with a Fluorescent CRISPR/Cas9 System." *Methods in Molecular Biology* 1411: 407–17.
- Anzalone, Andrea, Paolo Annibale, and Enrico Gratton. 2014. "3D Orbital Tracking in a Modified Two-Photon Microscope: An Application to the Tracking of Intracellular Vesicles." *Journal of Visualized Experiments: JoVE*, no. 92 (October): e51794.
- Armiger, Travis J., Stephen T. Spagnol, and Kris Noel Dahl. 2016. "Nuclear Mechanical Resilience but Not Stiffness Is Modulated by α II-Spectrin." *Journal of Biomechanics* 49 (16): 3983–89.

- Arsenovic, Paul T., Iswarya Ramachandran, Kranthidhar Bathula, Ruijun Zhu, Jiten D. Narang, Natalie A. Noll, Christopher A. Lemmon, Gregg G. Gundersen, and Daniel E. Conway. 2016. "Nesprin-2G, a Component of the Nuclear LINC Complex, Is Subject to Myosin-Dependent Tension." *Biophysical Journal* 110 (1): 34–43.
- Axelrod, D. 1981. "Cell-Substrate Contacts Illuminated by Total Internal Reflection Fluorescence." *The Journal of Cell Biology* 89 (1): 141–45.
- Axelrod, Daniel. 2001. "Total Internal Reflection Fluorescence Microscopy in Cell Biology." *Traffic*. <https://doi.org/10.1034/j.1600-0854.2001.21104.x>.
- Bacia, Kirsten, Sally A. Kim, and Petra Schwille. 2006. "Fluorescence Cross-Correlation Spectroscopy in Living Cells." *Nature Methods* 3 (2): 83–89.
- Bacia, Kirsten, Irina V. Majoul, and Petra Schwille. 2002. "Probing the Endocytic Pathway in Live Cells Using Dual-Color Fluorescence Cross-Correlation Analysis." *Biophysical Journal* 83 (2): 1184–93.
- Bacia, Kirsten, and Petra Schwille. 2003. "A Dynamic View of Cellular Processes by in Vivo Fluorescence Auto- and Cross-Correlation Spectroscopy." *Methods* 29 (1): 74–85.
- Bacia, K., Kim, S. A., & Schwille, P. 2006. "Fluorescence cross-correlation spectroscopy in living cells." *Nature Methods* 3 (2): 83–89.
- Bader, D. L., T. Ohashi, M. M. Knight, D. A. Lee, and M. Sato. 2002. "Deformation Properties of Articular Chondrocytes: A Critique of Three Separate Techniques." *Biorheology* 39 (1-2): 69–78.
- Bandyopadhyay, Debjyoti, Austin Cyphersmith, Jairo A. Zapata, Y. Joseph Kim, and Christine K. Payne. 2014. "Lysosome Transport as a Function of Lysosome Diameter." *PloS One* 9 (1): e86847.
- Banerjee, Bidisha, Dipanjan Bhattacharya, and G. V. Shivashankar. 2006. "Chromatin Structure Exhibits Spatio-Temporal Heterogeneity within the Cell Nucleus." *Biophysical Journal* 91 (6): 2297–2303.

- Barnes, Peter J. 2006. "Corticosteroids: The Drugs to Beat." *European Journal of Pharmacology* 533 (1-3): 2–14.
- Bashirzadeh, Yashar, Siddharth Chatterji, Dakota Palmer, Sandeep Dumbali, Shizhi Qian, and Venkat Maruthamuthu. 2018. "Stiffness Measurement of Soft Silicone Substrates for Mechanobiology Studies Using a Widefield Fluorescence Microscope." *Journal of Visualized Experiments: JoVE*, no. 137 (July).
<https://doi.org/10.3791/57797>.
- Benham-Pyle, Blair W., Beth L. Pruitt, and W. James Nelson. 2015. "Cell Adhesion. Mechanical Strain Induces E-Cadherin-Dependent Yap1 and β -Catenin Activation to Drive Cell Cycle Entry." *Science* 348 (6238): 1024–27.
- Benham-Pyle, Blair W., Joo Yong Sim, Kevin C. Hart, Beth L. Pruitt, and William James Nelson. 2016. "Increasing β -catenin/Wnt3A Activity Levels Drive Mechanical Strain-Induced Cell Cycle Progression through Mitosis." *eLife* 5 (October).
<https://doi.org/10.7554/eLife.19799>.
- Benham-Pyle, B. W., Pruitt, B. L. & Nelson, W. J. Cell adhesion. Mechanical strain induces E-cadherin-dependent Yap1 and beta-catenin activation to drive cell cycle entry. *Science* (New York, N.Y.) 348, 1024-1027, doi:10.1126/science.aaa4559 (2015).
- Berg, H. C. 1971. "How to Track Bacteria." *The Review of Scientific Instruments* 42 (6): 868–71.
- Bertrand, E., P. Chartrand, M. Schaefer, S. M. Shenoy, R. H. Singer, and R. M. Long. 1998. "Localization of ASH1 mRNA Particles in Living Yeast." *Molecular Cell* 2 (4): 437–45.
- Betzig, Eric, George H. Patterson, Rachid Sougrat, O. Wolf Lindwasser, Scott Olenych, Juan S. Bonifacino, Michael W. Davidson, Jennifer Lippincott-Schwartz, and Harald F. Hess. 2006. "Imaging Intracellular Fluorescent Proteins at Nanometer Resolution." *Science* 313 (5793): 1642–45.

- Bhattacharya, Dipanjan, Shefali Talwar, Aprotim Mazumder, and G. V. Shivashankar. 2009. "Spatio-Temporal Plasticity in Chromatin Organization in Mouse Cell Differentiation and during *Drosophila* Embryogenesis." *Biophysical Journal* 96 (9): 3832–39.
- Bohnsack, Markus T., Theis Stüven, Christa Kuhn, Volker C. Cordes, and Dirk Görlich. 2006. "A Selective Block of Nuclear Actin Export Stabilizes the Giant Nuclei of *Xenopus* Oocytes." *Nature Cell Biology* 8 (3): 257–63.
- Booth-Gauthier, Elizabeth A., Turi A. Alcoser, Ge Yang, and Kris N. Dahl. 2012. "Force-Induced Changes in Subnuclear Movement and Rheology." *Biophysical Journal* 103 (12): 2423–31.
- Borst, Piet. 2005. "Ethidium DNA Agarose Gel Electrophoresis: How It Started." *IUBMB Life* 57 (11): 745–47.
- Braccioli, Luca, and Elzo de Wit. 2019. "CTCF: A Swiss-Army Knife for Genome Organization and Transcription Regulation." *Essays in Biochemistry* 63 (1): 157–65.
- Bronshtein, I., E. Kepten, I. Kanter, S. Berezin, M. Lindner, Abena B. Redwood, S. Mai, et al. 2015. "Loss of Lamin A Function Increases Chromatin Dynamics in the Nuclear Interior." *Nature Communications* 6 (August): 8044.
- Burridge, K., K. Fath, T. Kelly, G. Nuckolls, and C. Turner. 1988. "Focal Adhesions: Transmembrane Junctions between the Extracellular Matrix and the Cytoskeleton." *Annual Review of Cell Biology* 4: 487–525.
- Butin-Israeli, Veronika, Stephen A. Adam, Nikhil Jain, Gabriel L. Otte, Daniel Neems, Lisa Wiesmüller, Shelly L. Berger, and Robert D. Goldman. 2015. "Role of Lamin b1 in Chromatin Instability." *Molecular and Cellular Biology* 35 (5): 884–98.
- Byron, Meg, Lisa L. Hall, and Jeanne B. Lawrence. 2013. "A Multifaceted FISH Approach to Study Endogenous RNAs and DNAs in Native Nuclear and Cell Structures." *Current Protocols in Human Genetics / Editorial Board, Jonathan L. Haines ... [et Al.]* Chapter 4 (January): Unit 4.15.

- Cain, Natalie E., Zeinab Jahed, Amy Schoenhofen, Venecia A. Valdez, Baila Elkin, Hongyan Hao, Nathan J. Harris, et al. 2018. "Conserved SUN-KASH Interfaces Mediate LINC Complex-Dependent Nuclear Movement and Positioning." *Current Biology: CB* 28 (19): 3086–97.e4.
- Calvi, Alessandra, Arnette Shi Wei Wong, Graham Wright, Esther Sook Miin Wong, Tsui Han Loo, Colin L. Stewart, and Brian Burke. 2015. "SUN4 Is Essential for Nuclear Remodeling during Mammalian Spermiogenesis." *Developmental Biology* 407 (2): 321–30.
- Camps, Jordi, Michael R. Erdos, and Thomas Ried. 2015. "The Role of Lamin B1 for the Maintenance of Nuclear Structure and Function." *Nucleus* 6 (1): 8–14.
- Cang, Hu, Chung M. Wong, C. Shan Xu, Abbas H. Rizvi, and Haw Yang. 2006. "Confocal Three Dimensional Tracking of a Single Nanoparticle with Concurrent Spectroscopic Readouts." *Applied Physics Letters* 88 (22): 223901.
- Capo-chichi, Callinice D., Kathy Q. Cai, Jennifer Smedberg, Parvin Ganjei-Azar, Andrew K. Godwin, and Xiang-Xi Xu. 2011. "Loss of A-Type Lamin Expression Compromises Nuclear Envelope Integrity in Breast Cancer." *Chinese Journal of Cancer* 30 (6): 415–25.
- Caridi, Christopher P., Carla D'Agostino, Taehyun Ryu, Grzegorz Zapotoczny, Laetitia Delabaere, Xiao Li, Varandt Y. Khodaverdian, et al. 2018. "Nuclear F-Actin and Myosins Drive Relocalization of Heterochromatic Breaks." *Nature* 559 (7712): 54–60.
- Case, Natasha, Jacob Thomas, Buer Sen, Maya Styner, Zhihui Xie, Kornelia Galior, and Janet Rubin. 2011. "Mechanical Regulation of Glycogen Synthase Kinase 3 β (GSK3 β) in Mesenchymal Stem Cells Is Dependent on Akt Protein Serine 473 Phosphorylation via mTORC2 Protein *." *The Journal of Biological Chemistry* 286 (45): 39450–56.
- Cawte, Adam D., Peter J. Unrau, and David S. Rueda. 2020. "Live Cell Imaging of Single RNA Molecules with Fluorogenic Mango II Arrays." *Nature Communications* 11 (1): 1283.

- Chambliss, Allison B., Shyam B. Khatau, Nicholas Erdenberger, D. Kyle Robinson, Didier Hodzic, Gregory D. Longmore, and Denis Wirtz. 2013. "The LINC-Anchored Actin Cap Connects the Extracellular Milieu to the Nucleus for Ultrafast Mechanotransduction." *Scientific Reports* 3 (January): 1087.
- Chang, Wakam, Eric S. Folker, Howard J. Worman, and Gregg G. Gundersen. 2013. "Emerin Organizes Actin Flow for Nuclear Movement and Centrosome Orientation in Migrating Fibroblasts." *Molecular Biology of the Cell* 24 (24): 3869–80.
- Chao, J. A., Y. Patskovsky, S. C. Almo, and R. H. Singer. 2008. "Structural Basis for the Coevolution of a Viral RNA-Protein Complex." *Nature Structural & Molecular Biology* 15 (1): 103–5.
- Chen, Bailing, Tao Lin, Xiaoxi Yang, Yiqiang Li, Denghui Xie, Wenhui Zheng, Haowen Cui, Weimin Deng, and Xin Tan. 2016. "Low-Magnitude, High-Frequency Vibration Promotes the Adhesion and the Osteogenic Differentiation of Bone Marrow-Derived Mesenchymal Stem Cells Cultured on a Hydroxyapatite-Coated Surface: The Direct Role of Wnt/ β -Catenin Signaling Pathway Activation." *International Journal of Molecular Medicine* 38 (5): 1531–40.
- Chen, Baohui, Luke A. Gilbert, Beth A. Cimini, Joerg Schnitzbauer, Wei Zhang, Gene-Wei Li, Jason Park, et al. 2013. "Dynamic Imaging of Genomic Loci in Living Human Cells by an Optimized CRISPR/Cas System." *Cell* 155 (7): 1479–91.
- Chen, Baohui, and Bo Huang. 2014. "Imaging Genomic Elements in Living Cells Using CRISPR/Cas9." *Methods in Enzymology* 546: 337–54.
- Chen, Bi-Chang, Wesley R. Legant, Kai Wang, Lin Shao, Daniel E. Milkie, Michael W. Davidson, Chris Janetopoulos, et al. 2014. "Lattice Light-Sheet Microscopy: Imaging Molecules to Embryos at High Spatiotemporal Resolution." *Science* 346 (6208): 1257998.
- Codelia, Veronica A., Gongping Sun, and Kenneth D. Irvine. 2014. "Regulation of YAP by Mechanical Strain through Jnk and Hippo Signaling." *Current Biology: CB* 24 (17): 2012–17.

- Cohen, Adam E., and W. E. Moerner. 2008. "Controlling Brownian Motion of Single Protein Molecules and Single Fluorophores in Aqueous Buffer." *Optics Express* 16 (10): 6941–56.
- Collins, Francis S. 1999. "Medical and Societal Consequences of the Human Genome Project." *The New England Journal of Medicine* 341 (1): 28–37.
- Collins, Francis S., Michael Morgan, and Aristides Patrinos. 2003. "The Human Genome Project: Lessons from Large-Scale Biology." *Science* 300 (5617): 286–90.
- Coskun, Ulas C., Matthew L. Ferguson, Alexander Vallmitjana, Anh Huynh, Julianna Goelzer, Yuansheng Sun, Shih-Chu Jeff Liao, Sunil Shah, Enrico Gratton, and Beniamino Barbieri. 2020. "Nano-Resolution in Vivo 3D Orbital Tracking System to Study Cellular Dynamics and Bio-Molecular Processes." In , 11246:1124614. International Society for Optics and Photonics.
- Coulon, Antoine, Matthew L. Ferguson, Valeria de Turrís, Murali Palangat, Carson C. Chow, and Daniel R. Larson. 2014. "Kinetic Competition during the Transcription Cycle Results in Stochastic RNA Processing." *eLife* 3 (October). <https://doi.org/10.7554/eLife.03939>.
- Crisp, Melissa, Qian Liu, Kyle Roux, J. B. Rattner, Catherine Shanahan, Brian Burke, Phillip D. Stahl, and Didier Hodzic. 2006. "Coupling of the Nucleus and Cytoplasm: Role of the LINC Complex." *The Journal of Cell Biology* 172 (1): 41–53.
- Crocker, J. C., M. T. Valentine, E. R. Weeks, T. Gisler, P. D. Kaplan, A. G. Yodh, and D. A. Weitz. 2000. "Two-Point Microrheology of Inhomogeneous Soft Materials." *Physical Review Letters* 85 (4): 888–91.
- Dahl, Kris Noel, Adam J. Engler, J. David Pajeroski, and Dennis E. Discher. 2005. "Power-Law Rheology of Isolated Nuclei with Deformation Mapping of Nuclear Substructures." *Biophysical Journal* 89 (4): 2855–64.
- Dame RT. 2005. "The role of nucleoid-associated proteins in the organization and compaction of bacterial chromatin." *Mol Microbiol.* 56 (4): 858-70.

- Darling, E. M. 2011. "Force Scanning: A Rapid, High-Resolution Approach for Spatial Mechanical Property Mapping." *Nanotechnology* 22 (17): 175707.
- Davis, Brandon J., and Mitchell R. O'Connell. 2020. "Put on Your Para-Spectacles: The Development of Optimized CRISPR-Cas13-Based Approaches to Image RNA Dynamics in Real Time." *Molecular Cell*.
- Denais, Celine M., Rachel M. Gilbert, Philipp Isermann, Alexandra L. McGregor, Mariska te Lindert, Bettina Weigelin, Patricia M. Davidson, Peter Friedl, Katarina Wolf, and Jan Lammerding. 2016. "Nuclear Envelope Rupture and Repair during Cancer Cell Migration." *Science* 352 (6283): 353–58.
- Deng, Wulan, Xinghua Shi, Robert Tjian, Timothée Lionnet, and Robert H. Singer. 2015. "CASFISH: CRISPR/Cas9-Mediated in Situ Labeling of Genomic Loci in Fixed Cells." *Proceedings of the National Academy of Sciences of the United States of America* 112 (38): 11870–75.
- De Sandre-Giovannoli, Annachiara, Rafaëlle Bernard, Pierre Cau, Claire Navarro, Jeanne Amiel, Irène Boccaccio, Stanislas Lyonnet, et al. 2003. "Lamin a Truncation in Hutchinson-Gilford Progeria." *Science* 300 (5628): 2055.
- Diakowski, Witold, Michał Grzybek, and Aleksander F. Sikorski. 2006. "Protein 4.1, a Component of the Erythrocyte Membrane Skeleton and Its Related Homologue Proteins Forming the Protein 4.1/FERM Superfamily." *Folia Histochemica et Cytobiologica / Polish Academy of Sciences, Polish Histochemical and Cytochemical Society* 44 (4): 231–48.
- Digman, Michelle A., Claire M. Brown, Parijat Sengupta, Paul W. Wiseman, Alan R. Horwitz, and Enrico Gratton. 2005. "Measuring Fast Dynamics in Solutions and Cells with a Laser Scanning Microscope." *Biophysical Journal* 89 (2): 1317–27.
- Digman, Michelle A., and Enrico Gratton. 2009. "Fluorescence Correlation Spectroscopy and Fluorescence Cross-Correlation Spectroscopy." *Wiley Interdisciplinary Reviews. Systems Biology and Medicine* 1 (2): 273–82.

- Ding, Xu, Rener Xu, Juehua Yu, Tian Xu, Yuan Zhuang, and Min Han. 2007. "SUN1 Is Required for Telomere Attachment to Nuclear Envelope and Gametogenesis in Mice." *Developmental Cell* 12 (6): 863–72.
- Dittrich, P. S., and P. Schwille. 2001. "Photobleaching and Stabilization Of Fluorophores Used for Single-Molecule Analysis. with One- and Two-Photon Excitation." *Applied Physics. B, Lasers and Optics* 73 (8): 829–37.
- Dolgosheina, Elena V., Sunny C. Y. Jeng, Shanker Shyam S. Panchapakesan, Razvan Cojocar, Patrick S. K. Chen, Peter D. Wilson, Nancy Hawkins, Paul A. Wiggins, and Peter J. Unrau. 2014. "RNA Mango Aptamer-Fluorophore: A Bright, High-Affinity Complex for RNA Labeling and Tracking." *ACS Chemical Biology* 9 (10): 2412–20.
- Donovan, Benjamin T., Anh Huynh, David A. Ball, Heta P. Patel, Michael G. Poirier, Daniel R. Larson, Matthew L. Ferguson, and Tineke L. Lenstra. 2019. "Live-Cell Imaging Reveals the Interplay between Transcription Factors, Nucleosomes, and Bursting." *The EMBO Journal* 38 (12).
<https://doi.org/10.15252/emj.2018100809>.
- Dostie, Josée, Todd A. Richmond, Ramy A. Arnaout, Rebecca R. Selzer, William L. Lee, Tracey A. Honan, Eric D. Rubio, et al. 2006. "Chromosome Conformation Capture Carbon Copy (5C): A Massively Parallel Solution for Mapping Interactions between Genomic Elements." *Genome Research* 16 (10): 1299–1309.
- Dou, Cai-Xia, Chaoyang Liu, Zhan-Ming Ying, Wanrong Dong, Fenglin Wang, and Jian-Hui Jiang. 2021. "Genetically Encoded Dual-Color Light-Up RNA Sensor Enabled Ratiometric Imaging of MicroRNA." *Analytical Chemistry* 93 (4): 2534–40.
- Driscoll, Tristan P., Brian D. Cosgrove, Su-Jin Heo, Zach E. Shurden, and Robert L. Mauck. 2015. "Cytoskeletal to Nuclear Strain Transfer Regulates YAP Signaling in Mesenchymal Stem Cells." *Biophysical Journal* 108 (12): 2783–93.

- Dubińska-Magiera, Magda, Katarzyna Koziół, Magdalena Machowska, Katarzyna Piekarowicz, Daria Filipczak, and Ryszard Rzepecki. 2019. “Emerin Is Required for Proper Nucleus Reassembly after Mitosis: Implications for New Pathogenetic Mechanisms for Laminopathies Detected in EDMD1 Patients.” *Cells* 8 (3). <https://doi.org/10.3390/cells8030240>.
- Dupont C, Armant DR, Brenner CA. 2009. “Epigenetics: definition, mechanisms and clinical perspective.” *Semin Reprod Med.* 27 (5): 351-7.
- Duval, Kayla, Hannah Grover, Li-Hsin Han, Yongchao Mou, Adrian F. Pegoraro, Jeffery Fredberg, and Zi Chen. 2017. “Modeling Physiological Events in 2D vs. 3D Cell Culture.” *Physiology* 32 (4): 266–77.
- Eckersley-Maslin, Melanie A., Jan H. Bergmann, Zsolt Lazar, and David L. Spector. 2013. “Lamin A/C Is Expressed in Pluripotent Mouse Embryonic Stem Cells.” *Nucleus* 4 (1): 53–60.
- ENCODE Project Consortium. 2012. “An Integrated Encyclopedia of DNA Elements in the Human Genome.” *Nature* 489 (7414): 57–74.
- Enderlein, Jörg. 2000. “Tracking of Fluorescent Molecules Diffusing within Membranes.” *Applied Physics. B, Lasers and Optics* 71 (5): 773–77.
- Eng, Chee-Huat Linus, Michael Lawson, Qian Zhu, Ruben Dries, Noushin Koulana, Yodai Takei, Jina Yun, et al. 2019. “Transcriptome-Scale Super-Resolved Imaging in Tissues by RNA seqFISH.” *Nature* 568 (7751): 235–39.
- Essawy, Nada, Camille Samson, Ambre Petitalot, Sophie Moog, Anne Bigot, Isaline Herrada, Agathe Marcelot, Ana-Andreea Arteni, Catherine Coirault, and Sophie Zinn-Justin. 2019. “An Emerin LEM-Domain Mutation Impairs Cell Response to Mechanical Stress.” *Cells* 8 (6). <https://doi.org/10.3390/cells8060570>.
- Fankhauser, David. n.d. “Heliocentric – David Fankhauser.” Accessed April 22, 2021. <https://fankhauserblog.wordpress.com/tag/heliocentric/>.
- Fejer, Szilard N. 2020. “Minimalistic Coarse-Grained Modeling of Viral Capsid Assembly.” *Progress in Molecular Biology and Translational Science* 170: 405–34.

- Femino, A. M., F. S. Fay, K. Fogarty, and R. H. Singer. 1998. "Visualization of Single RNA Transcripts in Situ." *Science* 280 (5363): 585–90.
- Fenn, Sebastian, Dennis Breitsprecher, Christian B. Gerhold, Gregor Witte, Jan Faix, and Karl-Peter Hopfner. 2011. "Structural Biochemistry of Nuclear Actin-Related Proteins 4 and 8 Reveals Their Interaction with Actin." *The EMBO Journal* 30 (11): 2153–66.
- Ferguson, Matthew L., and Daniel R. Larson. 2013. "Measuring Transcription Dynamics in Living Cells Using Fluctuation Analysis." *Methods in Molecular Biology* 1042: 47–60.
- Ferrara, Fortunato, Pawel Listwan, Geoffrey S. Waldo, and Andrew R. M. Bradbury. 2011. "Fluorescent Labeling of Antibody Fragments Using Split GFP." *PloS One* 6 (10): e25727.
- Filonov, Grigory S., Jared D. Moon, Nina Svensen, and Samie R. Jaffrey. 2014. "Broccoli: Rapid Selection of an RNA Mimic of Green Fluorescent Protein by Fluorescence-Based Selection and Directed Evolution." *Journal of the American Chemical Society* 136 (46): 16299–308.
- Furukawa, K., and Y. Hotta. 1993. "cDNA Cloning of a Germ Cell Specific Lamin B3 from Mouse Spermatocytes and Analysis of Its Function by Ectopic Expression in Somatic Cells." *The EMBO Journal* 12 (1): 97–106.
- Furusawa, Takashi, Mark Rochman, Leila Taher, Emiliós K. Dimitriadis, Kunio Nagashima, Stasia Anderson, and Michael Bustin. 2015. "Chromatin Decompaction by the Nucleosomal Binding Protein HMGN5 Impairs Nuclear Sturdiness." *Nature Communications* 6 (January): 6138.
- Gao, Qian, Ranjha Khan, Changping Yu, Manfred Alsheimer, Xiaohua Jiang, Hui Ma, and Qinghua Shi. 2020. "The Testis-Specific LINC Component SUN3 Is Essential for Sperm Head Shaping during Mouse Spermiogenesis." *The Journal of Biological Chemistry* 295 (19): 6289–98.

- Garcia, David A., Gregory Fettweis, Diego M. Presman, Ville Paakinaho, Christopher Jarzynski, Arpita Upadhyaya, and Gordon L. Hager. 2021. "Power-Law Behavior of Transcription Factor Dynamics at the Single-Molecule Level Implies a Continuum Affinity Model." *Nucleic Acids Research*, February. <https://doi.org/10.1093/nar/gkab072>.
- Gardel, M. L., M. T. Valentine, and D. A. Weitz. 2005. "Microrheology." *Microscale Diagnostic Techniques*. http://link.springer.com/chapter/10.1007/3-540-26449-3_1.
- Gelman, Andrew, Carlin, John B., Stern, Hal S., Dunson, David B., Vehtari, Aki, Rubin, Donald B. 2013. "Bayesian Data Analysis, Third Edition." *Chapman and Hall/CRC*. ISBN 978-1-4398-4095-5.
- Gerardo, Heloísa, Ana Lima, João Carvalho, João R. D. Ramos, Sofia Couceiro, Rui D. M. Travasso, Ricardo Pires das Neves, and Mário Grãos. 2019. "Soft Culture Substrates Favor Stem-like Cellular Phenotype and Facilitate Reprogramming of Human Mesenchymal Stem/stromal Cells (hMSCs) through Mechanotransduction." *Scientific Reports* 9 (1): 9086.
- Germann, James A., and Lloyd M. Davis. 2014. "Three-Dimensional Tracking of a Single Fluorescent Nanoparticle Using Four-Focus Excitation in a Confocal Microscope." *Optics Express* 22 (5): 5641–50.
- Ghosh, Soham, James G. Cimino, Adrienne K. Scott, Frederick W. Damen, Evan H. Phillips, Alexander I. Veress, Corey P. Neu, and Craig J. Goergen. 2017. "In Vivo Multiscale and Spatially-Dependent Biomechanics Reveals Differential Strain Transfer Hierarchy in Skeletal Muscle." *ACS Biomaterials Science & Engineering* 3 (11): 2798–2805.
- Ghosh, Soham, Victor Crespo Cuevas, Benjamin Seelbinder, and Corey P. Neu. 2020. "Image-Based Elastography of Heterochromatin and Euchromatin Domains in the Deforming Cell Nucleus." *bioRxiv*. <https://doi.org/10.1101/2020.04.17.047654>.

- Ghosh, Soham, Benjamin Seelbinder, Jonathan T. Henderson, Ryan D. Watts, Adrienne K. Scott, Alexander I. Veress, and Corey P. Neu. 2019. "Deformation Microscopy for Dynamic Intracellular and Intranuclear Mapping of Mechanics with High Spatiotemporal Resolution." *Cell Reports* 27 (5): 1607–20.e4.
- Gilchrist, Christopher L., Sietske W. Witvoet-Braam, Farshid Guilak, and Lori A. Setton. 2007. "Measurement of Intracellular Strain on Deformable Substrates with Texture Correlation." *Journal of Biomechanics* 40 (4): 786–94.
- Goelzer, Matthew, Amel Dudakovic, Melis Olcum, Buer Sen, Engin Ozcivici, Janet Rubin, Andre J. van Wijnen, and Gunes Uzer. 2020. "Lamin A/C Functions Independently from Mechanical Signaling during Adipogenesis." <https://doi.org/10.1101/2020.09.07.279828>.
- Goldberg, Martin W. 2017. "Nuclear Pore Complex Tethers to the Cytoskeleton." *Seminars in Cell & Developmental Biology* 68 (August): 52–58.
- Grashoff, Carsten, Brenton D. Hoffman, Michael D. Brenner, Ruobo Zhou, Maddy Parsons, Michael T. Yang, Mark A. McLean, et al. 2010. "Measuring Mechanical Tension across Vinculin Reveals Regulation of Focal Adhesion Dynamics." *Nature* 466 (7303): 263–66.
- Grasland-Mongrain, Pol, Ali Zorgani, Shoma Nakagawa, Simon Bernard, Lia Gomes Paim, Greg Fitzharris, Stefan Catheline, and Guy Cloutier. 2018. "Ultrafast Imaging of Cell Elasticity with Optical Microelastography." *Proceedings of the National Academy of Sciences of the United States of America* 115 (5): 861–66.
- Grimm, Jonathan B., Brian P. English, Heejun Choi, Anand K. Muthusamy, Brian P. Mehl, Peng Dong, Timothy A. Brown, et al. 2016. "Bright Photoactivatable Fluorophores for Single-Molecule Imaging." *Nature Methods* 13 (12): 985–88.
- Grimm, Jonathan B., Anand K. Muthusamy, Yajie Liang, Timothy A. Brown, William C. Lemon, Ronak Patel, Rongwen Lu, et al. 2017. "A General Method to Fine-Tune Fluorophores for Live-Cell and in Vivo Imaging." *Nature Methods* 14 (10): 987–94.

- Grimm, Jonathan B., Ariana N. Tkachuk, Liangqi Xie, Heejun Choi, Boaz Mohar, Natalie Falco, Kathy Schaefer, et al. 2020. "A General Method to Optimize and Functionalize Red-Shifted Rhodamine Dyes." *Nature Methods* 17 (8): 815–21.
- Grubert, Fabian, Rohith Srivas, Damek V. Spacek, Maya Kasowski, Mariana Ruiz-Velasco, Nasa Sinnott-Armstrong, Peyton Greenside, et al. 2020. "Landscape of Cohesin-Mediated Chromatin Loops in the Human Genome." *Nature* 583 (7818): 737–43.
- Grummt, Ingrid. 2006. "Actin and Myosin as Transcription Factors." *Current Opinion in Genetics & Development* 16 (2): 191–96.
- Guelen, Lars, Ludo Pagie, Emilie Brassat, Wouter Meuleman, Marius B. Faza, Wendy Talhout, Bert H. Eussen, et al. 2008. "Domain Organization of Human Chromosomes Revealed by Mapping of Nuclear Lamina Interactions." *Nature* 453 (7197): 948–51.
- Guilak, F., A. Ratcliffe, and V. C. Mow. 1995. "Chondrocyte Deformation and Local Tissue Strain in Articular Cartilage: A Confocal Microscopy Study." *Journal of Orthopaedic Research: Official Publication of the Orthopaedic Research Society* 13 (3): 410–21.
- Guilak, F., J. R. Tedrow, and R. Burgkart. 2000. "Viscoelastic Properties of the Cell Nucleus." *Biochemical and Biophysical Research Communications* 269 (3): 781–86.
- Guilluy, Christophe, Lukas D. Osborne, Laurianne Van Landeghem, Lisa Sharek, Richard Superfine, Rafael Garcia-Mata, and Keith Burridge. 2014. "Isolated Nuclei Adapt to Force and Reveal a Mechanotransduction Pathway in the Nucleus." *Nature Cell Biology* 16 (4): 376–81.
- Guo, Dong-Ge, Dian-Bing Wang, Chong Liu, Song Lu, Yu Hou, and Xian-En Zhang. 2019. "CRISPR-Based Genomic Loci Labeling Revealed Ordered Spatial Organization of Chromatin in Living Diploid Human Cells." *Biochimica et Biophysica Acta, Molecular Cell Research* 1866 (12): 118518.

- Ha, T., T. Enderle, D. F. Ogletree, D. S. Chemla, P. R. Selvin, and S. Weiss. 1996. "Probing the Interaction between Two Single Molecules: Fluorescence Resonance Energy Transfer between a Single Donor and a Single Acceptor." *Proceedings of the National Academy of Sciences of the United States of America* 93 (13): 6264–68.
- Hager, Gordon L., James G. McNally, and Tom Misteli. 2009. "Transcription Dynamics." *Molecular Cell* 35 (6): 741–53.
- Han, Shuo, Boxuan Simen Zhao, Samuel A. Myers, Steven A. Carr, Chuan He, and Alice Y. Ting. 2020. "RNA–protein Interaction Mapping via MS2- or Cas13-Based APEX Targeting." *Proceedings of the National Academy of Sciences of the United States of America* 117 (36): 22068–79.
- Haque, Farhana, David J. Lloyd, Dawn T. Smallwood, Carolyn L. Dent, Catherine M. Shanahan, Andrew M. Fry, Richard C. Trembath, and Sue Shackleton. 2006. "SUN1 Interacts with Nuclear Lamin A and Cytoplasmic Nesprins to Provide a Physical Connection between the Nuclear Lamina and the Cytoskeleton." *Molecular and Cellular Biology* 26 (10): 3738–51.
- Haque, Farhana, Daniela Mazzeo, Jennifer T. Patel, Dawn T. Smallwood, Juliet A. Ellis, Catherine M. Shanahan, and Sue Shackleton. 2010. "Mammalian SUN Protein Interaction Networks at the Inner Nuclear Membrane and Their Role in Laminopathy Disease Processes." *The Journal of Biological Chemistry* 285 (5): 3487–98.
- Harada, Takamasa, Joe Swift, Jerome Irianto, Jae-Won Shin, Kyle R. Spinler, Avathamsa Athirasala, Rocky Diegmiller, P. C. Dave P. Dingal, Irena L. Ivanovska, and Dennis E. Discher. 2014. "Nuclear Lamin Stiffness Is a Barrier to 3D Migration, but Softness Can Limit Survival." *The Journal of Cell Biology* 204 (5): 669–82.
- Haudenschild, Dominik R., Jianfen Chen, Nina Pang, Nikolai Steklov, Shawn P. Grogan, Martin K. Lotz, and Darryl D. D’Lima. 2011. "Vimentin Contributes to Changes in Chondrocyte Stiffness in Osteoarthritis." *Journal of Orthopaedic Research: Official Publication of the Orthopaedic Research Society* 29 (1): 20–25.

- Hayashi-Takanaka, Yoko, Kazuo Yamagata, Teruhiko Wakayama, Timothy J. Stasevich, Takashi Kainuma, Toshiki Tsurimoto, Makoto Tachibana, et al. 2011. "Tracking Epigenetic Histone Modifications in Single Cells Using Fab-Based Live Endogenous Modification Labeling." *Nucleic Acids Research* 39 (15): 6475–88.
- Hell, Stefan W., and Jan Wichmann. 1994. "Breaking the Diffraction Resolution Limit by Stimulated Emission: Stimulated-Emission-Depletion Fluorescence Microscopy." *Optics Letters*. <https://doi.org/10.1364/ol.19.000780>.
- Henderson, Jonathan T., Garrett Shannon, Alexander I. Veress, and Corey P. Neu. 2013. "Direct Measurement of Intranuclear Strain Distributions and RNA Synthesis in Single Cells Embedded within Native Tissue." *Biophysical Journal* 105 (10): 2252–61.
- Hernandez, Lidia, Kyle J. Roux, Esther Sook Miin Wong, Leslie C. Mounkes, Rafidah Mutalif, Raju Navasankari, Bina Rai, et al. 2010. "Functional Coupling between the Extracellular Matrix and Nuclear Lamina by Wnt Signaling in Progeria." *Developmental Cell* 19 (3): 413–25.
- Hnisz, Denes, Krishna Shrinivas, Richard A. Young, Arup K. Chakraborty, and Phillip A. Sharp. 2017. "A Phase Separation Model for Transcriptional Control." *Cell* 169 (1): 13–23.
- Ho, Brandon, Anastasia Baryshnikova, and Grant W. Brown. 2018. "Unification of Protein Abundance Datasets Yields a Quantitative *Saccharomyces Cerevisiae* Proteome." *Cell Systems* 6 (2): 192–205.e3.
- Ho, Chin Yee, Diana E. Jaalouk, Maria K. Vartiainen, and Jan Lammerding. 2013. "Lamin A/C and Emerin Regulate MKL1-SRF Activity by Modulating Actin Dynamics." *Nature* 497 (7450): 507–11.
- Ho, Chin Yee, and Jan Lammerding. 2012. "Lamins at a Glance." *Journal of Cell Science* 125 (Pt 9): 2087–93.
- Höfling, Felix, and Thomas Franosch. 2013. "Anomalous Transport in the Crowded World of Biological Cells." *Reports on Progress in Physics* 76 (4): 046602.

- Holaska, James M., Amy K. Kowalski, and Katherine L. Wilson. 2004. "Emerin Caps the Pointed End of Actin Filaments: Evidence for an Actin Cortical Network at the Nuclear Inner Membrane." *PLoS Biology* 2 (9): E231.
- Holaska, James M., and Katherine L. Wilson. 2007. "An Emerin 'Proteome': Purification of Distinct Emerin-Containing Complexes from HeLa Cells Suggests Molecular Basis for Diverse Roles Including Gene Regulation, mRNA Splicing, Signaling, Mechanosensing, and Nuclear Architecture." *Biochemistry* 46 (30): 8897–8908.
- Holaska, James M., Katherine L. Wilson, and Malini Mansharamani. 2002. "The Nuclear Envelope, Lamins and Nuclear Assembly." *Current Opinion in Cell Biology* 14 (3): 357–64.
- Horn, Henning F., Dae In Kim, Graham D. Wright, Esther Sook Miin Wong, Colin L. Stewart, Brian Burke, and Kyle J. Roux. 2013. "A Mammalian KASH Domain Protein Coupling Meiotic Chromosomes to the Cytoskeleton." *The Journal of Cell Biology* 202 (7): 1023–39.
- Hospital, Adam, Josep Ramon Goñi, Modesto Orozco, and Josep L. Gelpí. 2015. "Molecular Dynamics Simulations: Advances and Applications." *Advances and Applications in Bioinformatics and Chemistry: AABC* 8 (November): 37–47.
- Hou, Shangguo, Xiaoqi Lang, and Kevin Welsher. 2017. "Robust Real-Time 3D Single-Particle Tracking Using a Dynamically Moving Laser Spot." *Optics Letters* 42 (12): 2390–93.
- Hou, Weiwei, Denghui Zhang, Xiaoxia Feng, and Yi Zhou. 2020. "Low Magnitude High Frequency Vibration Promotes Chondrogenic Differentiation of Bone Marrow Stem Cells with Involvement of β -Catenin Signaling Pathway." *Archives of Oral Biology* 118 (July): 104860.
- Hsu, Chih-Yi, Robert J. Kurman, Russell Vang, Tian-Li Wang, Jan Baak, and Ie-Ming Shih. 2005. "Nuclear Size Distinguishes Low- from High-Grade Ovarian Serous Carcinoma and Predicts Outcome." *Human Pathology* 36 (10): 1049–54.

Im, Kyuseok, Sergey Mareninov, M. Fernando Palma Diaz, and William H. Yong. 2019. “An Introduction to Performing Immunofluorescence Staining.” *Methods in Molecular Biology* 1897: 299–311.

Indelicato, Giuliana, Paolo Cermelli, and Reidun Twarock. 2019. “A Coarse-Grained Model of the Expansion of the Human Rhinovirus 2 Capsid Reveals Insights in Genome Release.” *Journal of the Royal Society, Interface / the Royal Society* 16 (157): 20190044.

Iyer, K. Venkatesan, S. Pulford, A. Mogilner, and G. V. Shivashankar. 2012. “Mechanical Activation of Cells Induces Chromatin Remodeling Preceding MKL Nuclear Transport.” *Biophysical Journal* 103 (7): 1416–28.

Jaffe, Aron B., and Alan Hall. 2005. “Rho GTPases: Biochemistry and Biology.” *Annual Review of Cell and Developmental Biology* 21: 247–69.

Jaiswal, Devina, Zoe Moscato, Yuji Tomizawa, Kevin P. Claffey, and Kazunori Hoshino. 2019. “Elastography of Multicellular Spheroids Using 3D Light Microscopy.” *Biomedical Optics Express* 10 (5): 2409–18.

Jamieson K, Wiles ET, McNaught KJ, Sidoli S, Leggett N, Shao Y, Garcia BA, Selker EU. 2016. “Loss of HP1 causes depletion of H3K27me3 from facultative heterochromatin and gain of H3K27me2 at constitutive heterochromatin.” *Genome Res.* 26 (1): 97-107

Jeng, Sunny Scy, Robert J. Trachman 3rd, Florian Weissenboeck, Lynda Troung, Katie Link, Mette B. Jepsen, Jay Knutson, Ebbe Andersen, Adrian R. Ferré-D’Amaré, and Peter J. Unrau. 2020. “Fluorogenic Aptamers Resolve the Flexibility of RNA Junctions Using Orientation-Dependent FRET.” *RNA*, December. <https://doi.org/10.1261/rna.078220.120>.

Kanchanawong, Pakorn, Gleb Shtengel, Ana M. Pasapera, Ericka B. Ramko, Michael W. Davidson, Harald F. Hess, and Clare M. Waterman. 2010. “Nanoscale Architecture of Integrin-Based Cell Adhesions.” *Nature* 468 (7323): 580–84.

- Kapoor, Prabodh, Mingming Chen, Duane David Winkler, Karolin Luger, and Xuotong Shen. 2013. "Evidence for Monomeric Actin Function in INO80 Chromatin Remodeling." *Nature Structural & Molecular Biology* 20 (4): 426–32.
- Kapuscinski, J. 1995. "DAPI: A DNA-Specific Fluorescent Probe." *Biotechnic & Histochemistry: Official Publication of the Biological Stain Commission* 70 (5): 220–33.
- Kapuściński, J., and B. Skoczylas. 1978. "Fluorescent Complexes of DNA with DAPI 4',6-Diamidine-2-Phenyl indole.2HCl or DCI 4',6-Dicarboxyamide-2-Phenyl Indole." *Nucleic Acids Research* 5 (10): 3775–99.
- Kawashima, Satoshi, Hideaki Ogiwara, Shusuke Tada, Masahiko Harata, Ulrike Wintersberger, Takemi Enomoto, and Masayuki Seki. 2007. "The INO80 Complex Is Required for Damage-Induced Recombination." *Biochemical and Biophysical Research Communications* 355 (3): 835–41.
- Kennedy, Kelsey M., Lixin Chin, Robert A. McLaughlin, Bruce Latham, Christobel M. Saunders, David D. Sampson, and Brendan F. Kennedy. 2015. "Quantitative Micro-Elastography: Imaging of Tissue Elasticity Using Compression Optical Coherence Elastography." *Scientific Reports*. <https://doi.org/10.1038/srep15538>.
- Khatau, Shyam B., Christopher M. Hale, P. J. Stewart-Hutchinson, Meet S. Patel, Colin L. Stewart, Peter C. Searson, Didier Hodzic, and Denis Wirtz. 2009. "A Perinuclear Actin Cap Regulates Nuclear Shape." *Proceedings of the National Academy of Sciences of the United States of America* 106 (45): 19017–22.
- Killaars, Anouk R., Cierra J. Walker, and Kristi S. Anseth. 2020. "Nuclear Mechanosensing Controls MSC Osteogenic Potential through HDAC Epigenetic Remodeling." *Proceedings of the National Academy of Sciences of the United States of America* 117 (35): 21258–66.
- Kim, Jae-Yeol, Cheolhee Kim, and Nam Ki Lee. 2015. "Real-Time Submillisecond Single-Molecule FRET Dynamics of Freely Diffusing Molecules with Liposome Tethering." *Nature Communications* 6 (April): 6992.

- Kim, Jeong-Ki, Arghavan Louhghalam, Geonhui Lee, Benjamin W. Schafer, Denis Wirtz, and Dong-Hwee Kim. 2017. "Nuclear Lamin A/C Harnesses the Perinuclear Apical Actin Cables to Protect Nuclear Morphology." *Nature Communications* 8 (1): 2123.
- Kim, Sally A., Katrin G. Heinze, and Petra Schwille. 2007. "Fluorescence Correlation Spectroscopy in Living Cells." *Nature Methods* 4 (11): 963–73.
- Kim, Youngjo, Xiaobin Zheng, and Yixian Zheng. 2019. "Role of Lamins in 3D Genome Organization and Global Gene Expression." *Nucleus* 10 (1): 33–41.
- Kishi, Jocelyn Y., Sylvain W. Lapan, Brian J. Beliveau, Emma R. West, Allen Zhu, Hiroshi M. Sasaki, Sinem K. Saka, Yu Wang, Constance L. Cepko, and Peng Yin. 2019. "SABER Amplifies FISH: Enhanced Multiplexed Imaging of RNA and DNA in Cells and Tissues." *Nature Methods* 16 (6): 533–44.
- Kis-Petikova, Katarina, and Enrico Gratton. 2004. "Distance Measurement by Circular Scanning of the Excitation Beam in the Two-Photon Microscope." *Microscopy Research and Technique* 63 (1): 34–49.
- Klemm, S.L., Shipony, Z. & Greenleaf, W.J. 2019. "Chromatin accessibility and the regulatory epigenome." *Nat Rev Genet* 20, 207–220.
- Knight, M. M., J. van de Breevaart Bravenboer, D. A. Lee, G. J. V. M. van Osch, H. Weinans, and D. L. Bader. 2002. "Cell and Nucleus Deformation in Compressed Chondrocyte–alginate Constructs: Temporal Changes and Calculation of Cell Modulus." *Biochimica et Biophysica Acta (BBA) - General Subjects* 1570 (1): 1–8.
- Kong, Kristen Y. S., Sunny C. Y. Jeng, Batool Rayyan, and Peter J. Unrau. 2021. "RNA Peach and Mango: Orthogonal Two-Color Fluorogenic Aptamers Distinguish Nearly Identical Ligands." *RNA*, March. <https://doi.org/10.1261/rna.078493.120>.
- Kramer, Susanne, Elisabeth Meyer-Natus, Christian Stigloher, Hanna Thoma, Achim Schnauffer, and Markus Engstler. 2021. "Parallel Monitoring of RNA Abundance, Localization and Compactness with Correlative Single Molecule FISH on LR White Embedded Samples." *Nucleic Acids Research* 49 (3): e14.

- Krieger, Jan W., Anand P. Singh, Nirmalya Bag, Christoph S. Garbe, Timothy E. Saunders, Jörg Langowski, and Thorsten Wohland. 2015. "Imaging Fluorescence (cross-) Correlation Spectroscopy in Live Cells and Organisms." *Nature Protocols* 10 (12): 1948–74.
- Kudalkar, Emily M., Trisha N. Davis, and Charles L. Asbury. 2016. "Single-Molecule Total Internal Reflection Fluorescence Microscopy." *Cold Spring Harbor Protocols* 2016 (5). <https://doi.org/10.1101/pdb.top077800>.
- Kumar, Abhishek, and G. V. Shivashankar. 2016. "Dynamic Interaction between Actin and nesprin2 Maintain the Cell Nucleus in a Prestressed State." *Methods and Applications in Fluorescence* 4 (4): 044008.
- Kumar, Abhishek, Yicong Wu, Ryan Christensen, Panagiotis Chandris, William Gandler, Evan McCreedy, Alexandra Bokinsky, et al. 2014. "Dual-View Plane Illumination Microscopy for Rapid and Spatially Isotropic Imaging." *Nature Protocols* 9 (11): 2555–73.
- Lammerding, Jan, Loren G. Fong, Julie Y. Ji, Karen Reue, Colin L. Stewart, Stephen G. Young, and Richard T. Lee. 2006. "Lamins A and C but Not Lamin B1 Regulate Nuclear Mechanics." *The Journal of Biological Chemistry* 281 (35): 25768–80.
- Lander, E. S., L. M. Linton, B. Birren, C. Nusbaum, M. C. Zody, J. Baldwin, K. Devon, et al. 2001. "Initial Sequencing and Analysis of the Human Genome." *Nature* 409 (6822): 860–921.
- Larson, D. R., D. Zenklusen, B. Wu, J. A. Chao, and R. H. Singer. 2011. "Real-Time Observation of Transcription Initiation and Elongation on an Endogenous Yeast Gene." *Science* 332 (6028): 475–78.
- Latt, S. A., G. Stetten, L. A. Juergens, H. F. Willard, and C. D. Scher. 1975. "Recent Developments in the Detection of Deoxyribonucleic Acid Synthesis by 33258 Hoechst Fluorescence." *The Journal of Histochemistry and Cytochemistry: Official Journal of the Histochemistry Society* 23 (7): 493–505.

- Leemans, Christ, Marloes C. H. van der Zwalm, Laura Brueckner, Federico Comoglio, Tom van Schaik, Ludo Pagie, Joris van Arensbergen, and Bas van Steensel. 2019. “Promoter-Intrinsic and Local Chromatin Features Determine Gene Repression in LADs.” *Cell* 177 (4): 852–64.e14.
- Le, Huy Quang, Sushmita Ghatak, Ching-Yan Chloé Yeung, Frederik Tellkamp, Christian Günschmann, Christoph Dieterich, Assa Yeroslaviz, et al. 2016. “Mechanical Regulation of Transcription Controls Polycomb-Mediated Gene Silencing during Lineage Commitment.” *Nature Cell Biology* 18 (8): 864–75.
- Lenstra, Tineke L., Antoine Coulon, Carson C. Chow, and Daniel R. Larson. 2015. “Single-Molecule Imaging Reveals a Switch between Spurious and Functional ncRNA Transcription.” *Molecular Cell* 60 (4): 597–610.
- Lenstra, Tineke L., and Daniel R. Larson. 2016. “Single-Molecule mRNA Detection in Live Yeast.” *Current Protocols in Molecular Biology / Edited by Frederick M. Ausubel ... [et Al.]* 113 (January): 14.24.1–14.24.15.
- Leslie, Sabrina R., Alexander P. Fields, and Adam E. Cohen. 2010. “Convex Lens-Induced Confinement for Imaging Single Molecules.” *Analytical Chemistry*. <https://doi.org/10.1021/ac101041s>.
- Lessard, Guillaume A., Peter M. Goodwin, and James H. Werner. 2007. “Three-Dimensional Tracking of Individual Quantum Dots.” *Applied Physics Letters* 91 (22): 224106.
- Levi, Valeria, and Enrico Gratton. 2007. “Exploring Dynamics in Living Cells by Tracking Single Particles.” *Cell Biochemistry and Biophysics* 48 (1): 1–15.
- Levi, Valeria, Qiaoqiao Ruan, and Enrico Gratton. 2005. “3-D Particle Tracking in a Two-Photon Microscope: Application to the Study of Molecular Dynamics in Cells.” *Biophysical Journal* 88 (4): 2919–28.
- Levi, V., Q. Ruan, K. Kis-Petikova, and E. Gratton. 2003. “Scanning FCS, a Novel Method for Three-Dimensional Particle Tracking.” *Biochemical Society Transactions* 31 (Pt 5): 997–1000.

- Levi, V., Q. Ruan, M. Plutz, A. S. Belmont, and E. Gratton. 2005. "Chromatin Dynamics in Interphase Cells Revealed by Tracking in a Two-Photon Excitation Microscope." *Biophysical Journal* 89 (6): 4275–85.
- Libotte, Thorsten, Hafida Zaim, Sabu Abraham, V. C. Padmakumar, Maria Schneider, Wenshu Lu, Martina Munck, et al. 2005. "Lamin A/C-Dependent Localization of Nesprin-2, a Giant Scaffold at the Nuclear Envelope." *Molecular Biology of the Cell* 16 (7): 3411–24.
- Lieberman-Aiden, Erez, Nynke L. van Berkum, Louise Williams, Maxim Imakaev, Tobias Ragozy, Agnes Telling, Ido Amit, et al. 2009. "Comprehensive Mapping of Long-Range Interactions Reveals Folding Principles of the Human Genome." *Science* 326 (5950): 289–93.
- Li, G., G. Sudlow, and A. S. Belmont. 1998. "Interphase Cell Cycle Dynamics of a Late-Replicating, Heterochromatic Homogeneously Staining Region: Precise Choreography of Condensation/decondensation and Nuclear Positioning." *The Journal of Cell Biology* 140 (5): 975–89.
- Lim, Kai Y., Jonathan T. Henderson, and Corey P. Neu. 2013. "Cell and Tissue Deformation Measurements: Texture Correlation with Third-Order Approximation of Displacement Gradients." *Journal of Biomechanics* 46 (14): 2490–96.
- Lin, F., and H. J. Worman. 1993. "Structural Organization of the Human Gene Encoding Nuclear Lamin A and Nuclear Lamin C." *The Journal of Biological Chemistry* 268 (22): 16321–26.
- Liu, Qian, Dae In Kim, Janet Syme, Phyllis LuValle, Brian Burke, and Kyle J. Roux. 2010. "Dynamics of Lamin-A Processing Following Precursor Accumulation." *PloS One* 5 (5): e10874.
- Li, Yubin, Minghui Li, Bettina Weigel, Moritz Mall, Victoria P. Werth, and Ming-Lin Liu. 2020. "Nuclear Envelope Rupture and NET Formation Is Driven by PKC α -Mediated Lamin B Disassembly." *EMBO Reports* 21 (8): e48779.

- Lombardi, Maria L., Diana E. Jaalouk, Catherine M. Shanahan, Brian Burke, Kyle J. Roux, and Jan Lammerding. 2011. "The Interaction between Nesprins and Sun Proteins at the Nuclear Envelope Is Critical for Force Transmission between the Nucleus and Cytoskeleton." *The Journal of Biological Chemistry* 286 (30): 26743–53.
- Los, Georgyi V., Lance P. Encell, Mark G. McDougall, Danette D. Hartzell, Natasha Karassina, Chad Zimprich, Monika G. Wood, et al. 2008. "HaloTag: A Novel Protein Labeling Technology for Cell Imaging and Protein Analysis." *ACS Chemical Biology* 3 (6): 373–82.
- Lottersberger, Francisca, Roos Anna Karssemeijer, Nadya Dimitrova, and Titia de Lange. 2015. "53BP1 and the LINC Complex Promote Microtubule-Dependent DSB Mobility and DNA Repair." *Cell* 163 (4): 880–93.
- Lu, H. P., L. Xun, and X. S. Xie. 1998. "Single-Molecule Enzymatic Dynamics." *Science* 282 (5395): 1877–82.
- Lund, Eivind G., Isabelle Duband-Goulet, Anja Oldenburg, Brigitte Buendia, and Philippe Collas. 2015. "Distinct Features of Lamin A-Interacting Chromatin Domains Mapped by ChIP-Sequencing from Sonicated or Micrococcal Nuclease-Digested Chromatin." *Nucleus* 6 (1): 30–39.
- Luo, Yibo, In-Won Lee, Yu-Jin Jo, Suk Namgoong, and Nam-Hyung Kim. 2016. "Depletion of the LINC Complex Disrupts Cytoskeleton Dynamics and Meiotic Resumption in Mouse Oocytes." *Scientific Reports* 6 (February): 20408.
- Machesky, L. M., and R. H. Insall. 1998. "Scar1 and the Related Wiskott-Aldrich Syndrome Protein, WASP, Regulate the Actin Cytoskeleton through the Arp2/3 Complex." *Current Biology: CB* 8 (25): 1347–56.
- Magde, D., E. L. Elson, and W. W. Webb. 1974. "Fluorescence Correlation Spectroscopy. II. An Experimental Realization." *Biopolymers* 13 (1): 29–61.

- Ma, Hanhui, Li-Chun Tu, Ardalan Naseri, Maximiliaan Huisman, Shaojie Zhang, David Grunwald, and Thoru Pederson. 2016. "Multiplexed Labeling of Genomic Loci with dCas9 and Engineered sgRNAs Using CRISPRainbow." *Nature Biotechnology* 34 (5): 528–30.
- Makhija, Ekta, D. S. Jokhun, and G. V. Shivashankar. 2016. "Nuclear Deformability and Telomere Dynamics Are Regulated by Cell Geometric Constraints." *Proceedings of the National Academy of Sciences of the United States of America* 113 (1): E32–40.
- Mammoto, Akiko, Tadanori Mammoto, and Donald E. Ingber. 2012. "Mechanosensitive Mechanisms in Transcriptional Regulation." *Journal of Cell Science* 125 (Pt 13): 3061–73.
- Maston, Glenn A., Sara K. Evans, and Michael R. Green. 2006. "Transcriptional Regulatory Elements in the Human Genome." *Annual Review of Genomics and Human Genetics* 7: 29–59.
- Mathieu, Pattie S., and Elizabeth G. Lobo. 2012. "Cytoskeletal and Focal Adhesion Influences on Mesenchymal Stem Cell Shape, Mechanical Properties, and Differentiation down Osteogenic, Adipogenic, and Chondrogenic Pathways." *Tissue Engineering. Part B, Reviews* 18 (6): 436–44.
- Mazza, Davide, Timothy J. Stasevich, Tatiana S. Karpova, and James G. McNally. 2012. "Monitoring Dynamic Binding of Chromatin Proteins in Vivo by Fluorescence Correlation Spectroscopy and Temporal Image Correlation Spectroscopy." *Methods in Molecular Biology* 833: 177–200.
- Mazza, D., F. Mueller, T. J. Stasevich, and J. G. McNally. 2013. "Convergence of Chromatin Binding Estimates in Live Cells." *Nature Methods* 10 (8): 691–92.
- McCreery, Kaitlin P., Xin Xu, Adrienne K. Scott, Apresio K. Fajrial, Sarah Calve, Xiaoyun Ding, and Corey P. Neu. 2020. "Nuclear Stiffness Decreases with Disruption of the Extracellular Matrix in Living Tissues." *bioRxiv*.
<https://doi.org/10.1101/2020.08.28.273052>.

- McGeown, J. Graham. 2010. "Seeing Is Believing! Imaging Ca²⁺-Signalling Events in Living Cells." *Experimental Physiology* 95 (11): 1049–60.
- Meinke, Peter, Elisabetta Mattioli, Farhana Haque, Susumu Antoku, Marta Columbaro, Kees R. Straatman, Howard J. Worman, et al. 2014. "Muscular Dystrophy-Associated SUN1 and SUN2 Variants Disrupt Nuclear-Cytoskeletal Connections and Myonuclear Organization." *PLoS Genetics* 10 (9): e1004605.
- Mellad, Jason A., Derek T. Warren, and Catherine M. Shanahan. 2011. "Nesprins LINC the Nucleus and Cytoskeleton." *Current Opinion in Cell Biology* 23 (1): 47–54.
- Meyer, Adam J., Donna K. Almendrala, Minjoung M. Go, and Sharon Wald Krauss. 2011. "Structural Protein 4.1R Is Integrally Involved in Nuclear Envelope Protein Localization, Centrosome-Nucleus Association and Transcriptional Signaling." *Journal of Cell Science* 124 (Pt 9): 1433–44.
- Meyer, Mark B., Nancy A. Benkusky, Buer Sen, Janet Rubin, and J. Wesley Pike. 2016. "Epigenetic Plasticity Drives Adipogenic and Osteogenic Differentiation of Marrow-Derived Mesenchymal Stem Cells." *The Journal of Biological Chemistry* 291 (34): 17829–47.
- Michelman-Ribeiro, Ariel, Davide Mazza, Tilman Rosales, Timothy J. Stasevich, Hacene Boukari, Vikas Rishi, Charles Vinson, Jay R. Knutson, and James G. McNally. 2009. "Direct Measurement of Association and Dissociation Rates of DNA Binding in Live Cells by Fluorescence Correlation Spectroscopy." *Biophysical Journal* 97 (1): 337–46.
- Mishra, Dhruva K., Chad J. Creighton, Yiquan Zhang, Don L. Gibbons, Jonathan M. Kurie, and Min P. Kim. 2014. "Gene Expression Profile of A549 Cells from Tissue of 4D Model Predicts Poor Prognosis in Lung Cancer Patients." *International Journal of Cancer. Journal International Du Cancer* 134 (4): 789–98.

- Mislow, John M. K., James M. Holaska, Marian S. Kim, Kenneth K. Lee, Miriam Segura-Totten, Katherine L. Wilson, and Elizabeth M. McNally. 2002. "Nesprin-1alpha Self-Associates and Binds Directly to Emerin and Lamin A in Vitro." *FEBS Letters* 525 (1-3): 135–40.
- Moerner, W. E., and M. Orrit. 1999. "Illuminating Single Molecules in Condensed Matter." *Science* 283 (5408): 1670–76.
- Morisaki, Tatsuya, Kenneth Lyon, Keith F. DeLuca, Jennifer G. DeLuca, Brian P. English, Zhengjian Zhang, Luke D. Lavis, et al. 2016. "Real-Time Quantification of Single RNA Translation Dynamics in Living Cells." *Science* 352 (6292): 1425–29.
- Morita, Sumiyo, Takuro Horii, Mika Kimura, and Izuhito Hatada. 2020. "Synergistic Upregulation of Target Genes by TET1 and VP64 in the dCas9-SunTag Platform." *International Journal of Molecular Sciences* 21 (5). <https://doi.org/10.3390/ijms21051574>.
- Nava, Michele M., Yekaterina A. Miroshnikova, Leah C. Biggs, Daniel B. Whitefield, Franziska Metge, Jorge Boucas, Helena Vihinen, et al. 2020. "Heterochromatin-Driven Nuclear Softening Protects the Genome against Mechanical Stress-Induced Damage." *Cell* 181 (4): 800–817.e22.
- Newville, Matthew, Till Stensitzki, Daniel B. Allen, Michal Rawlik, Antonino Ingargiola, and Andrew Nelson. 2016. "Lmfit: Non-Linear Least-Square Minimization and Curve-Fitting for Python." *Astrophysics Source Code Library*. <https://ui.adsabs.harvard.edu/abs/2016ascl.soft06014N>.
- "Night Sky Viewing." n.d. Accessed April 22, 2021. <https://www.nps.gov/deto/planyourvisit/night-sky-viewing.htm>.
- N Peterson, Scott, and Keehwan Kwon. 2012. "The HaloTag: Improving Soluble Expression and Applications in Protein Functional Analysis." *Current Chemical Genomics* 6 (September): 8–17.

- Olmsted, J., 3rd, and D. R. Kearns. 1977. "Mechanism of Ethidium Bromide Fluorescence Enhancement on Binding to Nucleic Acids." *Biochemistry* 16 (16): 3647–54.
- O'Neil, Casey S., Jacie L. Beach, and Todd D. Gruber. 2018. "Thiazole Orange as an Everyday Replacement for Ethidium Bromide and Costly DNA Dyes for Electrophoresis." *Electrophoresis* 39 (12): 1474–77.
- Ouyang, Mingxing, Jie Sun, Shu Chien, and Yingxiao Wang. 2008. "Determination of Hierarchical Relationship of Src and Rac at Subcellular Locations with FRET Biosensors." *Proceedings of the National Academy of Sciences of the United States of America* 105 (38): 14353–58.
- Padmakumar, V. C., Thorsten Libotte, Wenshu Lu, Hafida Zaim, Sabu Abraham, Angelika A. Noegel, Josef Gotzmann, Roland Foisner, and Iakowos Karakesisoglou. 2005. "The Inner Nuclear Membrane Protein Sun1 Mediates the Anchorage of Nesprin-2 to the Nuclear Envelope." *Journal of Cell Science* 118 (Pt 15): 3419–30.
- Paige, Jeremy S., Karen Y. Wu, and Samie R. Jaffrey. 2011. "RNA Mimics of Green Fluorescent Protein." *Science* 333 (6042): 642–46.
- Palangat, Murali, and Daniel R. Larson. 2016. "Single-Gene Dual-Color Reporter Cell Line to Analyze RNA Synthesis in Vivo." *Methods* 103 (July): 77–85.
- Panchapakesan, Shanker Shyam S., Matthew L. Ferguson, Eric J. Hayden, Xin Chen, Aaron A. Hoskins, and Peter J. Unrau. 2017. "Ribonucleoprotein Purification and Characterization Using RNA Mango." *RNA* 23 (10): 1592–99.
- Pasapera, Ana M., Ian C. Schneider, Erin Rericha, David D. Schlaepfer, and Clare M. Waterman. 2010. "Myosin II Activity Regulates Vinculin Recruitment to Focal Adhesions through FAK-Mediated Paxillin Phosphorylation." *The Journal of Cell Biology* 188 (6): 877–90.
- Pastor, Richard W., Robert Zwanzig, and Attila Szabo. 1996. "Diffusion Limited First Contact of the Ends of a Polymer: Comparison of Theory with Simulation." *The Journal of Chemical Physics* 105 (9): 3878–82.

- Patterson, G. H., S. M. Knobel, W. D. Sharif, S. R. Kain, and D. W. Piston. 1997. "Use of the Green Fluorescent Protein and Its Mutants in Quantitative Fluorescence Microscopy." *Biophysical Journal* 73 (5): 2782–90.
- Pennacchio, Len A., Wendy Bickmore, Ann Dean, Marcelo A. Nobrega, and Gill Bejerano. 2013. "Enhancers: Five Essential Questions." *Nature Reviews. Genetics* 14 (4): 288–95.
- Pestic-Dragovich, L., L. Stojiljkovic, A. A. Philimonenko, G. Nowak, Y. Ke, R. E. Settlage, J. Shabanowitz, D. F. Hunt, P. Hozak, and P. de Lanerolle. 2000. "A Myosin I Isoform in the Nucleus." *Science* 290 (5490): 337–41.
- Peter, M., G. T. Kitten, C. F. Lehner, K. Vorburger, S. M. Bailer, G. Maridor, and E. A. Nigg. 1989. "Cloning and Sequencing of cDNA Clones Encoding Chicken Lamins A and B1 and Comparison of the Primary Structures of Vertebrate A- and B-Type Lamins." *Journal of Molecular Biology* 208 (3): 393–404.
- Phanstiel, Douglas H., Alan P. Boyle, Nastaran Heidari, and Michael P. Snyder. 2015. "Mango: A Bias-Correcting ChIA-PET Analysis Pipeline." *Bioinformatics* 31 (19): 3092–98.
- Philimonenko, Vlada V., Jian Zhao, Sebastian Iben, Hana Dingová, Katarína Kyselá, Michal Kahle, Hanswalter Zentgraf, et al. 2004. "Nuclear Actin and Myosin I Are Required for RNA Polymerase I Transcription." *Nature Cell Biology* 6 (12): 1165–72.
- Plessner, Matthias, Michael Melak, Pilar Chinchilla, Christian Baarlink, and Robert Grosse. 2015. "Nuclear F-Actin Formation and Reorganization upon Cell Spreading." *The Journal of Biological Chemistry* 290 (18): 11209–16.
- Pradhan, Roopali, Devika Ranade, and Kundan Sengupta. 2018. "Emerin Modulates Spatial Organization of Chromosome Territories in Cells on Softer Matrices." *Nucleic Acids Research* 46 (11): 5561–86.
- Prendergast, F. G., and K. G. Mann. 1978. "Chemical and Physical Properties of Aequorin and the Green Fluorescent Protein Isolated from *Aequorea forskålea*." *Biochemistry* 17 (17): 3448–53.

- Presman, Diego M., David A. Ball, Ville Paakinaho, Jonathan B. Grimm, Luke D. Lavis, Tatiana S. Karpova, and Gordon L. Hager. 2017. “Quantifying Transcription Factor Binding Dynamics at the Single-Molecule Level in Live Cells.” *Methods* 123 (July): 76–88.
- “Protocols.” n.d. Accessed April 25, 2021. <https://brugge.med.harvard.edu/protocols>.
- Purschke, Martin, Noemi Rubio, Kathryn D. Held, and Robert W. Redmond. 2010. “Phototoxicity of Hoechst 33342 in Time-Lapse Fluorescence Microscopy.” *Photochemical & Photobiological Sciences: Official Journal of the European Photochemistry Association and the European Society for Photobiology* 9 (12): 1634–39.
- Qi, Lei S., Matthew H. Larson, Luke A. Gilbert, Jennifer A. Doudna, Jonathan S. Weissman, Adam P. Arkin, and Wendell A. Lim. 2013. “Repurposing CRISPR as an RNA-Guided Platform for Sequence-Specific Control of Gene Expression.” *Cell* 152 (5): 1173–83.
- Raj, Arjun, Patrick van den Bogaard, Scott A. Rifkin, Alexander van Oudenaarden, and Sanjay Tyagi. 2008. “Imaging Individual mRNA Molecules Using Multiple Singly Labeled Probes.” *Nature Methods* 5 (10): 877–79.
- Ramasubramani, Vyas, Thi Vo, Joshua A. Anderson, and Sharon C. Glotzer. 2020. “A Mean-Field Approach to Simulating Anisotropic Particles.” *The Journal of Chemical Physics* 153 (8): 084106.
- Ranade, Devika, Roopali Pradhan, Muhunden Jayakrishnan, Sushmitha Hegde, and Kundan Sengupta. 2019. “Lamin A/C and Emerin Depletion Impacts Chromatin Organization and Dynamics in the Interphase Nucleus.” *BMC Molecular and Cell Biology* 20 (1): 11.
- Rao, Suhas S. P., Su-Chen Huang, Brian Glenn St Hilaire, Jesse M. Engreitz, Elizabeth M. Perez, Kyong-Rim Kieffer-Kwon, Adrian L. Sanborn, et al. 2017. “Cohesin Loss Eliminates All Loop Domains.” *Cell* 171 (2): 305–20.e24.

- Rao, Suhas S. P., Miriam H. Huntley, Neva C. Durand, Elena K. Stamenova, Ivan D. Bochkov, James T. Robinson, Adrian L. Sanborn, et al. 2014. "A 3D Map of the Human Genome at Kilobase Resolution Reveals Principles of Chromatin Looping." *Cell* 159 (7): 1665–80.
- Regoes, Attila, and Adrian B. Hehl. 2005. "SNAP-Tag Mediated Live Cell Labeling as an Alternative to GFP in Anaerobic Organisms." *BioTechniques* 39 (6): 809–10, 812.
- Reilly, Gwendolen C., and Adam J. Engler. 2010. "Intrinsic Extracellular Matrix Properties Regulate Stem Cell Differentiation." *Journal of Biomechanics* 43 (1): 55–62.
- Reis-Sobreiro, Mariana, Jie-Fu Chen, Tatiana Novitskaya, Sungyong You, Samantha Morley, Kenneth Steadman, Navjot Kaur Gill, et al. 2018. "Emerin Deregulation Links Nuclear Shape Instability to Metastatic Potential." *Cancer Research* 78 (21): 6086–97.
- Reynolds, Noel, Eoin McEvoy, Soham Ghosh, Juan Alberto Panadero Pérez, Corey P. Neu, and Patrick McGarry. 2020. "Investigation of Cell Nucleus Heterogeneity." *bioRxiv*. <https://doi.org/10.1101/2020.07.08.193854>.
- Riddick, Nadeene, Ken-Ichi Ohtani, and Howard K. Surks. 2008. "Targeting by Myosin Phosphatase-RhoA Interacting Protein Mediates RhoA/ROCK Regulation of Myosin Phosphatase." *Journal of Cellular Biochemistry* 103 (4): 1158–70.
- Ries, Jonas, and Petra Schwille. 2006. "Studying Slow Membrane Dynamics with Continuous Wave Scanning Fluorescence Correlation Spectroscopy." *Biophysical Journal* 91 (5): 1915–24.
- Röber, R. A., K. Weber, and M. Osborn. 1989. "Differential Timing of Nuclear Lamin A/C Expression in the Various Organs of the Mouse Embryo and the Young Animal: A Developmental Study." *Development* 105 (2): 365–78.

- Robinett, C. C., A. Straight, G. Li, C. Willhelm, G. Sudlow, A. Murray, and A. S. Belmont. 1996. "In Vivo Localization of DNA Sequences and Visualization of Large-Scale Chromatin Organization Using Lac Operator/repressor Recognition." *The Journal of Cell Biology* 135 (6 Pt 2): 1685–1700.
- Robson, Michael I., Alessa R. Ringel, and Stefan Mundlos. 2019. "Regulatory Landscaping: How Enhancer-Promoter Communication Is Sculpted in 3D." *Molecular Cell* 74 (6): 1110–22.
- Rønnov-Jessen, Lone, and Mina J. Bissell. 2009. "Breast Cancer by Proxy: Can the Microenvironment Be Both the Cause and Consequence?" *Trends in Molecular Medicine* 15 (1): 5–13.
- Roukos, Vassilis, Ty C. Voss, Christine K. Schmidt, Seungtaek Lee, Darawalee Wangsa, and Tom Misteli. 2013. "Spatial Dynamics of Chromosome Translocations in Living Cells." *Science* 341 (6146): 660–64.
- Rust, Michael J., Mark Bates, and Xiaowei Zhuang. 2006. "Sub-Diffraction-Limit Imaging by Stochastic Optical Reconstruction Microscopy (STORM)." *Nature Methods* 3 (10): 793–95.
- Sabari, Benjamin R., Alessandra Dall'Agnesse, Ann Boija, Isaac A. Klein, Eliot L. Coffey, Krishna Shrinivas, Brian J. Abraham, et al. 2018. "Coactivator Condensation at Super-Enhancers Links Phase Separation and Gene Control." *Science* 361 (6400). <https://doi.org/10.1126/science.aar3958>.
- Salpingidou, Georgia, Andrei Smertenko, Irena Hausmanowa-Petrucewicz, Patrick J. Hussey, and Chris J. Hutchison. 2007. "A Novel Role for the Nuclear Membrane Protein Emerin in Association of the Centrosome to the Outer Nuclear Membrane." *The Journal of Cell Biology* 178 (6): 897–904.
- Sanborn, Adrian L., Suhas S. P. Rao, Su-Chen Huang, Neva C. Durand, Miriam H. Huntley, Andrew I. Jewett, Ivan D. Bochkov, et al. 2015. "Chromatin Extrusion Explains Key Features of Loop and Domain Formation in Wild-Type and Engineered Genomes." *Proceedings of the National Academy of Sciences of the United States of America* 112 (47): E6456–65.

- Sato, Yuko, Timothy J. Stasevich, and Hiroshi Kimura. 2018. “Visualizing the Dynamics of Inactive X Chromosomes in Living Cells Using Antibody-Based Fluorescent Probes.” *Methods in Molecular Biology* 1861: 91–102.
- Savatier, Julien, Stéphan Jalaguier, Matthew L. Ferguson, Vincent Cavallès, and Catherine A. Royer. 2010. “Estrogen Receptor Interactions and Dynamics Monitored in Live Cells by Fluorescence Cross-Correlation Spectroscopy.” *Biochemistry* 49 (4): 772–81.
- Schwille, P., U. Haupts, S. Maiti, and W. W. Webb. 1999. “Molecular Dynamics in Living Cells Observed by Fluorescence Correlation Spectroscopy with One- and Two-Photon Excitation.” *Biophysical Journal* 77 (4): 2251–65.
- Seelbinder, Benjamin, Soham Ghosh, Alycia G. Berman, Stephanie E. Schneider, Craig J. Goergen, Sarah Calve, and Corey P. Neu. 2019. “Intra-Nuclear Tensile Strain Mediates Reorganization of Epigenetically Marked Chromatin During Cardiac Development and Disease.” *Cold Spring Harbor Laboratory*.
<https://doi.org/10.1101/455600>.
- Seelbinder, Benjamin, Adrienne K. Scott, Isabel Nelson, Stephanie E. Schneider, Kristin Calahan, and Corey P. Neu. 2020. “TENSCell: Imaging of Stretch-Activated Cells Reveals Divergent Nuclear Behavior and Tension.” *Biophysical Journal* 118 (11): 2627–40.
- Sefah, Kwame, Dihua Shangguan, Xiangling Xiong, Meghan B. O’Donoghue, and Weihong Tan. 2010. “Development of DNA Aptamers Using Cell-SELEX.” *Nature Protocols* 5 (6): 1169–85.
- Sen, Buer, Christophe Guilluy, Zhihui Xie, Natasha Case, Maya Styner, Jacob Thomas, Ipek Oguz, Clinton Rubin, Keith Burridge, and Janet Rubin. 2011. “Mechanically Induced Focal Adhesion Assembly Amplifies Anti-Adipogenic Pathways in Mesenchymal Stem Cells.” *Stem Cells* 29 (11): 1829–36.

- Sen, Buer, Christopher R. Paradise, Zhihui Xie, Jeyant Sankaran, Gunes Uzer, Maya Styner, Mark Meyer, Amel Dudakovic, Andre J. van Wijnen, and Janet Rubin. 2020. “ β -Catenin Preserves the Stem State of Murine Bone Marrow Stromal Cells Through Activation of EZH2.” *Journal of Bone and Mineral Research: The Official Journal of the American Society for Bone and Mineral Research* 35 (6): 1149–62.
- Sen, Buer, Maya Styner, Zhihui Xie, Natasha Case, Clinton T. Rubin, and Janet Rubin. 2009. “Mechanical Loading Regulates NFATc1 and Beta-Catenin Signaling through a GSK3beta Control Node.” *The Journal of Biological Chemistry* 284 (50): 34607–17.
- Sen, Buer, Zhihui Xie, Natasha Case, William R. Thompson, Gunes Uzer, Maya Styner, and Janet Rubin. 2014. “mTORC2 Regulates Mechanically Induced Cytoskeletal Reorganization and Lineage Selection in Marrow-Derived Mesenchymal Stem Cells.” *Journal of Bone and Mineral Research: The Official Journal of the American Society for Bone and Mineral Research* 29 (1): 78–89.
- Sen, Buer, Zhihui Xie, Natasha Case, Meiyun Ma, Clinton Rubin, and Janet Rubin. 2008. “Mechanical Strain Inhibits Adipogenesis in Mesenchymal Stem Cells by Stimulating a Durable Beta-Catenin Signal.” *Endocrinology* 149 (12): 6065–75.
- Sen, Buer, Zhihui Xie, Natasha Case, Maya Styner, Clinton T. Rubin, and Janet Rubin. 2011. “Mechanical Signal Influence on Mesenchymal Stem Cell Fate Is Enhanced by Incorporation of Refractory Periods into the Loading Regimen.” *Journal of Biomechanics* 44 (4): 593–99.
- Shaban, Haitham A., and Andrew Seeber. 2020. “Monitoring the Spatio-Temporal Organization and Dynamics of the Genome.” *Nucleic Acids Research* 48 (7): 3423–34.
- Shah, Parisha P., Greg Donahue, Gabriel L. Otte, Brian C. Capell, David M. Nelson, Kajia Cao, Varun Aggarwala, et al. 2013. “Lamin B1 Depletion in Senescent Cells Triggers Large-Scale Changes in Gene Expression and the Chromatin Landscape.” *Genes & Development* 27 (16): 1787–99.

- Shah, Sheel, Yodai Takei, Wen Zhou, Eric Lubeck, Jina Yun, Chee-Huat Linus Eng, Noushin Koulana, et al. 2018. "Dynamics and Spatial Genomics of the Nascent Transcriptome by Intron seqFISH." *Cell* 174 (2): 363–76.e16.
- Shashkova, Sviatlana, and Mark C. Leake. 2017. "Single-Molecule Fluorescence Microscopy Review: Shedding New Light on Old Problems." *Bioscience Reports* 37 (4). <https://doi.org/10.1042/BSR20170031>.
- Shimi, Takeshi, Takako Koujin, Miriam Segura-Totten, Katherine L. Wilson, Tokuko Haraguchi, and Yasushi Hiraoka. 2004. "Dynamic Interaction between BAF and Emerin Revealed by FRAP, FLIP, and FRET Analyses in Living HeLa Cells." *Journal of Structural Biology* 147 (1): 31–41.
- Shraim, Ala'a S., Abdelrahim Hunaiti, Abdalla Awidi, Walhan Alshaer, Nidaa A. Ababneh, Bashaer Abu-Irmaileh, Fadwa Odeh, and Said Ismail. 2020. "Developing and Characterization of Chemically Modified RNA Aptamers for Targeting Wild Type and Mutated c-KIT Receptor Tyrosine Kinases." *Journal of Medicinal Chemistry* 63 (5): 2209–28.
- Shweta, Him, Moirangthem Kiran Singh, Kavita Yadav, Sachin Dev Verma, Nibedita Pal, and Sobhan Sen. 2017. "Effect of T·T Mismatch on DNA Dynamics Probed by Minor Groove Binders: Comparison of Dynamic Stokes Shifts of Hoechst and DAPI." *The Journal of Physical Chemistry. B* 121 (48): 10735–48.
- Simon, Dan N., and Katherine L. Wilson. 2011. "The Nucleoskeleton as a Genome-Associated Dynamic 'Network of Networks.'" *Nature Reviews. Molecular Cell Biology* 12 (11): 695–708.
- Singer, R. H., and D. C. Ward. 1982. "Actin Gene Expression Visualized in Chicken Muscle Tissue Culture by Using in Situ Hybridization with a Biotinated Nucleotide Analog." *Proceedings of the National Academy of Sciences of the United States of America* 79 (23): 7331–35.

- Stasevich, Timothy J., Florian Mueller, Ariel Michelman-Ribeiro, Tilman Rosales, Jay R. Knutson, and James G. McNally. 2010. "Cross-Validating FRAP and FCS to Quantify the Impact of Photobleaching on in Vivo Binding Estimates." *Biophysical Journal* 99 (9): 3093–3101.
- Stavreva, Diana A., David A. Garcia, Gregory Fettweis, Prabhakar R. Gudla, George F. Zaki, Vikas Soni, Andrew McGowan, et al. 2019. "Transcriptional Bursting and Co-Bursting Regulation by Steroid Hormone Release Pattern and Transcription Factor Mobility." *Molecular Cell* 75 (6): 1161–77.e11.
- Stavreva, Diana A., Waltraud G. Müller, Gordon L. Hager, Carolyn L. Smith, and James G. McNally. 2004. "Rapid Glucocorticoid Receptor Exchange at a Promoter Is Coupled to Transcription and Regulated by Chaperones and Proteasomes." *Molecular and Cellular Biology* 24 (7): 2682–97.
- Stepanenko, Olesya V., Vladislav V. Verkhusha, Irina M. Kuznetsova, Vladimir N. Uversky, and K. K. Turoverov. 2008. "Fluorescent Proteins as Biomarkers and Biosensors: Throwing Color Lights on Molecular and Cellular Processes." *Current Protein & Peptide Science* 9 (4): 338–69.
- Stephens, Andrew D., Edward J. Banigan, Stephen A. Adam, Robert D. Goldman, and John F. Marko. 2017. "Chromatin and Lamin A Determine Two Different Mechanical Response Regimes of the Cell Nucleus." *Molecular Biology of the Cell* 28 (14): 1984–96.
- Stephens, Andrew D., Edward J. Banigan, and John F. Marko. 2019. "Chromatin's Physical Properties Shape the Nucleus and Its Functions." *Current Opinion in Cell Biology* 58 (June): 76–84.
- Stephens, Andrew D., Patrick Z. Liu, Edward J. Banigan, Luay M. Almassalha, Vadim Backman, Stephen A. Adam, Robert D. Goldman, and John F. Marko. 2018. "Chromatin Histone Modifications and Rigidity Affect Nuclear Morphology Independent of Lamins." *Molecular Biology of the Cell* 29 (2): 220–33.
- Stephens, David J., and Victoria J. Allan. 2003. "Light Microscopy Techniques for Live Cell Imaging." *Science* 300 (5616): 82–86.

- Stortz, Martin, Juan Angiolini, Esteban Mocskos, Alejandro Wolosiuk, Adali Pecci, and Valeria Levi. 2018. "Mapping the Dynamical Organization of the Cell Nucleus through Fluorescence Correlation Spectroscopy." *Methods* 140-141 (May): 10–22.
- Strickfaden, Hilmar, Thomas O. Tolsma, Ajit Sharma, D. Alan Underhill, Jeffrey C. Hansen, and Michael J. Hendzel. 2020. "Condensed Chromatin Behaves like a Solid on the Mesoscale In Vitro and in Living Cells." *Cell* 183 (7): 1772–84.e13.
- Swift, Joe, Irena L. Ivanovska, Amnon Buxboim, Takamasa Harada, P. C. Dave P. Dingal, Joel Pinter, J. David Pajerowski, et al. 2013. "Nuclear Lamin-A Scales with Tissue Stiffness and Enhances Matrix-Directed Differentiation." *Science* 341 (6149): 1240104.
- Tajik, Arash, Yuejin Zhang, Fuxiang Wei, Jian Sun, Qiong Jia, Wenwen Zhou, Rishi Singh, Nimish Khanna, Andrew S. Belmont, and Ning Wang. 2016. "Transcription Upregulation via Force-Induced Direct Stretching of Chromatin." *Nature Materials* 15 (12): 1287–96.
- Takahashi, Yuto, Shogo Hiratsuka, Nanako Machida, Daisuke Takahashi, Junpei Matsushita, Pavel Hozak, Tom Misteli, Kei Miyamoto, and Masahiko Harata. 2020. "Impairment of Nuclear F-Actin Formation and Its Relevance to Cellular Phenotypes in Hutchinson-Gilford Progeria Syndrome." *Nucleus* 11 (1): 250–63.
- Talwar, Shefali, Abhishek Kumar, Madan Rao, Gautam I. Menon, and G. V. Shivashankar. 2013. "Correlated Spatio-Temporal Fluctuations in Chromatin Compaction States Characterize Stem Cells." *Biophysical Journal* 104 (3): 553–64.
- Tanenbaum, Marvin E., Luke A. Gilbert, Lei S. Qi, Jonathan S. Weissman, and Ronald D. Vale. 2014. "A Protein-Tagging System for Signal Amplification in Gene Expression and Fluorescence Imaging." *Cell* 159 (3): 635–46.
- Taylor, John Robert. 1997. "An introduction to error analysis." *University Science Books*.

- Thompson, Russell E., Daniel R. Larson, and Watt W. Webb. 2002. "Precise Nanometer Localization Analysis for Individual Fluorescent Probes." *Biophysical Journal* 82 (5): 2775–83.
- Tirat, Aline, Felix Freuler, Thomas Stettler, Lorenz M. Mayr, and Lukas Leder. 2006. "Evaluation of Two Novel Tag-Based Labelling Technologies for Site-Specific Modification of Proteins." *International Journal of Biological Macromolecules* 39 (1-3): 66–76.
- Toan, Ngo Minh, Greg Morrison, Changbong Hyeon, and D. Thirumalai. 2008. "Kinetics of Loop Formation in Polymer Chains." *The Journal of Physical Chemistry. B* 112 (19): 6094–6106.
- Toh, Kee Chua, Nisha M. Ramdas, and G. V. Shivashankar. 2015. "Actin Cytoskeleton Differentially Alters the Dynamics of Lamin A, HP1 α and H2B Core Histone Proteins to Remodel Chromatin Condensation State in Living Cells." *Integrative Biology: Quantitative Biosciences from Nano to Macro* 7 (10): 1309–17.
- Tokunaga, M., N. Imamoto, and K. Sakata-Sogawa. 2008. "Highly Inclined Thin Illumination Enables Clear Single-Molecule Imaging in Cells." *Nature Methods* 5 (2): 159–61.
- Trzaskoma, Paweł, Błażej Ruszczycki, Byoungkoo Lee, Katarzyna K. Pels, Katarzyna Krawczyk, Grzegorz Bokota, Andrzej A. Szczepankiewicz, et al. 2020. "Ultrastructural Visualization of 3D Chromatin Folding Using Volume Electron Microscopy and DNA in Situ Hybridization." *Nature Communications* 11 (1): 2120.
- Tuerk, C., and L. Gold. 1990. "Systematic Evolution of Ligands by Exponential Enrichment: RNA Ligands to Bacteriophage T4 DNA Polymerase." *Science* 249 (4968): 505–10.
- Turner, C. E., J. R. Glenney, and K. Burridge. 1990. "Paxillin: A New Vinculin-Binding Protein Present in Focal Adhesions." *The Journal of Cell Biology* 111 (3): 1059–68.

- Tutucci, Evelina, Maria Vera, Jeetayu Biswas, Jennifer Garcia, Roy Parker, and Robert H. Singer. 2018. "An Improved MS2 System for Accurate Reporting of the mRNA Life Cycle." *Nature Methods* 15 (1): 81–89.
- Uzer, Gunes, Guniz Bas, Buer Sen, Zhihui Xie, Scott Birks, Melis Olcum, Cody McGrath, Maya Styner, and Janet Rubin. 2018. "Sun-Mediated Mechanical LINC between Nucleus and Cytoskeleton Regulates β catenin Nuclear Access." *Journal of Biomechanics* 74 (June): 32–40.
- Uzer, Gunes, William R. Thompson, Buer Sen, Zhihui Xie, Sherwin S. Yen, Sean Miller, Guniz Bas, et al. 2015. "Cell Mechanosensitivity to Extremely Low-Magnitude Signals Is Enabled by a LINCed Nucleus." *Stem Cells* 33 (6): 2063–76.
- Valentine, M. T., P. D. Kaplan, D. Thota, J. C. Crocker, T. Gisler, R. K. Prud'homme, M. Beck, and D. A. Weitz. 2001. "Investigating the Microenvironments of Inhomogeneous Soft Materials with Multiple Particle Tracking." *Physical Review E, Statistical, Nonlinear, and Soft Matter Physics* 64 (6 Pt 1): 061506.
- Vera, Maria, Evelina Tutucci, and Robert H. Singer. 2019. "Imaging Single mRNA Molecules in Mammalian Cells Using an Optimized MS2-MCP System." *Methods in Molecular Biology* 2038: 3–20.
- Vergnes, Laurent, Miklós Péterfy, Martin O. Bergo, Stephen G. Young, and Karen Reue. 2004. "Lamin B1 Is Required for Mouse Development and Nuclear Integrity." *Proceedings of the National Academy of Sciences of the United States of America* 101 (28): 10428–33.
- Versaevel, Marie, Jean-Baptiste Braquenier, Maryam Riaz, Thomas Grevesse, Joséphine Lantoine, and Sylvain Gabriele. 2014. "Super-Resolution Microscopy Reveals LINC Complex Recruitment at Nuclear Indentation Sites." *Scientific Reports* 4 (December): 7362.
- Versaevel, Marie, Thomas Grevesse, and Sylvain Gabriele. 2012. "Spatial Coordination between Cell and Nuclear Shape within Micropatterned Endothelial Cells." *Nature Communications* 3 (February): 671.

- Vorburger, K., C. F. Lehner, G. T. Kitten, H. M. Eppenberger, and E. A. Nigg. 1989. "A Second Higher Vertebrate B-Type Lamin. cDNA Sequence Determination and in Vitro Processing of Chicken Lamin B2." *Journal of Molecular Biology* 208 (3): 405–15.
- Walker, D., H. Htun, and G. L. Hager. 1999. "Using Inducible Vectors to Study Intracellular Trafficking of GFP-Tagged Steroid/nuclear Receptors in Living Cells." *Methods* 19 (3): 386–93.
- Wang, Siyuan, Jun-Han Su, Feng Zhang, and Xiaowei Zhuang. 2016. "An RNA-Aptamer-Based Two-Color CRISPR Labeling System." *Scientific Reports* 6 (May): 26857.
- Wang, Yang, Liang-Zhong Yang, and Ling-Ling Chen. 2020. "Protocol for Dynamic Imaging of RNA in Living Cells by CRISPR-Cas13 System." *STAR Protocols* 1 (1): 100037.
- Wan, Yihan, Dimitrios G. Anastasakis, Joseph Rodriguez, Murali Palangat, Prabhakar Gudla, George Zaki, Mayank Tandon, et al. 2021. "Dynamic Imaging of Nascent RNA Reveals General Principles of Transcription Dynamics and Stochastic Splice Site Selection." *Cell*, May. <https://doi.org/10.1016/j.cell.2021.04.012>.
- Waring, M. J. 1965. "Complex Formation between Ethidium Bromide and Nucleic Acids." *Journal of Molecular Biology* 13 (1): 269–82.
- Wilhelmsen, Kevin, Sandy H. M. Litjens, Ingrid Kuikman, Ntambua Tshimbalanga, Hans Janssen, Iman van den Bout, Karine Raymond, and Arnoud Sonnenberg. 2005. "Nesprin-3, a Novel Outer Nuclear Membrane Protein, Associates with the Cytoskeletal Linker Protein Plectin." *The Journal of Cell Biology* 171 (5): 799–810.
- Wilusz, Rebecca E., Eric M. Darling, Michael P. Bolognesi, Stefan Zauscher, and Farshid Guilak. 2009. "The Inhomogeneous Mechanical Properties of the Pericellular Matrix of Articular Cartilage Measured In Situ by Atomic Force Microscopy." In *Summer Bioengineering Conference*, 48913:1065–66. American Society of Mechanical Engineers.

- Worman, H. J., J. Yuan, G. Blobel, and S. D. Georgatos. 1988. "A Lamin B Receptor in the Nuclear Envelope." *Proceedings of the National Academy of Sciences of the United States of America* 85 (22): 8531–34.
- Wu, Bin, Young J. Yoon, and Robert H. Singer. 2014. "Visualization of Stimulation Dependent Localization of Single Endogenous mRNAs to Dendritic Spines." *Biophysical Journal* 106 (2): 400a.
- Yang, J-W, L. Yang, R-G Luo, and J-F Xu. 2020. "Corticosteroid Administration for Viral Pneumonia: COVID-19 and beyond." *Clinical Microbiology and Infection: The Official Publication of the European Society of Clinical Microbiology and Infectious Diseases* 26 (9): 1171–77.
- Yang, Liang-Zhong, Yang Wang, Si-Qi Li, Run-Wen Yao, Peng-Fei Luan, Huang Wu, Gordon G. Carmichael, and Ling-Ling Chen. 2019. "Dynamic Imaging of RNA in Living Cells by CRISPR-Cas13 Systems." *Molecular Cell* 76 (6): 981–97.e7.
- Yildiz, Ahmet, Joseph N. Forkey, Sean A. McKinney, Taekjip Ha, Yale E. Goldman, and Paul R. Selvin. 2003. "Myosin V Walks Hand-over-Hand: Single Fluorophore Imaging with 1.5-Nm Localization." *Science* 300 (5628): 2061–65.
- Zhang, Qiuping, Rose-Marie Minaisah, Elisa Ferraro, Chen Li, Lauren J. Porter, Can Zhou, Fang Gao, et al. 2016. "N-Terminal Nesprin-2 Variants Regulate β -Catenin Signalling." *Experimental Cell Research* 345 (2): 168–79.
- Zhang, Q., J. N. Skepper, F. Yang, J. D. Davies, L. Hegyi, R. G. Roberts, P. L. Weissberg, J. A. Ellis, and C. M. Shanahan. 2001. "Nesprins: A Novel Family of Spectrin-Repeat-Containing Proteins That Localize to the Nuclear Membrane in Multiple Tissues." *Journal of Cell Science* 114 (Pt 24): 4485–98.
- Zhang, Ting, Wenhui Zhou, Xiaoya Lin, Mohammad Rizwan Khan, Sha Deng, Mi Zhou, Guiping He, Chengyong Wu, Ruijie Deng, and Qiang He. 2021. "Light-up RNA Aptamer Signaling-CRISPR-Cas13a-Based Mix-and-Read Assays for Profiling Viable Pathogenic Bacteria." *Biosensors & Bioelectronics* 176 (March): 112906.

- Zhou, Haibo, Junlai Liu, Changyang Zhou, Ni Gao, Zhiping Rao, He Li, Xinde Hu, et al. 2018. "In Vivo Simultaneous Transcriptional Activation of Multiple Genes in the Brain Using CRISPR-dCas9-Activator Transgenic Mice." *Nature Neuroscience* 21 (3): 440–46.
- Zhou, Rui, and Yi Qin Gao. 2020. "Polymer Models for the Mechanisms of Chromatin 3D Folding: Review and Perspective." *Physical Chemistry Chemical Physics: PCCP* 22 (36): 20189–201.
- Zhou, Zhaocai, Xiulian Du, Zheng Cai, Xiaomin Song, Hongtao Zhang, Takako Mizuno, Emi Suzuki, et al. 2012. "Structure of Sad1-UNC84 Homology (SUN) Domain Defines Features of Molecular Bridge in Nuclear Envelope." *The Journal of Biological Chemistry* 287 (8): 5317–26.
- Zhuang, Xiaowei. 2009. "Nano-Imaging with Storm." *Nature Photonics* 3 (7): 365–67.
- Zink, Daniele, Nicolas Sadoni, and Ernst Stelzer. 2003. "Visualizing Chromatin and Chromosomes in Living Cells." *Methods* 29 (1): 42–50.
- Zoorob, Roger, and Dawn Cender. 1998. "A Different Look at Corticosteroids." August 1, 1998. <https://www.aafp.org/afp/1998/0801/p443.html>.

APPENDIX I

Fluorescence Labeling Methods for Single Molecule Experiments

Abstract

Single-molecule experiments have emerged as an invaluable tool in the biosciences, a mainstay technique that offers both spatial and temporal resolution with relatively minimal perturbation to the sample as compared with many other biophysical techniques. These experiments rely heavily on fluorescent labeling as a tool to investigate molecular interactions, track biomolecule dynamics, and in turn gain insights into their biological functions. A prerequisite to these experiments is the optimization of specific fluorophores for DNA, RNA, and protein, with the desired photophysical properties. While many successful labeling strategies have historically been available for imaging of DNA and protein, there is an emerging field in live cell, single molecule imaging of RNA. Here, we outline the recent advances in biomolecule fluorescence labeling, focusing primarily on relevant techniques for the visualization of RNA's spatial and temporal dynamics. The advantages and limitations of the currently available fluorescence labeling strategies are summarized along with perspectives on future research directions.

Introduction

For the spatial and temporal measurement of biological processes in living cells and tissues, there is no substitute for light microscopy. The limited interaction of photons, with highly sensitive biological matter, in combination with high contrast provided by fluorescence labeling allows us to visualize biochemical processes directly. 3D structure and function are known to be inherently tied, but “seeing is believing”, and therefore visualizing live cells in action is critical for determining the guiding principles which are key to understanding the highly dynamic, ultra-synchronized genome. The provocation

lies in creating highly specific labels that are photostable for long periods of time for live cell imaging. Non-specific labels like DAPI have been available for many years and they have provided valuable information on the whole genome. The real challenge lies in developing labels that are specific and viable for use in a living cell. Such labels would provide biologically relevant information on not only the localization of the biomolecules, but also the timing of their interactions. Significant advances have been made in imaging technology and now require the next wave of fluorescent labels to overcome the lingering challenges to fully visualize a single living cell at the single molecule level. Here we provide a brief overview of the labeling technologies available for DNA, RNA, and protein, highlighting specifically the recent advances in live-cell single molecule techniques of visualizing RNA (Figure A.1). Finally, we will discuss the directions and opportunities for synergistic labeling approaches (Figure A.2). Together these labeling strategies promise to provide invaluable insights into the dynamics of gene expression, regulation, and functionality.

Imaging DNA

Visualizing DNA, its structure and behavior are critical to understanding the human genome. Once thought to be random and simplistic, the 4D genome is being revealed as an organized, information rich entity whose synchronized structuring and restructuring plays a critical role in how the genome is accessed and in turn expressed. In pursuit of observing the genome in action there have been a variety of specific, safe, bright labels developed, but to date there is no universally ideal method to fit all microscopy needs. Determination of which microscopy method to use must be made based on the research question being asked. Here we will describe the labeling tools

currently available along with their advantages and disadvantages to determine which microscopy methods best answer the research question.

DAPI/Hoechst

Two mainstay DNA specific dyes are available. These dyes, DAPI and Hoechst, intercalate into the minor groove of DNA and fluoresce blue (~461 nm). They have both been used since the mid-70's. While both exhibit weak fluorescence in solution, they strongly fluoresce when bound to DNA (Latt et al. 1975; Kapuściński and Skoczylas 1978), making them an ideal label for chromatin. It is important to note that while Hoechst and DAPI can interact with RNA and fluoresce, they do not fluoresce anywhere near as brightly as they do with DNA. Both of these fluorescent molecules bind to the minor groove of DNA (Kapusinski 1995), which not only inhibits cell division, but also becomes cytotoxic to many cell types (Shweta et al. 2017). There are protocols for live cell imaging using Hoechst (Purschke et al. 2010), but neither DAPI nor Hoechst staining are ideal labeling methods for studying chromatin dynamics as they are nonspecific (Zink, Sadoni, and Stelzer 2003).

DNA FiSH

DNA FiSH, or fluorescence in-situ hybridization, which was developed in the mid-80's allowed for a great advance in labeling a specific gene locus using fluorescently tagged single stranded DNA Oligos. While Hoechst and DAPI are indiscriminate in their DNA labeling, DNA FiSH labels specific DNA sequences in fixed cells (Camps, Erdos, and Ried 2015; Byron, Hall, and Lawrence 2013). This technology has continued to advance through further methods such as signal amplification by exchange reaction (SABER), which overcomes background fluorescence and not bright enough labels

(Kishi et al. 2019). Despite significant improvements in probe design and detection methods this technique remains primarily a fixed cell method (Gelali et al. 2018).

TetR and LacR

Another advance came in 1996, Robinett et al. demonstrated that it was possible to label a specific chromatin locus in living cells with a GFP-fusion protein through the LacR system (Robinett et al. 1996). Through this novel DNA labeling system, the authors were able to fluorescently image a specific DNA locus over time in mitotic cells. This method uses the integration of prokaryotic operon sequences into the DNA. Through homologous recombination, random integration, or retroviral integration specific genes can be labeled with GFP or similar labels. LacR and its kin technology, TetR, provide the additional benefit of a stable cell line. These systems no longer require the addition of labeling probes to see specific gene loci, instead with this technology specific sequences of DNA can be imaged in live cells over many generations (Robinett et al. 1996; Roukos et al. 2013).

CRISPR/Cas9

CRISPR/Cas9 genome editing technology has not only enhanced our ability to modify the genome, but also visualize specific, endogenous genomic loci in living cells. Deactivated Cas9 (dCas9) has provided the technological advancement necessary to visualize and measure the dynamics of multiple unique genes simultaneously (Baohui Chen and Huang 2014; Anton, Leonhardt, and Markaki 2016; Baohui Chen et al. 2013; Qi et al. 2013). dCas9 repurposes the CRISPR gene editing system for DNA labeling using a nuclease dead Cas9 that has been tagged with a fluorescent protein and sequence specific guide RNAs. Alternatively, the guide RNA can be tagged with multiple PP7

loops that bind GFP coat proteins (S. Wang et al. 2016). This technology has been used to track repetitive elements within telomeres (Baohui Chen et al. 2013). CRISPR/Cas9 labeling can visualize up to six unique gene loci concurrently within a live cell, a method known as CRISPRainbow (Ma et al. 2016). This labeling method is ideal for live cell imaging and it also does not require the laborious gene editing of the TetR and LacR systems (Anton, Leonhardt, and Markaki 2016; G. Li, Sudlow, and Belmont 1998).

Imaging RNA

RNA is the linchpin of the central dogma, and therefore the visualization of it is critical to understanding the inner workings of the genome. While less than 3% of the genome is eventually transcribed into protein, conservatively more than 62% of the genome is transcribed into RNA (ENCODE Project Consortium 2012). Imaging of RNA is not a new concept; in fact, it has been a core scientific pursuit since the 1970s. Since then, there have been advances from visualizing extracted RNA in gels to imaging single RNA transcripts within a single living cell.

Ethidium Bromide

Currently there is no truly indeterminate RNA label that is comparable to DAPI or Hoechst, although ethidium bromide has been used to visualize RNA. While ethidium bromide does indeed label RNA when the RNA folds back on itself it can intercalate into the base pairing, it does not label specifically. It labels both DNA and RNA indiscriminately (Olmsted and Kearns 1977; Waring 1965). Ethidium bromide fluoresces bright orange when bound, though its fluorescence is diminished in the presence of water. This makes it ideal for visualizing DNA and RNA gels (Borst 2005), but it limits its value *in situ* in fluorescence microscopy. Additionally, ethidium bromide is excited with

UV light and in and of itself it is a mutagen, making this label both toxic to the cell and potentially toxic to the researcher (O'Neil, Beach, and Gruber 2018).

RNA FiSH

RNA FiSH provided one of the first significant advances in the visualization of specific RNA transcripts. This method, much like DNA FiSH, utilizes sequence-specific fluorescent probes to label target RNAs. This visualization technique can be used for not only detecting RNA transcripts, but also quantifying RNA molecules. All of this is done without extracting the RNA from the cell. By using a large number of labeled probes, both the location and number of RNA can be quantified (Raj et al. 2008; Femino et al. 1998; Singer and Ward 1982). While this approach provides a strong signal and significantly reduces background noise, it is inefficient in the detection of RNAs that are compact and abundant (Kramer et al. 2021). There are historically several major issues with RNA FiSH including the lack of live-cell RNA dynamics and inability to properly visualize dense structures of RNA. In recent years much work has been completed in the optimization of this technique. A recent paper showed the visualization of RNA granules using RNA FiSH through a new technique known as LR White (Kramer et al. 2021), which was a major advance in the visualization of dense structures of RNA. Additionally, this technique has been adapted to provide not only RNA localization data, but also sequencing data through seqFISH (Eng et al. 2019; S. Shah et al. 2018). While there have been great advances in improving the versatility of this tool, it remains limited to fixed-cell experiments.

MS2/PP7

A live cell labelling method for RNA is the MS2/PP7 system. RNA bacteriophage coat proteins bind to the integrated stem loop sequence within the specific RNA of interest (Bertrand et al. 1998; Chao et al. 2008; Larson et al. 2011; Vera, Tutucci, and Singer 2019). It has been widely used for RNA localization and RNA synthesis studies. This method is based on binding of fluorescent molecules to repetitive stem loops that have been introduced into the gene of interest. MS2 plasmids have been made available on Addgene and they can be used to perform a stable transfection and generate a stable cell line (Coulon et al. 2014). Each individual stem loop binds to a dimer of a chimeric protein composed of the phage protein, a nuclear localization signal and a fluorescent protein such as green fluorescent protein (GFP) (Lenstra and Larson 2016). Multiplexing of the stem loops is usually required for a bright enough signal to image. This allows for visualization of a mRNA throughout its entire life cycle (Tutucci et al. 2018). Since PP7-RNA and MS2-RNA are very specific, both can be used simultaneously within a given cell, allowing for two colors or two RNAs to be visualized at the same time (Coulon et al. 2014). While it does allow for the visualization of actively transcribed RNA, this technique does suffer from requiring lots of genome editing. MS2/PP7 labeling typically has around 24 stem loop repeats, and in this it is not truly a “single molecule” technique.

CRISPR/Cas13

The future of RNA labelling lies with dCas13, a method similar to dCas9, which exploits CRISPR/Cas technology. This method relies on endonuclease-deficient, programmable guide RNAs that target specific sequences of RNA and fluorescent-protein fused Cas that have been catalytically deactivated. Together the guide RNA and

fluorescent Cas protein are able to locate a specific sequence of RNA and fluorescently label it. This labeling strategy when paired with the proper microscopy technique can provide spatial and temporal information on RNA dynamics in a living cell (L.-Z. Yang et al. 2019; Y. Wang, Yang, and Chen 2020). Recently this technology was piloted in the imaging of NEAT1. NEAT1 is a moderately expressed long-noncoding RNA (lncRNA) that is spatially restricted and is a critical component of paraspeckles. These characteristics make it an ideal tool for RNA-imaging screening because of its multiple copies and colocalization. This group showed that multiple, but not all, Cas13 orthologs tested yielded a significant signal-to-noise ratio and were highly specific (L.-Z. Yang et al. 2019). In addition to being a great tool for imaging RNA localization, it has also been shown to be valuable in the imaging of live-cell RNA-protein interactions (Han et al. 2020). While these preliminary studies show promise, there is still much to be done in optimizing the guide RNAs, visualizing less abundant RNAs, and minimizing background fluorescence noise (Davis and O'Connell 2020).

RNA Aptamers

Another new labeling technique that is gaining popularity is RNA aptamers like RNA Spinach (Paige, Wu, and Jaffrey 2011); (Dolgosheina et al. 2014). RNA Spinach and similar aptamers like RNA Mango (Dolgosheina et al. 2014) and RNA Broccoli (Filonov et al. 2014), were designed and selected through Systematic Evolution of Ligands by EXponential Enrichment (SELEX) (Sefah et al. 2010; Tuerk and Gold 1990). The aptamers that result from this selection bind specifically to fluorophore derivatives with nanomolar affinity. Binding results in a fluorescence increase of up to 1,000-fold. This technique provides a significant advance over the MS2-RNA and PP7-RNA systems

in that there is a significant enhancement of fluorescence upon binding, lowering the fluorescence background that is typically significant in the MS2/PP7 method. In addition to lowering background fluorescence, RNA Mango can be visualized for long periods of time due to bleached fluorophore replacement (Cawte, Unrau, and Rueda 2020). It was also recently shown that the Mango array did not negatively affect the localization of the labeled RNA (Cawte, Unrau, and Rueda 2020). The visualization of RNA aptamers such as RNA Mango has been used in conjunction with single-molecule fluorescence cross correlation spectroscopy (Panchapakesan et al. 2017). The extent of the usefulness of RNA aptamers for labeling is still being explored, but it appears promising with novel work being conducted in the labeling of microRNAs (Dou et al. 2021), dual color imaging (Kong et al. 2021), and the development of RNA aptamers for Förster resonance energy transfer (FRET) (Jeng et al. 2020). This propitious new method has the capacity to visualize RNA dynamics as no other label has.

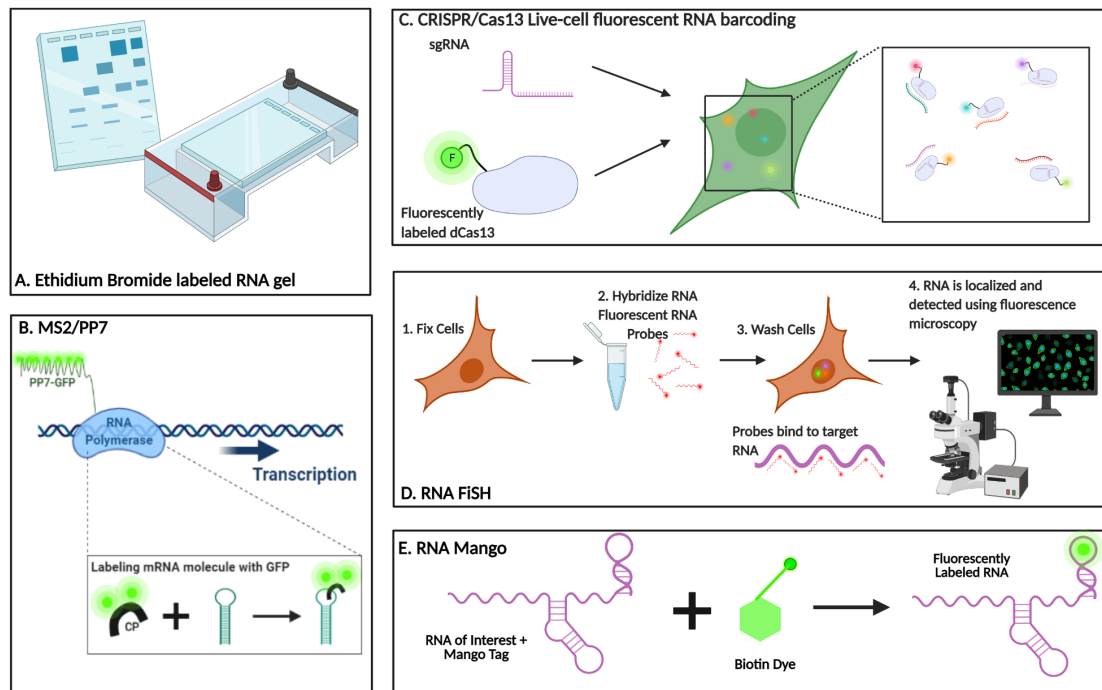


Figure A.1 Methods of Fluorescently Labeling RNA

A. Ethidium Bromide can be used to label DNA and RNA nonspecifically B. MS2/PP7 labeling technology uses GFP/coat protein molecules that bind to RNA stem loops to label the specific RNA of interest C. CRISPR/Cas13 technology uses a fluorescently labeled dCas13 molecule and a specific guide RNA to target a RNA of interest D. RNA FiSH uses fluorescent RNA probes to label RNAs of interest E. RNA Mango is an RNA aptamer that can be added on to a target RNA. When the TO1-Biotin dye is added the RNA of interest fluoresces.

Imaging Protein

Visualizing protein within a living cell is critical for determining the structure and function of the cell. It is currently estimated that *Saccharomyces cerevisiae* have 5,858 unique proteins within their proteome and on average 42 million proteins expressed at a given time (B. Ho, Baryshnikova, and Brown 2018). Proteins are known to play roles in cellular trafficking, metabolism, gene expression, cell mobility and so much more. These further underscores the importance of visualizing proteins and characterizing their

synchronized behavior within a living cell. For visualization there are several fluorescent labeling options available.

GFP

A major advance in biomolecular imaging came in the form of the first fluorescence protein label. Green fluorescent protein (GFP), which was first purified from *Aequorea victoria* (Prendergast and Mann 1978), can not only be purified and synthesized, but it can be integrated into a cell so that the protein of interest is labeled in fluorescent green (Stepanenko et al. 2008). GFP is now a part of a growing family of fluorescent proteins that can be not only green, but also orange-red, far-red, cyan, blue and yellow (Stepanenko et al. 2008; Patterson et al. 1997). Since GFP and proteins like it are naturally derived fluorophores, they are much less cytotoxic to cells than many comparable fluorophores (Patterson et al. 1997). They also have the additional benefit of having 100% labeling efficiency without requiring microinjections or the addition of fluorescent probes.

SunTag

Fusing a fluorescent tag to the protein of interest is one of the most straightforward ways to track and visualize proteins, but it can often have unforeseen effects on the cell in the form of toxic protein aggregations or high phototoxicity which is often due to the use of a CMV promoter. SunTag addresses these issues by fusing a SunTag scaffold to the protein instead of the fluorophore directly. This scaffold allows for the binding of multiple fluorescent proteins, therefore increasing brightness. This is a significant improvement over GFP which is not particularly photostable and requires up to an hour to mature. SunTag reduced maturation time to zero so you can now visualize

translation. It has recently been shown that by simply swapping in SunTag they were able to decrease their laser power by 80% while still having a better signal-to-noise ratio (Tanenbaum et al. 2014). Additionally, SunTag shows significantly less undesired protein aggregation (Tanenbaum et al. 2014). The SunTag technology in combination with Cas9 technology has recently been used to visualize activation of a gene and synthesis of RNA (H. Zhou et al. 2018; Morita et al. 2020).

IF

Immunofluorescence (IF) is a labeling technique that allows for detection and localization of a wide range of biomolecules in many different sample types. It is an excellent technique for sensitivity and signal amplification and can be used with a wide range of microscopy techniques. There are two main ways of labeling the biomolecules: directly through a primary antibody or indirectly through a secondary antibody (Im et al. 2019). Whether using the direct or indirect staining method, the antibodies are conjugated to a fluorophore. While this is a very specific technique it does have the significant limitation of only being conducted on fixed cells, therefore limiting its usefulness in determining dynamics. While it is limited in studying protein dynamics, it has been useful in determining the nuclear and cellular structure.

SNAP/Halo

An additional tool that has been developed recently for advanced protein imaging studies are self-labeling protein tags such as HaloTag (Los et al. 2008) and SNAP-tag (Regoes and Hehl 2005). These tags are expressed on the protein of interest and fluorescence when small fluorescent probes bind with the tag. Originally fluorescent proteins like GFP were used, but of late there has been a shift towards dyes. One such

class of dye known as “Janelia Fluor” (JF) dyes are often used. They are small, membrane permeable chemically derived dyes that provide improved brightness and photostability (Grimm et al. 2016). This class of dyes allows for spectral tuning of the fluorophores through the incorporation and substitution of azetidine groups. This unique property has yielded a palette of labels with excitation ranging from blue to the far-red (Grimm et al. 2017, 2020).

Fabs

Another label is fluorescent antibody fragments (Fabs), a fluorescent protein labeling technique that uses antibodies which lack the Fc component to specifically tag proteins of interest (Ferrara et al. 2011). The fluorophore is conjugated to a single chain antibody specific to the protein of interest. It has been combined with confocal and super-resolution microscopy to image the dynamic changes of nuclear transcription factors as well as epigenetic histone modifications (Conic et al. 2018). This labeling technique was recently utilized in the labeling and imaging of epigenetic markers such as H3K9 acetylation and H3K27 acetylation, as well as a histone methylation in inactivated X-chromosomes and embryos (Sato, Stasevich, and Kimura 2018; Hayashi-Takanaka et al. 2011). It has great potential to yield valuable information on the proteins regulating gene expression.

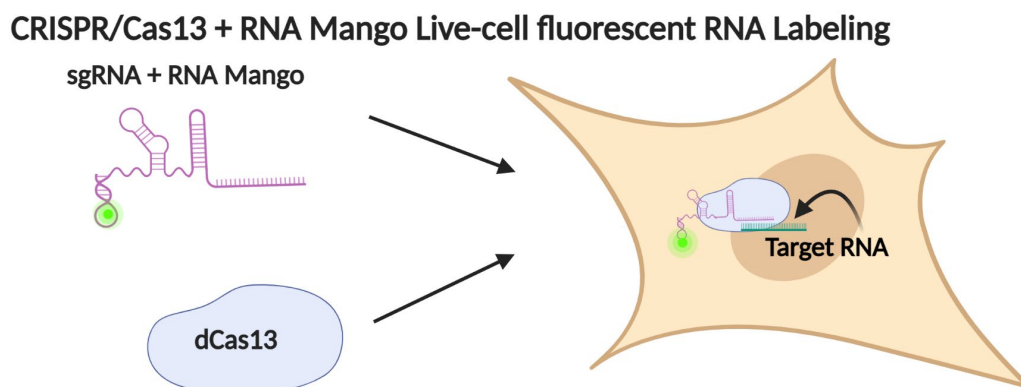


Figure A.2 CRISPR/Cas13 + RNA Mango Live-cell fluorescent RNA Labeling

RNA Mango can be added on to the guide RNA typically used for CRISPR/Cas labeling. Multiple different RNA aptamers could be used to obtain multiple colors and the labeling of multiple different RNA sequences within the same cell using the same dCas13 enzyme.

Future Perspectives

The labeling strategies discussed above promise to provide invaluable insights into gene expression dynamics and RNA function when deployed strategically and synergistically. As the middle step in the central dogma its visualization is crucial to understanding the genome and its dynamics. Highly specific fluorescent labels that are photostable for long periods of time are necessary for taking these kinds of measurements in a living cell. As highlighted in this review there are a wide range of labeling strategies available that lend themselves to specific experiments based on their advantages and disadvantages. Major advances have been made in adapting fluorescent labels for live cell imaging, increasing brightness of the probes, decreasing off-target or undesired biomolecular interactions, and simplifying the labeling process. Despite these great strides, there is still work to be done. While many studies focus on simplifying or improving currently available methods, the daunting, yet necessary task ahead is to

combine the benefits of currently available techniques into a new and improved method. One such example is shown by Zhang et al. in their proof-of-concept experiments employing both Cas13 and Broccoli in a pathogenic bacterium (T. Zhang et al. 2021). Additionally, we propose that RNA Mango and Cas13 could be combined to deal with issues like fluorescent background and laborious genome editing. We surmise that attaching the RNA Mango to a CRISPR guide RNA would provide a bright signal, reduce photobleaching and phototoxicity, and provide a more streamlined labeling process. Uniquely combining fluorescent labeling strategies should reveal previously undiscovered truths about the genome, biomolecular kinetics, and the role of structure in the function of a living cell.

APPENDIX II

Nuclear Envelope Mechanobiology: Linking the Nuclear Structure and Function

Abstract

Cellular responses rely on effective sensing and intra-cellular transduction of environmental information. This information is either coded in the extracellular matrix as biochemical cues or activated by mechanosensitive signaling cascades through dynamic environmental force gradients. The nucleus, central to cellular activity, relies on both direct mechanical input as well as its molecular transducers to sense external stimuli and respond by regulating intra-nuclear chromatin organization that determines cell function and fate. In mesenchymal stem cells of musculoskeletal tissues, changes in nuclear structures are emerging as a key modulator of their differentiation and proliferation programs. While significant advances were made in the understanding of nuclear structure and gene expression separately, studying the nuclear mechanics and gene transcription in tandem has been challenging. In this review we will first introduce the structural elements of the nucleoskeleton and discuss the current literature on how nuclear structure and signaling are altered in relation to environmental and tissue level mechanical cues. We will focus on state-of-the-art methods that can measure nuclear structure and mechanics of living nuclei with a particular emphasis on the methodologies that can be used in conjunction to visualize DNA, RNA, and protein dynamics in live cells in response to various forms of mechanical stimulation. Ultimately, combining real-time nuclear deformations and chromatin dynamics can be a powerful tool to study mechanisms of how forces affect the dynamics of genome function.

Introduction

Cells both sense and adapt to dynamic mechanical environments in tissues. Cellular mechanosensation is accomplished through a variety of structures and proteins

that reside within the plasma membrane, the cytoskeleton, and the nucleus. Depending on the type of sensory element and the external stimuli, mechanical signals are either converted into biochemical signaling cascades or physically transmitted to the intracellular structures (Table AII.1). This conversion of extracellular deformations into intracellular information is called mechanotransduction. For example, application of extracellular mechanical signals such as substrate strain first activates focal adhesions, protein plaques smaller than 200nm comprised of integrins, focal adhesion kinase (FAK), talin, paxilin, vinculin, and zyxin, that enable direct connections between the extracellular matrix (ECM) and the cell (Kanchanawong et al. 2010). In stem cells, strain application recruits signaling complexes to focal adhesions, essentially turning them into intracellular signaling relays for extracellular mechanical information (Burrige et al. 1988). Upon mechanical challenge, more structural elements, such as vinculin, paxilin and talin, as well as signaling molecules, including FAK, Src, and Akt, are recruited into focal adhesions (Grashoff et al. 2010; Turner, Glenney, and Burrige 1990; Pasapera et al. 2010; Sen et al. 2011; Sen et al. 2014). These signaling events in focal adhesions in turn activate adaptations of cell cytoskeleton where compressive forces on microtubules balance the contractile pulling forces generated by F-actin stress fibers. Numerous proteins maintain the structural adaptation of the F-actin cytoskeleton, including actin related protein (Arp) 2/3 complexes that maintain branching (Machesky and Insall 1998), formin homology 1 & 2 domain containing proteins that regulate the end-to-end actin formation (Blanchoin 2014). Changes in the F-actin contractility and tension are largely regulated by Rho GTPases, such as RhoA, Ras, and CDC42A (Jaffe and Hall 2005). RhoA for example, recruits myosin light chain kinase to F-actin fibers through its effector

protein ROCK, which in turn activates the dimerized motor protein myosin II to generate tension by pulling F-actin bundles together (Riddick, Ohtani, and Surks 2008). Not only these changes in cytoskeletal contractions are directly transmitted to cell nuclei through nuclear envelope proteins such as Linker of Nucleoskeleton and Cytoskeleton (LINC) complex (Arsenovic et al. 2016), restructuring events also result in activation of a number of signaling molecules, most notably, β -catenin, and YAP/TAZ. Following a strain for example both β catenin and YAP are activated (de-phosphorylated) in the cytoplasm (Sen et al. 2008; Codelia, Sun, and Irvine 2014). Following their activation by mechanical force both β -catenin (Case et al. 2011; Sen et al. 2009) and YAP/TAZ (Driscoll et al. 2015; Benham-Pyle, Pruitt, and Nelson 2015; Thompson et al. 2020) enter cell nuclei through nuclear pores to act as co-transcriptional factors for regulating cell function. In this way, mechanical information, whether directly through cytoskeletal networks or through intermediate molecular transducers has to transmit through the nuclear envelope and into the nucleus to direct cell function and fate.

Nuclear Structure and Mechanical Force

LINC Complex

The Linker of Nucleoskeleton and Cytoskeleton (LINC) complex forms a physical link between the cytoskeleton and nucleus. Located in the nuclear envelope the LINC complex is formed from multiple proteins that connect to actin, microtubules, and intermediate filaments in the cytoskeleton (Q. Zhang et al. 2001; Crisp et al. 2006; Mellad, Warren, and Shanahan 2011; Wilhelmsen et al. 2005). LINC complex proteins can be categorized into two main groups: those that are located on the outer nuclear membrane (ONM) forming connections to the cytoskeleton and span into the perinuclear

space (PNS); and those that are located in the inner nuclear membrane (INM) creating connections between proteins inside the nucleus and LINC complex proteins in the ONM (Q. Zhang et al. 2001; Crisp et al. 2006; Mellad, Warren, and Shanahan 2011; Wilhelmsen et al. 2005). LINC complex proteins that form the first group are nesprin proteins. In mammalian cells there are four main forms of nesprins, nesprins 1-4. While there are a number of smaller analogs of nesprins found elsewhere in the cell such as N-terminal nesprin-2 that binds to cell-cell junctions (Qiuping Zhang et al. 2016), we will focus on the nesprins that facilitate nucleo-cytoskeletal connectivity and mechanosignaling. Nesprins bind to cytoskeletal elements via their N-termini protruding into the cytoplasm. Their C-termini extend into the PNS where a conserved KASH (Klarsicht, ANC-1, and Syne Homology) domain binds to other major LINC complex proteins called SUN proteins (Q. Zhang et al. 2001; Crisp et al. 2006; Mellad, Warren, and Shanahan 2011; Wilhelmsen et al. 2005). Other unique ONM proteins such as KASH5 and Jaw1 that are involved in regulation of cell shape by binding to microtubules but their role in mechanosignaling requires further investigation (Horn et al. 2013; Kozono et al. 2018). Nesprins play an important role in mechanosignaling. During mechanical stimulation, the RhoA signaling pathway is activated, forming F-actin stress fibers over the nucleus creating an “actin cap” (Khatau et al. 2009; Versaevel, Grevesse, and Gabriele 2012; J.-K. Kim et al. 2017; Chambliss et al. 2013). Nesprins bind to these actin fibers and then regulate nuclear morphology, orientation, and motility (Khatau et al. 2009; Versaevel, Grevesse, and Gabriele 2012; J.-K. Kim et al. 2017; Chambliss et al. 2013). Mechanical stimulation through regulation of cell shape increases the number of nesprin associations with the actin cap in both Human HUVAC (Toh, Ramdas, and

Shivashankar 2015; Versaevel et al. 2014; Makhija, Jokhun, and Shivashankar 2016; Kumar and Shivashankar 2016) and mouse NIH-3T3 cells (Toh, Ramdas, and Shivashankar 2015; Versaevel et al. 2014; Makhija, Jokhun, and Shivashankar 2016; Kumar and Shivashankar 2016). Depletion of nesprins negatively impacts mechanical response as actin cap does not form during shear stress (Chambliss et al. 2013) and mesenchymal stem cells (MSCs) are not able to mechanically activate osteogenesis through extracellular matrix (ECM) stiffening (Killaars, Walker, and Anseth 2020). Furthermore, the loss of nesprins leads to the dysfunctional mechanoregulation of differentiation in MSCs, pushing their differentiation away from osteogenesis and into adipogenesis (Killaars, Walker, and Anseth 2020). Interestingly, while substrate strain activates the focal adhesion signaling independent of nesprin function (Sen, Guilly, et al. 2011; Uzer et al. 2015) strain-induced YAP nuclear entry is inhibited when nesprin-1 is depleted in stem cells (Driscoll et al. 2015). This data indicates that nesprins provide a unique target that will allow for the investigation into nuclear mechanical signaling and mechanoresponse independent of cytoplasmic mechanoresponse events. Therefore, nesprins provide a unique target that will allow for the investigation into nuclear mechanical signaling and mechanoresponse independent of cytoplasmic mechanoresponse events. While future research into the LINC complex via nesprins is needed a considerable amount of research into the LINC complex SUN proteins has been done, which we will discuss next.

There are two main SUN proteins in the LINC complex in somatic mammalian cells, SUN1 and SUN2. The other SUN proteins SUN3-5 are also found in the LINC complex but are found mainly in germline cells (Gao et al. 2020; Crisp et al. 2006; Calvi

et al. 2015). SUN proteins are located in the INM and form trimers (Z. Zhou et al. 2012) that bind to the KASH domain of nesprins in the PNS via their C-terminal SUN domains, anchoring nesprins to the nuclear envelope (Haque et al. 2006; Padmakumar et al. 2005). Extending into the nucleus the N-terminal of SUN proteins binds to lamin A/C (Haque et al. 2006), emerin (Haque et al. 2010) and chromatin (Ding et al. 2007). It is important to note that through its connection with emerin, the LINC complex directly connects the cytoskeleton to intranuclear actin and chromatin via barrier-to-autointegration factor (BAF) (Mellad, Warren, and Shanahan 2011; Salpingidou et al. 2007). Depletion of SUN proteins disrupts centrosome orientation, nuclear positioning (Cain et al. 2018; Meinke et al. 2014; Lombardi et al. 2011), and meiosis (Killaars, Walker, and Anseth 2020). Important in these processes are microtubules. SUN proteins regulate microtubule dependent DNA repair (Lottersberger et al. 2015) and spindle formation (Luo et al. 2016). Therefore, an important regulatory role of SUN proteins is revealed: regulation of cell proliferation and meiosis. While one aspect of SUN protein effects is centered around microtubule regulation of proliferation, SUN proteins also regulate mechanical response. Mechanical stimulation via low intensity vibration (LIV), strain and ECM activates mechanically sensitive biomolecular pathways such as Yes-associated-protein (YAP) and β -catenin/Wnt pathways (Sen et al. 2020; Benham-Pyle, Pruitt, and Nelson 2015; Benham-Pyle et al. 2016; Sen et al. 2008; Sen, Guilluy, et al. 2011) that in turn regulate both proliferation and differentiation (W. Hou et al. 2020; Y. Zhang et al. 2016; Bailing Chen et al. 2016; Sen, Xie, et al. 2011; Uzer et al. 2015; Benham-Pyle, Pruitt, and Nelson 2015; Sen et al. 2020; Zhao et al. 2008). SUN proteins regulate mechanical response to strain and atomic force microscopy-induced cell deformation by restricting YAP

(Elosegui-Artola et al. 2017) and β -catenin (Sen et al. 2009; Uzer et al. 2018) entry into the nucleus by disrupting nuclear pore complex organization (Goldberg 2017; Liu et al. 2007). Additionally, SUN proteins are required for mechanoreponse and mechanoregulation of adipogenesis in MSCs (W. Hou et al. 2020; Y. Zhang et al. 2016; Bailing Chen et al. 2016; Sen, Xie, et al. 2011; Uzer et al. 2015) during low intensity vibration (LIV). Interestingly, de-coupling of nesprins and SUN proteins also inhibits mechanoreponse to LIV (W. Hou et al. 2020; Y. Zhang et al. 2016; Bailing Chen et al. 2016; Sen, Xie, et al. 2011; Uzer et al. 2015). Decoupling of the LINC complex also decreases nuclear strain and deformation during microneedle manipulation indicating physical force transmission from the cytoskeleton into the nucleus is lost during loss of function of the LINC complex (Lombardi et al. 2011). Additionally, isolated nuclei lose their ability to stiffen during magnetic bead displacement pulling on nesprin-1 during simultaneous SUN1 and SUN2 depletion (Guilluy et al. 2014). However, strain can overcome the depletion of SUN proteins and decoupling of the LINC complex (W. Hou et al. 2020; Y. Zhang et al. 2016; Bailing Chen et al. 2016; Sen, Xie, et al. 2011; Uzer et al. 2015; Lombardi et al. 2011). It is clear that the LINC complex is of important for cellular functioning and mechanoreponse and is the lynchpin by which mechanical and biomolecular signals enter the nucleus. However, the LINC complex does not account for all regulatory mechanisms of mechanoreponse in the nucleus. Other factors such as chromatin and lamin A/C affect cellular outcomes due to mechanical signals. These other systems cannot be underestimated in their contribution to cellular mechanics and mechanoreponse and require further investigation in tandem with the LINC complex to determine their interconnected roles in mechanoreponse.

Emerin

Emerin is a LEM-domain (LAP2 β , emerin, MAN1) family protein that is found in the endoplasmic reticulum and in the nuclear envelope. In the nuclear envelope, emerin is found on the ONM and INM. Emerin is a pointed end actin capping protein that is capable of regulating actin dynamics in both intra and extra nuclear compartments (Holaska, Kowalski, and Wilson 2004). SUN2 levels are significantly decreased in mutated emerin cells compared to wild type, playing a role in altered F-actin dynamics and nuclear structure (Essawy et al. 2019). Other emerin mutation isoforms cause misshaped nuclei, disorganized microtubule networks, and irregular cell shape (Dubińska-Magiera et al. 2019). Emerin's role in mechanical signaling revolves around regulating nuclear stiffness and binding to the actin-cap. During nuclear tension via nesprin-1-coated magnetic tweezers, the tyrosine kinase Src is activated, which in turn Src phosphorylates emerin to increase nuclear stiffness. During emerin knockdown or expression of mutated, non-phosphorylated emerin, isolated nuclei do not experience nuclear stiffening during force application (Guilluy et al. 2014). During mechanical strain, emerin increases its association with F-actin at the ONM and decreases its association with lamin A/C at the INM (Le et al. 2016). The mutated emerin isoform Δ K37 reduces actin-cap formation and actin organization in response to stiff substrates and cyclic strain (Reis-Sobreiro et al. 2018). While emerin regulates the physical connection of the nucleus to the cytoskeleton, its role has redundancy with that of the LINC complex. During LIV, depletion of emerin in MSCs does not impede mechanoactivation of the focal adhesions (W. Hou et al. 2020; Y. Zhang et al. 2016; Bailing Chen et al. 2016; Sen, Xie, et al. 2011; Uzer et al. 2015). However, emerin has

been shown to have a major impact on chromatin organization. As mentioned previously, emerin connects the LINC complex (Mislow et al. 2002; Haque et al. 2010) to the chromatin through BAF and to lamin A (Holaska, Wilson, and Mansharamani 2002). As a result of this important connection, depleting emerin results in the dispersion of chromatin from the periphery to the center of the nucleus (Pradhan, Ranade, and Sengupta 2018). Additionally, emerin dependent switching of heterochromatin from H3K9me3 to H3K27me3 occurs during strain (Le et al. 2016). In DLD-1 cells co-depletion of emerin and lamin A/C results in mislocalization of chromosomes (Ranade et al. 2019). Chromosome 19, which is positioned in the center of the nucleus, experiences relocalization to the periphery of the nucleus while chromosome 18 at the periphery sees no changes in positioning. Fluorescence recovery after photobleaching (FRAP) of H2A shows chromatin mobility increase of chromatin located internally of the nucleus which was aided by increased activity of nuclear myosin-1 (NM1) and nuclear actin during lamin A/C-emerin co-depletion (Ranade et al. 2019). The effects seen from the loss of emerin function range from loss of nuclear stiffness to chromatin organization, indicating emerin's important role in the nuclear envelope. However, most of the effects from the loss of emerin also require other nuclear envelope and nucleoskeleton elements like that of lamin A/C and F-actin. This indicates that emerin's involvement in regulating nuclear structure and mechanoreponse is more intricate than previously believed. Therefore, these interactions with chromatin, LINC complex, and lamin A/C must be further explored to fully understand emerin's regulatory role in the nucleus during mechanical stimulation. Further insight into emerin's potential role in regulating intra-nuclear actin should also be explored. As emerin associates with the actin-cap, regulates actin dynamics (Holaska,

Kowalski, and Wilson 2004; C. Y. Ho et al. 2013), and actin-driven nuclear positioning (Chang et al. 2013) emerlin's regulatory role on intranuclear actin could affect DNA repair and chromosome organization. Emerlin's role in the nuclear envelope is important, but its effects are dependent upon other nuclear envelope and nucleoskeleton proteins. Indicating other proteins in the nucleus are also important during mechanoresponse and mechanoregulation of the nucleus.

Spectrin, Intranuclear Actin, and Other Nuclear Proteins

Spectrins are tetramer proteins formed by association of two α - β heterodimers and are encoded in seven genes that are alternatively spliced to form different isoforms. Three types of spectrins are found in the nucleus: α II-spectrin, β IV Σ 5-spectrin, and β III-spectrin of which α II-spectrin is the most common (Simon and Wilson 2011). Spectrin creates a network of nucleoskeleton proteins through crosslinking nuclear actin and protein 4.1, providing elastic properties as nuclei lacking α II-spectrin have decreased recovery of nuclei shape after compression (Armiger, Spagnol, and Dahl 2016). Spectrin also plays an important role in DNA homologous recombination repair (HRR), nonhomologous end-joining (NHEJ), and nucleotide excision repair (NER) through recruiting DNA repair proteins to the repair site (Lambert 2018; Sridharan et al. 2003). In addition to actin and protein 4.1, spectrins also associate with lamin A, lamin B, SUN2, emerlin, and MYO1C. Knockdown of protein 4.1, a spectrin-actin stabilizer (Diakowski, Grzybek, and Sikorski 2006), results in nuclear blebbing and mislocalization of α II-spectrin, emerlin, actin, and lamin A (A. J. Meyer et al. 2011; Simon and Wilson 2011).

Actin is present in the nucleus as either monomeric G-actin or polymeric F-actin. The F-actin polymers in the nucleus differ from that of the cytoskeleton in that F-actin

polymers in the nucleus form short, anti-parallel structures that are bound to lamin A, lamin B, and emerin (Simon, Zastrow, and Wilson 2010). Intra-nuclear actin binding to emerin causes intra-nuclear actin polymerization and is linked to localizing chromatin remodeling complexes (Holaska, Kowalski, and Wilson 2004; Holaska and Wilson 2007). Binding of F-actin to lamin A has also been associated with regulating actin polymerization as cells lacking lamin A form rod-like structures of F-actin in the nucleus (Simon, Zastrow, and Wilson 2010). G-actin monomers are required for proper DNA repair (Kawashima et al. 2007) and chromatin modifications (Kapoor et al. 2013; Fenn et al. 2011). Blocking intra-nuclear G-actin export out of the nucleus stabilizes nuclei and prevents nuclear rupture, indicative of increased mechanical competence (Bohnsack et al. 2006). Intra-nuclear F-actin also increases during cell spreading which is likely to exert complex loading on nuclei. Intranuclear F-actin formations due to cell spreading are prevented when lamin A/C, SUN1/2, or emerin are depleted (Plessner et al. 2015). Myosin motor proteins are also found in the nucleus and are unsurprisingly associated with the nuclear actin. Nuclear Myosin 1 (NM1) was the first nuclear myosin protein found in the nucleus and is an isoform of MYO1C produced by an alternative transcription start site of the *Myo1c* gene. Strain activates nuclear myosins and increases nuclear myosin localization to the INM, as well as increases of emerin-actin association. NM1 has been shown to be required for proper RNA polymerase I and II transcription through moving chromatin to transcription initiation sites (Pestic-Dragovich et al. 2000; Philimonenko et al. 2004; Grummt 2006). When myosins I and V are depleted via RNAi, myosin I and V cannot relocalize to repair sites for heterochromatic double strand breaks (Caridi et al. 2018). While other myosin proteins have been found in the nucleus their

impact on nuclear function is still under investigation. Additionally, nuclear actin has a role in regulating chromatin organization and structure during mechanical stimulation, but this avenue of research has yet to be fully explored. Therefore, research into nuclear actin and other nuclear proteins should investigate their roles in regulating nuclear response to mechanical signals.

Nuclear Lamins

One family of nuclear proteins that has been extensively investigated are the lamins. The lamin family of proteins are type V intermediate filaments and consist of lamin A, lamin B, and lamin C. Alternative splicing of the *LMNA* gene produces either lamin A or lamin C (Lin and Worman 1993) and together are termed lamin A/C. Another lamin family protein is lamin B which has three isoforms: lamin B1 encoded by *LMNB1* gene, lamin B2 and lamin B3 which are encoded by *LMNB2* and are formed via alternative splicing (Burke and Stewart 2013). Lamin B1 and lamin B2 are found in somatic cells while lamin B3 is found in spermatid cells (Furukawa and Hotta 1993; Vorburger et al. 1989; Peter et al. 1989). Together lamin A/C and lamin B proteins form the majority of the nuclear lamina located at the INM. Lamin A/C proteins are associated with emerin, the LINC complex via SUN1/2, intranuclear actin, BAF, histones, and DNA (Burke and Stewart 2013; C. Y. Ho and Lammerding 2012). Lamin B binds to emerin, intra-nuclear actin and DNA, which DNA binding is done through the nuclear envelope protein lamin binding receptor (LBR) (C. Y. Ho and Lammerding 2012). Each lamin family protein has a distinct role in nuclear structure and function. During the loss of lamin A/C the nucleus experiences blebbing, wrinkling, loss of circularity, increased volume, height, area, and decreased cellular and nuclei stiffening (Goelzer et al. 2020;

Dorland et al. 2019; Sullivan et al. 1999). This loss of structural properties causes increased migration and proliferation (Hsu et al. 2005; Capo-chichi et al. 2011; Harada et al. 2014). Investigation into lamin A/C shows that during lamin A/C depletion fibroblasts are unable to harness apical F-actin fibers that are formed during substrate strain (J.-K. Kim et al. 2017). This inability to associate with F-actin fibers is observed in progeria models. In progeria, a devastating early aging disease, a silent mutation in *LMNA* causes permanent farnesylation, preventing proteolytic cleavage causing progerin, a misfolded form of lamin A, to build up at the nuclear (De Sandre-Giovannoli et al. 2003; Liu et al. 2010). *LMNA* mutation results in the increased phosphorylation of ERK1/2. *LMNA* dependent phosphorylation of ERK1/2 causes the phosphorylation of FHOD1/3, inhibiting actin bundling at the nuclear envelope (Antoku et al. 2019). The regulatory role of lamin A/C in connecting to F-actin fibers results in the loss of nuclear positioning (Antoku et al. 2019), nuclear movement (Antoku et al. 2019), and negates jasplakinolide-induced nuclear F-actin formation in fibroblasts leading to reduced transcription (Takahashi et al. 2020). These observations of lamin A/C loss and nuclear morphology alterations are constant throughout any mechanical force stimulation method. Fluid shear stress (FSS) in mouse embryonic fibroblasts (MEF) and C2C12 cells that are *LMNA* *-/-* experience no alignment to fluid shear causing the loss of localization of nesprin-2 and nesprin-3 to the nuclear envelope (Chambliss et al. 2013; Libotte et al. 2005). During cell shape regulation via microstamps depletion of lamin A/C causes increased nuclei size fluctuation in rectangular cells (Makhija, Jokhun, and Shivashankar 2016). These discoveries unearthed the role of lamin A/C in regulating nuclear morphology and

mechanical properties. However, lamin B is also present in the nuclear lamina and has its own role in the nucleus.

Unlike lamin A/C that is largely expressed in committed or multipotential cell types, lamin B is found in the brain cells of mice at birth and are expressed in early stages of embryonic development (Röber, Weber, and Osborn 1989; Eckersley-Maslin et al. 2013). While lamin A/C binds to NPCs and emerin, lamin B does not. Instead lamin B binds to lamin B receptors (LBR) in the nuclear membrane linking lamin B to the nuclear envelope (Worman et al. 1988). Similar to lamin A/C related laminopathies, mutation of *LMNB1* and *LMNB2* are also linked to diseases. For example, adult-onset leukodystrophy which causes demyelination of the central nervous system and is linked to duplication of *LMNB1*. Heterozygous mutation of *LMNB2* is linked to acquired partial lipodystrophy which presents as a loss of subcutaneous tissue in the neck, arms, legs, and face (Hernandez et al. 2010). Depletion of lamin B results in chromatin instability and increased DNA double strand breaks (Butin-Israeli et al. 2015), chromatin reorganization (P. P. Shah et al. 2013), and increased senescence similar to that of progeria (P. P. Shah et al. 2013). Alterations to nuclear structure occur as well as increasing micronuclei (Butin-Israeli et al. 2015) and nuclear rupture (Vergnes et al. 2004; Y. Li et al. 2020). Lamin B has a critical role for the proper development of mice as *LMNB1* *-/-* mice experience reduced survival after birth and increased bone ossification (Vergnes et al. 2004). Lamin B therefore has an important role in maintaining normal nuclear functioning. However, the role of lamin B during mechanical signaling is not as vital and is different from the role of lamin A/C. The role differences between lamin A/C and lamin B are largely seen during mechanical stimulation of the nucleus. Modulation of

extracellular matrix (ECM) stiffness causes mechanical force effects on lamin A/C protein levels, lamin A/C structure, and nuclear lamina organization. Decreasing ECM stiffness decreases lamin A/C levels and causes re-localization of lamin A/C and lamin B into the interior of the nucleus (Pradhan, Ranade, and Sengupta 2018) and causes the deformation and folding of lamin A/C (Swift et al. 2013). In MSCs ECM stiffness alters LBR:lamin A/C ratios. Softer extracellular matrices induce LBRs to be highly expressed relative to lamin A/C (Lammerding et al. 2006) correlating with increased adipogenesis while stiffer ECM induces a lower LBR/lamin A relationship pushing the MSCs to osteogenesis (Lammerding et al. 2006). While these results show a role for lamin A/C, lamin B, and LBRs in mechanosensing pathways, cells with defective lamin B experience little changes in gene expression during mechanical stimulation (Lammerding et al. 2006) which further supports that lamin A/C is the main target to regulate mechanical signals and mechanoregulation. Indeed, further research into lamin A/C through microstamp cell shape regulation shows that cells forced into rectangular shapes increase lamin A association at the nuclear envelope (Toh, Ramdas, and Shivashankar 2015), decrease nuclear size fluctuations (Makhija, Jokhun, and Shivashankar 2016), and induce osteogenic differentiation (Mathieu and Lobo 2012). Contrastingly, cells forced into circular shapes have decreased lamin A association with nuclear envelope (Toh, Ramdas, and Shivashankar 2015), large nucleus size fluctuations (Makhija, Jokhun, and Shivashankar 2016), increased chromatin and telomere diffusion (Makhija, Jokhun, and Shivashankar 2016), and inducement into adipogenesis (Mathieu and Lobo 2012). Lamin A/C therefore has a more important role in regulating cellular and nuclear response to mechanical signals. However, we have shown that mechanoregulation of

adipogenic differentiation in MSCs is independent of lamin A/C indicating that lamin A/C may have a limited or at least overlapping functionality with other nuclear proteins during mechanically induced repression of adipogenesis (Goelzer et al. 2020). Further research into the role of the nuclear lamina, specifically, lamin A/C, is needed during mechanoregulation of differentiation in combination with other nuclear envelope elements such as emerin or the LINC complex to fully elucidate the full mechanoregulatory effects of nuclear envelope proteins.

Chromatin

As the organized and packaged structure of histones and DNA, chromatin provides the nucleus with a mechanism to regulate not only genomic expression but also genomic organization and nuclear structural properties. Chromatin is known to associate with SUN proteins (Ding et al. 2007), emerin, lamin A/C through DNA binding domains and BAF, to lamin B via LBRs, and other nuclear proteins. Chromatin domains that are in proximity to and associate with the nuclear lamins are called lamin-associated-domains (LAD) (Guelen et al. 2008; Lund et al. 2015) (Figure AII.1A). These domains have been shown to be correlated with heterochromatin, producing repression of gene expression of genes located in the LADs (Leemans et al. 2019). However, this model of LAD-mediated repression at the nuclear periphery does not account for the changes in the 3D chromatin organization observed under lamin depleted cells. Disabling the interaction of chromatin and nuclear lamins results in the loss of the inter and intra-interactions between topological-associated domains (TADs) at both the periphery and internal regions of the nucleus (Y. Kim, Zheng, and Zheng 2019). Additionally, loss of lamin A/C alters chromatin diffusion (Bronshtein et al. 2015). Therefore, disabling the interaction of

chromatin with the nuclear lamins not only affects the nuclear periphery but alters 3D organization of chromatin. Mechanical forces also regulate chromatin structure. Soft ECM induces increases in euchromatin (Gerardo et al. 2019) and localization of chromosomes 1, 18, and 19 to the nuclear interior, and upon replating on stiffer substrates only chromosome 18 experiences recovered localization (Pradhan, Ranade, and Sengupta 2018). Substrate strain causes an increase of heterochromatin and switching of heterochromatin from H3K9me3 to H3K27me3 (Le et al. 2016; Nava et al. 2020). Direct magnetic bead shear stress on the nucleus of Chinese hamster ovary (CHO) cells also shows that chromatin is induced into an open state and increases gene expression (Tajik et al. 2016). Depletion of SUN1/2, lamin B, lamin A/C, emerin, and BAF all cause similar chromatin movement and gene expression as magnetic bead shear stress (Tajik et al. 2016). Ultimately, these alterations of chromatin structure have major regulatory effects on differentiating stem cells. In MSCs, the heterochromatin marker H3K27me3 is decreased in cells differentiating into adipocytes, while the euchromatin markers H3K9ac, H3K4me3, and H4K5ac see an increase (M. B. Meyer et al. 2016; Sen et al. 2020). Alterations to chromatin are one of the first steps in cellular responses to mechanical signals. Understanding how stem cells alter their chromatin structure and organization in response to mechanical forces is required to truly understand and manipulate stem cell fate.

As the main house for DNA, it is a logical conclusion that both alteration to nuclei structure and mechanical force stimulation would alter chromatin. However, chromatin also has an important role in regulating the nuclear response to mechanical forces and regulating nuclear morphology. Disruption of chromatin structure via chromatin digestive

MNase protein retards cell stiffening in response to low levels of strain displacement ($<3\mu\text{m}$) (A. D. Stephens et al. 2017). Additionally, increases in heterochromatin induces nuclear stiffening (A. D. Stephens et al. 2017, 2018) while increases in euchromatin results in decreased stiffness (A. D. Stephens et al. 2017, 2018). Reduced H1, a histone protein that stabilizes formation of condensed chromatin, does not alter heterochromatin markers but does result in decreased nuclear rigidity inducing increased nuclei fragility (Furusawa et al. 2015). Additionally, decreased levels of heterochromatin also result in blebbing and protrusion of the nuclear envelope independent of lamin A/C (A. D. Stephens et al. 2018; Furusawa et al. 2015; A. D. Stephens, Banigan, and Marko 2019). Therefore, chromatin is a vital nuclear element that regulates gene expression, nuclear morphology, and nuclear mechanics. In order to fully understand how the nucleus responds to and senses mechanical signals the interaction of chromatin and nuclear proteins must be further explored. Specifically, understanding the connections between chromatin and the nuclear envelope proteins is of great importance. As mechanical signals enter the nucleus through the nuclear envelope proteins, like that of the LINC complex, and are transferred to the chromatin, understanding the chromatin dynamics is of vital importance. A potential tool to investigate these dynamics is fluorescence microscopy, as the advancement of fluorescence microscopy beyond the diffraction limited spot has now provided a way to visualize these dynamics at the single molecule level, providing a launching point for further exploration and quantification of these changes that have not been achievable before.

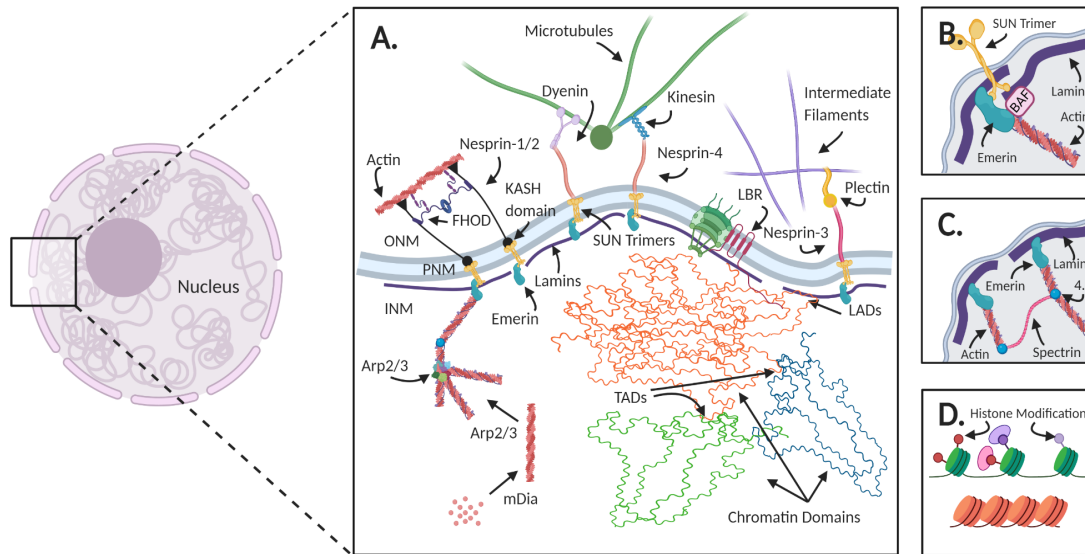
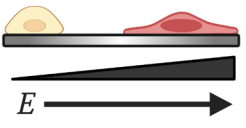
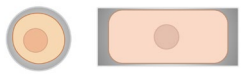
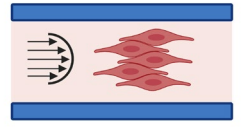


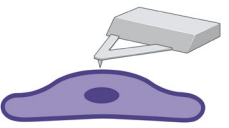


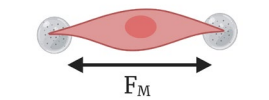
Figure AII.1 Nuclear Structure

A. Nuclear structural proteins interact with the cytoskeleton, chromatin, and the nuclear membrane to stabilize the nucleus and provide mechanosensing functions. Chromatin domains that bind to the nuclear lamins are called lamin-associated-domains (LAD). These domains have been shown to be correlated with heterochromatin, producing repression of gene expression of genes in the LADs. B. Emerin connects the LINC complex, via Sun1/2 and nesprin-1/2 to the chromatin through BAF and lamin A. C. The intranuclear actin network is formed through the crosslinking of short F-actin fibers via protein 4.1 and spectrin. This provides elastic structural properties to the nucleus. D. Chromatin domains conserve epigenetic histone modifications. Changes of histone modifications, TADs, and LADs all result in changes in gene expression and cell differentiation.

Table AII.1 Common in vitro mechanical force stimulation methods and their major studied outcomes

Mechanical Force	Major Outcomes	Description	Benefits	Drawbacks
 <p>Extracellular Matrix Stiffness</p>	<p>Focal adhesion activation, Actin cytoskeleton polymerization, nuclear stiffening, stem cell differentiation, chromatin organization</p>	<p>Stiffening or softening of extracellular matrix to induce homologous mechanical responses to that of native tissue</p>	<p>Replicates to native tissue mechanics No additional machines or apparatus required to induce mechanical signals</p>	<p>Expensive to purchase Can have uneven stiffness profiles across surfaces Harder to image live or fixed cells</p>
 <p>Micropillars and Microstamps</p>	<p>Cytoskeleton, nucleus shape, stem cell differentiation, chromatin organization</p>	<p>Restricting cell shape through physical impediments or shape of adherent surface</p>	<p>Easy to manufacture Isolate's function of cell shape in cellular functions Can image live or fixed cells</p>	<p>Low cell density Partial homology to tissue environment</p>
 <p>Fluid Shear Stress</p>	<p>Cell and nucleus orientation, cytoskeleton remodeling</p>	<p>Mimicry of fluid shear stress forces found in vasculature systems</p>	<p>High homology to vasculature forces Easy to mimic human pathologies</p>	<p>Requires use of specially designed bioreactors Fluid force can be non-uniform between experiment sets</p>

 <p>Strain</p>	<p>Actin cytoskeleton, cell differentiation, focal adhesion signaling, nuclear stiffness, chromatin organization</p>	<p>Stretching of adherent substrate to produce dynamic or static strain forces</p>	<p>Easy to regulate forces Induces strong regulation of differentiation and stimulation of the actin cytoskeleton</p>	<p>Requires expensive strain application machinery Limited by size of specialized cell culture plates</p>
 <p>Low Intensity Vibration</p>	<p>Focal Adhesions, cell differentiation, cell proliferation, nuclear stiffness</p>	<p>Low magnitude strain induced by low amplitude, high frequency vibration</p>	<p>Similar homology to muscle-induced vibration forces observed in native tissue Can be utilized in cell culture, tissues, and mammalian models</p>	<p>Limited by size of vibration surface area Requires long term exposure to mechanical signals</p>
 <p>Atomic Force Microscopy</p>	<p>Cell and nuclear stiffness, force induced translocation of mechanically sensitive biomolecules</p>	<p>Probing of individual cells and nuclei with rounded-tip atomic force microscopy</p>	<p>Provides high resolution stiffness measurement of cells and nuclei Targeted mechanical activation of mechosensitive signaling pathways</p>	<p>Does not provide population-based measurements Hard to determine if measuring proper target versus non-desired targets</p>

 <p data-bbox="293 394 495 468">Magnetic Bead Stretching</p>	<p data-bbox="581 226 797 548">Force induced translocation of mechanically sensitive biomolecules, nuclei mechano-response, actin cytoskeleton, chromatin</p>	<p data-bbox="820 226 954 510">Use of magnetic beads to induce physical strain on individual cells</p>	<p data-bbox="1011 226 1203 604">Allows for targeted strain on an individual cell level Can induce targeted chromatin structure changes</p>	<p data-bbox="1226 226 1393 569">Does not provide population-based measurements Requires use of special equipment</p>
---	---	--	---	---

Characterization of Nuclear Structure and Mechanics

The nucleus is a mechanosensitive organelle of the cell that allows for gene regulation and adaptation as an active response to biophysical stimuli from the cytoskeleton and surrounding environment. Numerous methodologies have been developed to probe nuclear structure and mechanics, including fluorescence anisotropy (Banerjee, Bhattacharya, and Shivashankar 2006; Bhattacharya et al. 2009; Shaban and Seeber 2020), micropipette aspiration (Bader et al. 2002; Farshid Guilak et al. 2005), nanoindentation (Darling 2011; Wilusz et al. 2009), and image-based assessment of aspect ratios (Haudenschild et al. 2011; Knight et al. 2002), volume (F. Guilak, Ratcliffe, and Mow 1995; Abusara et al. 2011), deformable image registration (Gilchrist et al. 2007; Lim, Henderson, and Neu 2013), and deformation microscopy (Ghosh et al. 2019). Characterization of bulk or local structure and mechanics is possible for isolated cells or nuclei, and additionally of cells embedded in two- and three-dimensional microenvironments. Like most biological structures, the nucleus is well-known to exhibit complex (e.g., nonlinear, time-dependent) properties, and available methods allow for the

characterization of this behavior following a wide range of mechanical perturbations (F. Guilak, Tedrow, and Burgkart 2000; Guilluy et al. 2014).

Nuclear Structure

Recent research reveals that the nuclear structure, with distinct euchromatin and heterochromatin subdomains, demonstrates a scale-dependent and solid-like behavior under some conditions that provides insight for the physical organization and regulation of the genome (Strickfaden et al. 2020). While microscopy methods like fluorescence microscopy and fluorescence recovery after photobleaching provide the ability to visualize the nuclear interior, additional methods are required to provide value-added characterization of nuclear structure. The morphology of the nucleus is commonly assessed based on measurement of the aspect ratio, volume, or a characteristic dimension such as major/minor axes (Knight et al. 2002; Gilchrist et al. 2007; Seelbinder et al. 2020). Morphological analysis of this type commonly considers geometric changes of the nuclear periphery using automated or semi-automated algorithms and does not provide any intranuclear spatial information. A major strength of nuclear morphology measurements is the ability to assess large numbers of cells in a high-throughput manner, enabling population-level analysis of treatment responses, often at the cost of detailed intranuclear spatial information.

Intranuclear Strain

Local mechanical deformations, i.e., displacements and strains within the nuclear interior, may be related directly to altered transcriptional activities, possibly through the alteration and regulation of chromatin domains (Mammoto, Mammoto, and Ingber 2012). While the measurement of local deformation may reveal fundamental mechanobiological

mechanisms, direct imaging of intranuclear mechanics is challenging. Commonly, fluorescent microscopy of viable cells is required to capture and tag the deforming nucleus in multiple (e.g., resting and mechanically loaded or stretched) states to allow for a description of motion of the nucleus in a “current” configuration with respect to an initial “reference” configuration. Widefield and confocal microscopy can be used to visualize living cells before and after deformation (Lim, Henderson, and Neu 2013), and a natural extension of imaging modalities to include modern methods like super-resolution microscopy are possible.

Spatial mapping of deformation within the nucleus is accomplished using fluorescence anisotropy (Talwar et al. 2013), and texture correlation (Gilchrist et al. 2007; Henderson et al. 2013). Recently, deformation microscopy, based on hyperelastic warping and deformable image registration (Ghosh et al. 2019), demonstrated the ability to map biophysical and biochemical interactions due to substrate stiffness or hyperosmotic changes, or LINC disruption treatments, and have been used broadly to describe the mechanics of nuclei in cardiomyocytes, chondrocytes, and skeletal muscle *in vivo* (Ghosh et al. 2019; Henderson et al. 2013; Ghosh et al. 2017). Additionally, detailed strain patterns have been associated with distinct epigenetic modifications that impact development (Seelbinder et al. 2019). The use of hyperelasticity enables the measurement of complex nuclear behavior, including nonlinear elasticity in two and three dimensions, that would be expected to sufficiently describe intranuclear deformation for most anticipated applications. Certainly, nuclei have demonstrated extreme deformations, such as in migratory cancer cells in constrained geometries (Denais et al. 2016), and yet

recovery of the nucleus is observed, aligning more with hyperelastic, and not plastic or permanent, deformation behavior.

Intranuclear Stiffness

Emerging methods also enable the description of the mechanical properties of heterochromatin and euchromatin domains. One method is intranuclear rheology (Booth-Gauthier et al. 2012; Dahl et al. 2005) which tracks the passive movement of fiduciary markers such as fluorescent beads but may suffer from limitations including the possible invasive nature of bead insertion and the impact of embedded beads on cell viability. Atomic force microscopy with a needle-tip probe has recently demonstrated the ability to directly map the nuclear envelope and cell membrane stiffness in within native tissue (McCreery et al. 2020), and showed that the nuclear stiffness decreases with disruption of the extracellular matrix in living tissues, further emphasizing the physical links connecting the nucleus to the surrounding microenvironment. Optical microscopy-based (Grasland-Mongrain et al. 2018; Jaiswal et al. 2019; Kennedy et al. 2015) elastography is a powerful potential method to measure the distribution of mechanical properties noninvasively within the nucleus. Based on techniques like deformable image registration and inverse finite element methods, image-based elastography of heterochromatin and euchromatin domains in the deforming cell nucleus is now possible (Ghosh et al. 2020; Reynolds et al. 2020).

Linking Nuclear Mechanics and Mechanobiology

While characterization of the nucleus structure and mechanics is possible using numerous methods, still lacking are studies that carefully link biomechanics with cell and nuclear biological activity. Methods are required that allow for the rapid acquisition of

biomechanical data coupled simultaneously with techniques that capture activities like rapid gene expression in response to mechanical loading. High spatial resolution imaging is needed to probe the single-cell level, ideally in complex three-dimensional microenvironments like hydrogels or native tissue. New methods explore combinatorial methods, including the use of photobleaching with unique Förster Resonance Energy Transfer (FRET) pairs (Ouyang et al. 2008; Iyer et al. 2012), or deformable image registration with independent assessments of histone modifications or LINC disruption (Seelbinder et al. 2019).

Visualizing Chromatin Dynamics in Living Cells

In the sections leading here we have detailed the mechano-responsive structures that make up nucleus as well as methods to apply mechanical force as well as methods to measure nuclear mechanics. While it is accepted that 3D structure and function of the nucleus and chromatin are inherently connected, “seeing is believing” (McGeown 2010), and therefore visualizing is critical to understanding the structure and function of the genome. There are an increasing number of studies aimed at understanding how mechanical signals regulate nuclear mechanics at higher resolution, while at the same time there are several state-of-the-art optical techniques under-utilized in the field of mechanobiology that are capable of visualizing nuclear dynamics. In this section we will first focus on current methods of labeling DNA, RNA, and proteins in living cells and discuss details of different imaging modalities that can be used to discern the motion of these labeled structures. Finally, we will discuss possible approaches that can be combined to perform correlative measurements of mechanical stimulation and gene

expression at high resolution as these may provide critical information about the relationship between mechanics and spatiotemporal (3D+1D) dynamics of the nucleus.

Fluorescent Biomolecule Labeling

There are a variety of labeling strategies available for visualizing biomolecules. Each provides varying pros and cons, making them ideal for different experimental questions. Some questions to consider when choosing a label method include: Is the experimental imaging going to be performed in live cells? How bright does my fluorophore need to be? Do I want the flexibility of adding my probe before each experiment or do I want the stability of having a self-labeling cell line? How important is fluorescent background and labeling efficiency? Based on the answers to these questions, the proper labeling method for your experiment can be identified (Table AII.2). Below we highlight the most promising methods for imaging the nucleus while it undergoes mechanical stimulation.

The newest addition to genome editing, CRISPR, has revolutionized our ability to edit the genome as well as visualize it. Deactivated Cas9 (dCas9) provides the technology necessary to document the dynamic properties of different gene loci simultaneously (Baohui Chen and Huang 2014; Deng et al. 2015; Guo et al. 2019; Anton, Leonhardt, and Markaki 2016; S. Wang et al. 2016; Ma et al. 2016; Baohui Chen et al. 2013; Qi et al. 2013). dCas9 uses the CRISPR gene editing system for DNA labeling with a fluorescently tagged Cas9 in combination with specifically engineered guide RNAs (gRNA). This method can be used to successfully image multiple gene loci simultaneously within a living cell, which makes it an ideal labeling method for studying chromatin dynamics during mechanical stimulation (Ma et al. 2016). Similarly, dCas13, a

molecule like dCas9, targets complementary sequences of RNA. Together the gRNA and dCas13 protein can locate a specific sequence of RNA and fluorescently label it. While this method of RNA labelling is still in development, it promises a versatile method for labelling RNA's which have not been modified through the insertion of an RNA hairpin or other sequence. In this system either the gRNA (Deng et al. 2015) or dCas13 molecule (L.-Z. Yang et al. 2019) may be fluorescently labelled. Like dCas9 it suffers from low affinity but that can be overcome through multimerization of the guide RNAs. Now specific sequences of RNA can be labeled for real-time imaging and tracking (L.-Z. Yang et al. 2019).

Another newer option for live-cell imaging of RNA are RNA aptamers like RNA Mango (Dolgosheina et al. 2014), RNA Spinach (Paige, Wu, and Jaffrey 2011), and RNA Broccoli (Filonov et al. 2014). RNA aptamers are sequences designed as molecular beacons and selected through SELEX (Sefah et al. 2010; Tuerk and Gold 1990). The resulting aptamer is capable of binding specific fluorophore derivatives with nanomolar affinity. This results in an increased fluorescence of up to 1,000-fold. The main advantage of this method is that it provides a fluorescence enhancement upon binding, lowering the considerable fluorescence background that is typically present in other methods such as dCas9 and dCas13. This technology for visualization of RNA Mango has been used in conjunction with single-molecule fluorescence microscopy on a wide range of projects including visualizing RNA complexes in live *C. elegans* (Cawte, Unrau, and Rueda 2020) and protein tyrosine kinase activity (Shraim et al. 2020). While this method is still very new it holds promise for visualizing RNA dynamics as no other label has, providing invaluable information of the inner workings of the nucleus and the results

of mechostimulus on the transcriptome. An additional tool that has been developed recently for advanced protein imaging studies are self-labeling protein tags such as HaloTag and SNAP-tag (Tirat et al. 2006; N Peterson and Kwon 2012). These self-labeling organic protein tags can be inserted into cloning vectors (Tirat et al. 2006), allowing for a specific binding site for fluorophores. The SNAP-tag and HaloTag technology can be used with a wide range of fluorophores, allowing for more flexibility than with fluorescent proteins alone. They are often used in conjunction with small, membrane permeable chemically derived dyes like “Janelia Fluor” (JF) dyes that are known to be highly photostable (Grimm et al. 2016). There are many labeling options available (Table AII.2), but the ones described above CRISPR/Cas, RNA Aptamers, and HaloTag promise to be the most valuable for characterizing the dynamics of DNA, RNA, and protein while the nucleus is undergoing mechanical perturbations.

Table AII.2 Fluorescence Labeling Technologies

Label	Target Biomolecule	Description	Benefits	Drawbacks
DAPI & Hoechst stains	DNA	These dyes fluoresce when they intercalate into the minor groove of DNA. (Latt et al. 1975; Kapuściński and Skoczylas 1978; Kapuscinski 1995)	Requires minimal sample preparation Labels all DNA indiscriminately	Primarily for fixed samples Cannot label specific genes
FiSH	DNA/RNA	Fluorescence in-situ hybridization (FiSH) labels gene loci or RNA specifically with fluorescently labeled single stranded probes. (Byron, Hall, and Lawrence 2013; Camps, Erdos, and Ried 2015)	Labels DNA gene loci or RNA specifically Multiple gene loci labeled at one time	Cannot be used for live cell imaging Requires specific probe design
LacR & TetR	DNA	LacR and TetR specifically label chromatin locus in living cells with a GFP-fusion protein (Robinett et al. 1996; Roukos et al. 2013).	Results in stable cell line that can be used over and over Specific gene loci and individual gene loci can be imaged in live cells over multiple generation without the addition of probes	Requires integration of prokaryotic operon sequences into the DNA The gene editing may result in abnormal gene expression profiles
dCas9	DNA	dCas9 uses the CRISPR gene editing system for DNA labeling with a fluorescently tagged nuclease dead Cas9 in combination with specifically engineered guide RNAs (Baohui	Live cell imaging without laborious or disruptive gene editing Multiple gene loci labeled at one time	Requires multiple CRISPR/Cas9 to produce a bright enough signal for imaging The binding affinity of CRISPR/Cas9 is

		Chen and Huang 2014; Deng et al. 2015; Guo et al. 2019; Anton, Leonhardt, and Markaki 2016; S. Wang et al. 2016; Ma et al. 2016; Baohui Chen et al. 2013; Qi et al. 2013).	Ideal for studying chromatin dynamics	highly dependent upon the gRNA sequence
MS2/PP7	RNA	Fluorescent molecules bind to repetitive stem loops that have been introduced into the gene of interest. Each stem loop, of which there are often up to 24 copies, binds to a dimer of a chimeric protein composed of the phage protein, a nuclear localization signal and a fluorescent protein (Lenstra and Larson 2016).	Actively transcribing RNA can be imaged in real-time within a cell Since MS2-RNA and PP7-RNA are sequence specific, both can be used simultaneously within a given cell, allowing for multiple RNAs to be visualized at the same time.	Can only be used to label two distinct RNAs at a time The multimerization of the stem loops results in a bulky label that can alter RNA kinetics
dCas13	RNA	dCas13 uses the CRISPR gene editing system for RNA labeling with a nuclease dead Cas13 in combination with specifically engineered guide RNAs (Deng et al. 2015). Either the gRNA or the Cas13 can be fluorescently tagged.	Versatile method for labelling RNA's which have not been modified through the insertion of an RNA hairpin or other sequence Sequence specific Ideal for studying RNA dynamics	Requires multiple copies of the RNA of interest and multiple CRISPR/Cas13 to produce a bright enough signal for imaging The binding affinity of CRISPR/Cas13 is highly dependent upon the gRNA sequence
RNA Aptamers	RNA	RNA aptamers, like RNA Mango (Dolgosheina et al. 2014), are sequences designed as molecular	Provides a fluorescence enhancement upon binding (up to 1000x),	Requires binding to a target molecule to fluoresce

		beacons and selected through SELEX (Sefah et al. 2010; Tuerk and Gold 1990). The resulting aptamer is capable of binding specific fluorophore derivatives with nanomolar affinity.	lowering the considerable fluorescence background that is typically present	Requires specific environmental parameters to perform optimally (magnesium concentration, temperature, ect.)
Fluorescent Protein Tags (ex. GFP)	Protein	Fluorescent proteins can be inserted into a cell line so that as a protein is expressed it fluoresces (Stepanenko et al. 2008).	Proteins are produced directly by the cell 100% labeling efficiency	These protein labels are bulky and can change protein dynamics
HaloTag and SNAP-tag	Protein	Self-labeling protein tags such as HaloTag and SNAP-tag (Tirat et al. 2006; N Peterson and Kwon 2012) are organic protein tags that can be inserted into cloning vectors (Tirat et al. 2006), allowing for a specific binding site for fluorophores.	Can be used with a wide range of fluorophores Improved brightness and photostability Self-labeling	Does not have 100% labeling efficiency, therefore “dark” or unlabeled proteins sometimes occur Requires gene editing
Fluorescent Antibody Fragments (Fabs)	Protein	This is a technique that uses monoclonal antibodies which lack the Fc component to specifically tag proteins of interest (Ferrara et al. 2011). The fluorophore is conjugated to a single chain antibody specific to the protein of interest (Sato, Stasevich, and Kimura 2018).	Ideal method of quantifying the timing of post-translational modifications and their effects in living cells	Challenging to design probes Low yield when designing Fabs

Fluorescence Imaging Techniques

For the study of living cells and tissues there is no substitute for light microscopy. The limited interaction of photons with biological matter combined with superb contrast provided by fluorescent labelling allows us to study both the prevalence and subcellular organization of selected biomolecules within living cells and tissues. The ever-growing list of highly specific fluorescent labels makes fluorescence microscopy one of the techniques of choice for studying nuclear architecture and function (D. J. Stephens and Allan 2003). In the last decade the nucleus, which was a proverbial black box has been unmasked as a highly dynamic, ultra-structured entity that is dynamically reforming based on biochemical cues from the microenvironment and mechanical cues from the tissue. This evolution of scientific understanding is in large part due to advances in light microscopy and new creative imaging techniques (Trzaskoma et al. 2020; Bashirzadeh et al. 2018).

The methods we will discuss here can provide information about nuclear structure and mechanics. One of the main methods is visualizing tracer particles. Depending upon its size, a tracer particle may sample and provide information on either the micro or macro environment of the local nuclear region through the generalized stokes einstein's equation (Crocker et al. 2000). Confinement of a particle within a region of the nucleus may also allow determination of phase separated domains which have been reported to correlate with specific histone modifications and transcriptional activity (Sabari et al. 2018; Hnisz et al. 2017). Methods such as fluorescence anisotropy can also characterize properties of the local environment of a tracer particle. If mechanical stimulus is applied to the nucleus, particle image velocimetry can be used as a control to quantify the applied

stress or strain rate. Microrheology may be applied after mechanical stimulus to determine its effect on the local nuclear environment of a tracer particle (Gardel, Valentine, and Weitz 2005). Another more novel application in fluorescence microscopy, is to monitor changes in gene expression affected by mechanical stimulus. It may be that in some cases there is a direct relationship between gene activation or repression and the mechanical environment of the nucleus. While this effect is well known in population measurements of stem cell differentiation (Reilly and Engler 2010), it has never been directly verified at the single cell or single molecule level.

As with determining the appropriate fluorescent label for the experimental question, there are a variety of labeling techniques with benefits and drawbacks. Some focus on temporal resolution at the expense of spatial resolution. Others are focused on determining molecular interactions and binding events. The below chart provides an overview of techniques that are available and useful in determining the structure and function of nuclear architecture and its role in nuclei's mechanoresponsiveness (Table AII.3). We will then further highlight several methods that promise to be valuable.

Table AII.3 Fluorescence Imaging Techniques

Technique	Description	Benefits	Drawbacks
Colocalization	The observation of spatial overlap between different fluorescent labels, which reveals associations and interactions between two molecules (Dunn, Kamocka, and McDonald 2011; Adu-Gyamfi et al. 2012).	Can be conducted on widefield, confocal, and superresolution microscopes Shows biomolecular associations and co-distributions	Limited spatial and temporal resolution Limited by resolution as the colocalization of two probes does not always signify association.
Fluorescence Recovery After Photobleaching (FRAP)	FRAP is used to determine the kinetics and diffusion of various biomolecules by intentionally photobleaching a portion of the sample and then observing how the fluorescence distribution returns to its previous state (Vijayaraghavan et al. 2018; Darzacq et al. 2007; Sen Gupta et al. 2018; Wachsmuth et al. 2003; Ranade et al. 2019).	Useful for finding ratios of bound and unbound molecules, as well as localization data Turns photobleaching, which is generally avoided, into a desirable	The photobleaching process can be destructive to the sample because of the high light intensity Sometimes incomplete fluorescence recovery occurs due to obstruction of diffusion A local temperature increase at the photobleached site can affect the calculated diffusion rate (Abbaci et al. 2008)
Fluorescence Correlation Spectroscopy (FCS)	FCS utilizes fluctuations in fluorescence intensity in small detection volumes in samples of low concentration to investigate molecular dynamics (Magde, Elson, and Webb 1974)(V. Levi et al.	Kinetics data can be measured in a living cell Number of molecules of interest and their	Requires high labeling efficiency in order to get accurate kinetics data Only counts the molecules in the

	2003; Digman et al. 2005; Digman and Gratton 2009)(Schwille et al. 1999; Bacia, Majoul, and Schwille 2002; Ries and Schwille 2006; Dittrich and Schwille 2001; S. A. Kim, Heinze, and Schwille 2007).	molecular brightness can be calculated	observation volume, not the entire field of view
Single Particle Tracking (SPT)	SPT is a microscopy tool that allows the movement of individual particles to be followed within living cells. It provides information on molecular dynamics over time (Qian, Sheetz, and Elson 1991; Thompson, Larson, and Webb 2002).	Monitors the trajectories of individual biomolecules in living cells Good for studying localization dynamics	Requires extremely low fluorescent background and very bright labels Requires highly sensitive cameras Requires TIRF or HILO microscopes Photobleaching (due to widefield imaging)
3D Orbital Tracking	3D orbital tracking uses a unique scanning pattern. Instead of exciting the molecule directly, the laser passing around the bright spot indirectly excites it, resulting in a longer imaging window(V. Levi et al. 2003; Valeria Levi, Ruan, and Gratton 2005).	Minimal photobleaching Can collect data for long periods of time	Can only track one particle at a time Only collects data on the molecule being tracked, not the rest of the field of view
Förster Resonance Energy Transfer (FRET)	FRET exploits the energy transfer that occurs between two chromophores that are in close proximity. The donor when in an excited state can transfer its energy to the acceptor through dipole-dipole coupling (Helms 2008). The excitation is accompanied by light emission and the transfer of	FRET is a nondestructive spectroscopic technique Characterized molecular interactions with high accuracy (on the 1-10nm scale)	Low signal-to-noise ratio Sensitivity of probes to pH, temperature, ionic concentration, etc..

	energy is characterized by a loss of light emission. The efficiency of this transfer can be used to calculate small changes in distance between the chromophores (Pollok and Heim 1999).		
Fluorescence Lifetime Imaging (FLIM)	FLIM specifically measures how long a fluorophore stays in an excited state before emitting a photon (Digman et al. 2008; Datta et al. 2020).	Can detect molecular variations of fluorophores that are not apparent with spectral techniques alone Ideal tool for removing background fluorescence intensity Collects lifetime measurements for every pixel within the image	Difficult to conduct in live cells because there are not enough photons per pixel Requires in-depth data analysis

Fluorescence Correlation Spectroscopy (FCS) utilizes fluctuations in fluorescence intensity in small detection volumes in samples of low concentration to investigate molecular dynamics namely, diffusion, molecular conformations, binding events, and chemical reaction kinetics (Magde, Elson, and Webb 1974). It was first developed by Elliot, Magde and Webb (Magde, Elson, and Webb 1974) and later developed by Gratton et al. (V. Levi et al. 2003; Digman et al. 2005; Digman and Gratton 2009; Schwille et al. 1999; Bacia, Majoul, and Schwille 2002; Ries and Schwille 2006; Dittrich and Schwille 2001; S. A. Kim, Heinze, and Schwille 2007) and many others for scanning multiple labels and two photon excitation and was eventually extended to the study of transcription (Larson et al. 2011), translation (Morisaki et al. 2016) and splicing (Coulon et al. 2014) and more recently gene activation (Stavreva et al. 2019; Donovan et al.

2019). FCS is conducted by measuring fluctuations in fluorescence intensity as fluorescent molecules enter and exit an illuminated space. Large jumps in intensity signify larger molecules or multiplexes as opposed to small jumps in intensity that signify smaller, individual molecules. Similarly, slow changes in intensity indicate slower moving, often larger molecules, while quick fluctuations in intensity indicate faster moving, often smaller molecules. FCS calculations are done using a correlation curve from the fluctuations in intensity. The taller the curve the lower the concentration of molecules within the observation volume. The longer the curve, the slower they are moving (Magde, Elson, and Webb 1974). FCS was originally conducted on homogenized samples in a cuvette, now this technique has been extended for use in live cell microscopy (Bacia and Schwille 2003). The cell now acts as the confined space like the cuvette. Not only can single biomolecules be analyzed through FCS, but multiple molecules can be studied simultaneously, and their intermolecular interactions can be quantified as well by using fluorescence cross correlation spectroscopy (FCCS) (Bacia, Kim, and Schwille 2006; Digman and Gratton 2009). FCCS has been used extensively to quantify the kinetics of transcription factor binding and elongation as well as many other biomolecular interactions within the nucleus (Stortz et al. 2018; Mazza et al. 2012; Savatier et al. 2010).

Single Particle Tracking (SPT) is a method that requires bright and stable fluorescent labelling, highly sensitive CCD or sCMOS cameras and extremely low fluorescent background. In living cells this can only be achieved using a Total Internal Reflection Fluorescence (TIRF) (Daniel Axelrod 2001; D. Axelrod 1981) or Highly inclined illuminated optical sheet (HILO) (Tokunaga, Imamoto, and Sakata-Sogawa

2008) microscopes. SPT can be useful in determining the trajectories of individual particles with nanometer precision providing dynamic information about biomolecule locations. One of the major challenges with SPT is photobleaching. Even with improved fluorophores photobleaching often occurs within seconds or at most minutes on a widefield microscope, reducing the temporal resolution of correlative measurements. Recent advances have been made in this area with the development of lattice light sheet (B.-C. Chen et al. 2014) and other microscopy methods (Kumar et al. 2014), and has also been addressed by combining SPT with FCS and 3D orbital tracking (Larson et al. 2011; Coulon et al. 2014; Donovan et al. 2019; Stavreva et al. 2019). This synergistic approach has been successfully used to visualize transcription factor binding dynamics (Presman et al. 2017).

3D orbital tracking, which was developed in 2005 by Levi and Gratton et al. (Valeria Levi, Ruan, and Gratton 2005; V. Levi et al. 2005) gets around photobleaching issues by changing the laser scanning pattern from x-y to a circular orbit (Valeria Levi, Ruan, and Gratton 2005). Instead of exciting the molecule directly, the laser passing around the bright spot indirectly excites it, resulting in a longer imaging window (V. Levi et al. 2003; Valeria Levi, Ruan, and Gratton 2005). This method has been used to acquire quantitative, single-cell, live data on transcription factor binding and elongation (Donovan et al. 2019; Stavreva et al. 2019), as well as study lysosome active transport and free diffusion (Valeria Levi, Ruan, and Gratton 2005; Coskun et al. 2020). In addition to information on transcription factor binding and transcriptional activity, a laplace transformation of the mean squared displacement (MSD) of the 3D trajectory of a

gene locus by orbital tracking may also give information on the complex viscoelastic modulus of the nuclear compartment (Valentine et al. 2001).

Moving forward it is becoming increasingly necessary to combine these techniques to both validate findings as well as discover new information about nuclear structure and dynamics. By combining techniques, both spatially and temporally relevant data can be gleaned. FRAP and FRET are being used in conjunction to determine the dynamics of BAF and emerin interactions (Shimi et al. 2004). Colocalization and FRAP together showed that the crosstalk seen between the cytoskeleton and the nucleus is in large part regulated by lamin A/C and emerin modulating structural cytoskeletal proteins like actin (Ranade et al. 2019). FCCS and 3D orbital tracking have been used synergistically to determine the kinetics of transcription factor binding and RNA synthesis (Stavreva et al. 2019). It is not enough to solely study RNA, DNA-Protein interactions, or chromatin-chromatin interactions; each must be combined to understand how nuclear structure and gene expression are affected by mechanical and environmental cues. Not only is it powerful to combine two imaging techniques or two sequencing techniques, when both sequencing and imaging are combined unique research questions can be addressed.

Future Directions

Recent advances in the field of nuclear mechanobiology clearly indicates that the nucleus is not a passive element but actively participates in regulating cell phenotype in response to extracellular and cytoskeletal mechanical cues. As highlighted in this review, large numbers of proteins as well as inter-related structural and signaling events propose a daunting task for researchers who like to study the mechanical basis of nuclear

function. While many studies focus on simplifying assumptions, mechanistic understanding of nuclear mechanobiology requires inherently complex live-cell approaches that utilize innovative experimental designs using versatile model systems such as mesenchymal stem cells that rely on reconfigurations chromatin and nucleoskeleton for their differentiation programs. Further, some of the methods highlighted here provide a high level of control on cell geometrical constraints as well as applying precise dynamic mechanical forces. Therefore, uniquely combining powerful models with experimental mechanics such as “deformation microscopy” and with state-of-the-art visualization techniques to track mRNA transcription within a gene locus, should yield currently unstudied correlations between subnuclear mechanics and mRNA transcription and significantly advance the current scientific knowledge in how external mechanical force regulates cell function by altering nuclear interior.